Neural dynamics of the anesthetized brain and the control of conscious states

by

Jacob A. Donoghue

Sc.B., Brown University (2009)

Submitted to the Department of Brain and Cognitive Sciences
in partial fulfillment of the requirements for the degree of

Doctor of Philosophy

at the

MASSACHUSETTS INSTITUTE OF TECHNOLOGY

June 2019

Signature redacted

Author . . . . . .
Department of Brain and Cognitive Sciences
May 8, 2019

Signature redacted

Certified by . . . . . .
Earl K. Miller
Picower Professor of Neuroscience
Thesis Supervisor

Signature redacted

Accepted by . . . . . .
Matthew A. Wilson
Sherman Fairchild Professor of Neuroscience and Picower Scholar
Director of Graduate Education for Brain and Cognitive Sciences

Neural dynamics of the anesthetized brain and the control of conscious states

by

Jacob A. Donoghue

Submitted to the Department of Brain and Cognitive Sciences
on May 8, 2019, in partial fulfillment of the
requirements for the degree of
Doctor of Philosophy

Abstract

General anesthesia (GA) reversibly induces unconsciousness. It is arguably the most powerful brain state manipulation that clinicians and researchers can reliably perform. However, the mechanisms underlying GA at the neural systems level are underexplored and largely not understood. To link neural dynamics to the loss of consciousness, we measured spiking activity and local field potentials (LFPs) from multiple cortical and thalamic regions while monkeys were pharmacologically rendered unconscious. In Chapter 2, we examine effects of the GABAergic anesthetic propofol across prefrontal cortices (PFC), parietal cortex, temporal cortex, and the mediodorsal and intralaminar thalamic nuclei. Propofol decreased brain-wide spiking and high-frequency LFPs (e.g. gamma, 30-80Hz) while producing prominent slow cortical oscillations (0-4 Hz). These slow rhythms were incoherent across PFC yet synchronized in frontoparietal networks. Electrical stimulation of the central thalamus immediately and continuously reversed the neurophysiological effects of propofol and awakened the anesthetized monkeys. Thus, we interpret GABAergic anesthetics to produce unconsciousness via fragmented network dynamics facilitated by subcortical arousal pathway inhibition. In Chapter 3, we explore an alternative unconscious state mediated by the anti-glutamatergic anesthetic ketamine. Ketamine substantially increased spiking and gamma rhythms while eliminating beta (13-25 Hz) power and coherence across the cortical areas studied in Chapter 2. In anesthesia, slow waves interrupted high-frequency activity globally and PFC uniquely entrained central thalamic LFPs. Seemingly, ketamine harnesses an excitatory mechanism to disrupt conscious processing, overwhelming cortex with disordered spiking activity and binding thalamo-prefrontal flexibility. In Chapter 4, we describe our model for closed-loop control of GA in monkeys. We established and implemented a pharmacokinetic-pharmacodynamic paradigm within an optimal control framework that automatically titrated propofol using an LFP-derived GA biomarker. Together, this collection of work demonstrates the distinct network mechanisms that can drive GA and the systems-level approach to enhanced control of conscious states.

Thesis Supervisor: Earl K. Miller
Title: Picower Professor of Neuroscience

We shall not cease from exploration
And the end of all our exploring
Will be to arrive where we started
And know the place for the first time.

-- T.S. Eliot, Little Gidding (1942)

Acknowledgements

To appropriately acknowledge all of the individuals who contributed to these works and my own development over the course of this Ph.D. program would require another, much longer thesis. The substantial efforts taken by those around me have been invaluable in every aspect of what is contributed with this work.

Foremost, Earl. I thank my advisor Earl Miller for the unparalleled environment he provided for me to grow into a scientist. This diverse collection of work is truly a testament to what makes you great; Earl, you foster an infectious passion for scientific inquiry, provide the freedom and resources to pursue fully the questions we find most interesting, and challenge our views to ensure our hypotheses are rigorously evaluated by thoughtful experiments. Thank you for making this the best imaginable place to obtain my Ph.D.— it has been the most exciting and important part of my academic career.

I thank Emery Brown, my MD/PhD advisor, for teaching me to think as a rigorous, curious, and compassionate physician-scientist. Through late-night whiteboarding sessions and patent-drafting marathons, you've shown me how to take theory into practice. You have embedded these skills in me and I aspire to elegantly transform my scientific discoveries into better care for patients, just as you do.

I am thankful to my additional committee members for their support and valuable feedback throughout my research program. Bob Desimone and Nancy Kopell, through explicit advice and thoughtful conversations, my ability to perform and derive meaning from experiments is better because of you.

When opportunity or disaster strikes (and remember, we're a monkey lab!), my fellow labmates were always there to help me succeed. Whether diving in with me to epic, 14-hour MRI surgery sessions or providing emotional support upon the discovery of yet more unsynchronized data, there was no shortage of technical and intellectual feats, especially from Andre Bastos, Scott Brincat, Sourish Chakravarty, Meredith Mahnke, Roman Loonis, Mikael Lundqvist, Simon Kornblith, Marek Kowalski, Jefferson Roy, and Jorge Yanar. And without help of a few other impressive lab members, this work *truly* would be impossible. Tiergan, Mr. Jones, Mary, Edith, Cheerio, Galileo, and Jonah— may the grapes be ripe in your journeys to come.

My parents, unwittingly, hooked me on the brain. Phrases like "demyelinating" and "precentral gyrus" casually crossed the dinner table with my father busy inventing brain-machine interfaces for paralyzed patients and my mom caring for children with neurological disorders in her clinic. Thank you both for showing me how much joy and fulfillment can come from dedicating one's life to understanding the complexities of the brain and how to improve science and society alike.

Finally, I thank my sidekick Kathleen, my brother Noah, and my friends and family who have sustained and encouraged me throughout this academic adventure. You made all this possible and you made it fun.

Dedication

Kathleen, Jarrett, Keith, Noah, Mom and Dad. You are each superhumans. Your magic is palpable. Your selfless heroics vitalize those around you and enable us, mere mortals, to accomplish what we cannot imagine. I am infinitely grateful for the incredible sacrifice, love, and support you have given to me to make this possible— over and over again. I dedicate this work to you and all of the friends that have made my journey extraordinary.

Contents

List of Figures

Chapter 1

Introduction

1.1 Gentlemen! This is no humbug.

John Collins Warren, M.D. purportedly proclaimed these celebrated words upon the miraculous discovery of general anesthesia (GA) in the operating amphitheater at Massachusetts General Hospital on October 16, 1846. Concentrated in a sea sponge in a glass bulb, aerosolized ether was inhaled by a fortunate dental patient, who awoke following neck surgery without having felt discomfort. The discovery, bringing the conquest of pain, spread rapidly across America and Europe. Medicine was instantly and permanently transformed. Surgical procedures no longer resembled the gruesome affairs of medieval barber surgeons, but a controlled, humane practice that enabled a contemporary focus on the comfort and care of the patient.

Currently, over 60,000 patients each day are placed into a pharmacologically-induced, reversible state of unconsciousness, analgesia, amnesia and immobility alongside

maintained physiological stability— a state referred to as *general anesthesia*[1] (Purdon et al., 2013). Many modern anesthetics are structurally similar to the original diethyl ether administered that famed day the Ether Dome in 1846, though a shift has gone increasingly to involve and favor intravenous general anesthetics, such as propofol. There have been substantial efforts to enhance the physiological monitoring of patients during general anesthesia in an attempt to both ensure patient safety and stability, as well as to obtain improved metrics for the human body under GA. Some monitoring techniques are standard of care. Classic cardiovascular metrics recorded from electrocardiogram (ECG) such as heart rate and rhythm and airway monitoring to gauge respiratory metrics such as breathing rate and end-tidal carbon dioxide are essential in all clinical general anesthesia settings.

Brain monitoring via electroencephalographic (EEG) recordings from the scalp has been used extensively more recently to better track correlates of the unconscious state during clinical procedures. Spectral indices have emerged commercially to report a biomarker of depth of general anesthesia for a given patient through proprietary algorithms relating higher frequency brain waves to the lower frequency brain waves. Nevertheless, clinicians still more commonly rely on observable features of a patient (e.g. movement or responsiveness), and cardiovascular and respiratory vital signs to estimate level of unconsciousness. However, it's not that brain-derived analytics don't provide insight as to what is happening in the brain under general anesthesia. Quantitative EEG, breaking down spectral and waveform features of the extracranially recorded signals, even has been shown to reflect global neural metabolic activity, such as brain glucose utilization

[1] For the avoidance of doubt, we disambiguate *general anesthesia* from the commonly utilized term *anesthesia*, which often inappropriately combines drugs that are used to produce unconsciousness (*general anesthetics*, e.g. propofol), those that only produce conscious sedation but potentiate general anesthetics (*general anesthesia adjuncts*, e.g. dexmedetomidine or benzodiazepines), and those that that strictly cause focal insensitivity to pain or touch at the site of injection or the territory covered by the targeted nerve (*local anesthetics*, e.g. lidocaine).

(Alkire, 1998). Surprisingly, though, these advances have not translated to a greatly enhanced understanding on the neural processes giving rise to unconsciousness.

Extensive work has been done to understand the mechanisms of action of anesthetic drugs at the molecular and cellular level. Chemical structures, receptor-subunit binding affinities, changes in ion channel dynamics and downstream intracellular metabotropic pathways, single-neuron response activity— these features can all be effortlessly searched in classic reference texts to identify fundamental features of a given anesthetic compound. From these textbook specifics, detailed pharmacokinetic and pharmacodynamic models can be built to explain compartment saturations and clearance rates, but not unconsciousness. Nevertheless, understanding the mechanisms of clinically-used anesthetic agents at this scale sets the stage for exploring how populations of neurons in higher-order networks transform in GA. First, we review several major classes of drugs used to induce and maintain unconsciousness in humans and animals.

1.2 Molecular Effects of General Anesthetic Agents and Adjuncts

Intravenous General Anesthetic Agents

Propofol, nicknamed the Propofol, nicknamed the "milk of amnesia" for its white appearing emulsion, is a strongly lipophilic compound acting predominantly by increasing inhibition potentiating GABA-A receptors (Figure 1-1). Like most general anesthetics, propofol also has cross-reactivity with several other major cell receptor-classes. Most notably, it increases glycinergic inhibition at spinal cord synapses and slightly reduces cholinergic, NMDA, and AMPA-receptor activity(Alkire, Hudetz, & Tononi, 2008). It is often preferred for its rapid onset of action and high tolerability among adult patients, though is notably used with caution in children due to the risk of a potentially lethal "propofol infusion syndrome".

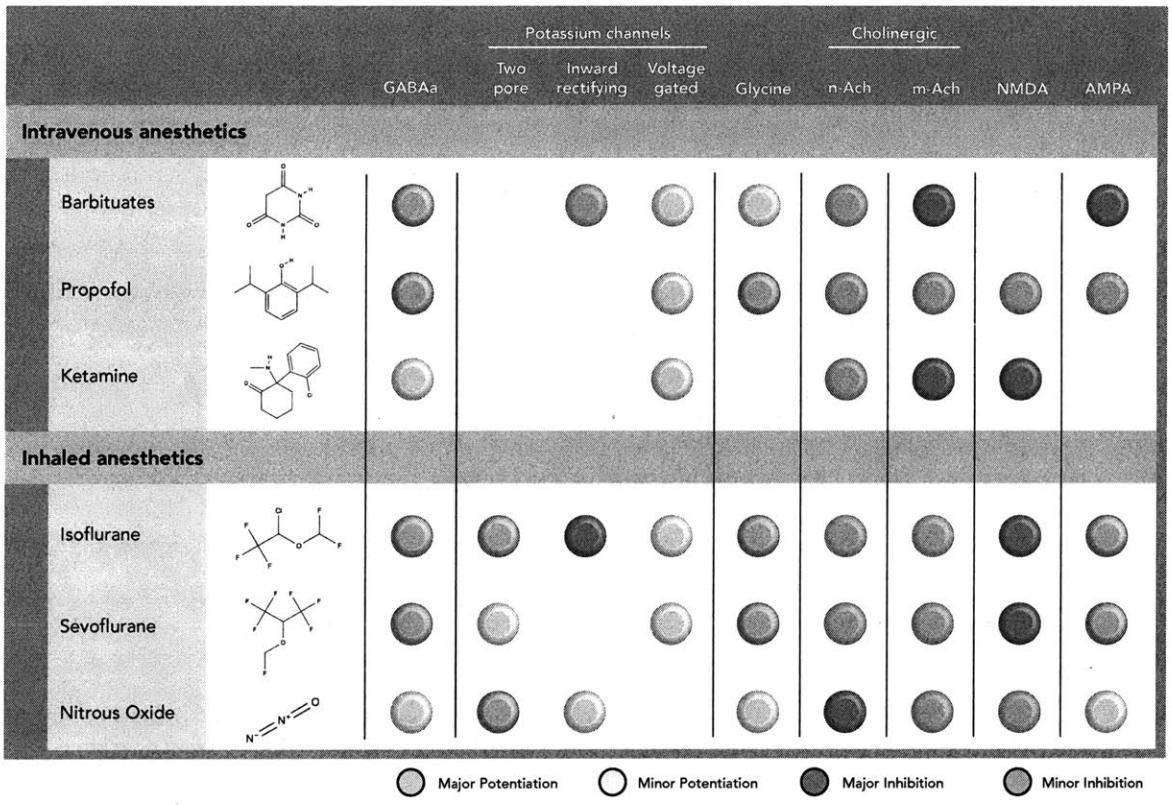

Figure 1–1: Chemical structures, molecular receptor targets, and mechanism of receptor-actions for the major classes of intravenous (top) and inhaled (lower) general anesthetic compounds. Figure adapted from (Alkire et al., 2008).

Barbiturates are barbituric acid-derived central nervous system depressants that drive sedation, anxiolysis, hypnosis, and even death at high doses. Barbiturates, much like propofol, exhibit most of their global inhibitory effects by potentiating the GABA-A receptor. Unlike propofol, barbiturates are potent inhibitors of AMPA receptors and muscarinic acetylcholine receptors (propofol is a mild inhibitor). In addition, they slightly potentiate glycinergic and voltage-gated potassium channels across the brain. Given the profound sedation these drugs are capable of producing, barbiturates are among the front-line therapy (alongside benzodiazepines and propofol) for terminating persistent seizures,

such as in patients experiencing refractory status epilepticus (Betjemann & Lowenstein, 2015).

Ketamine is a very different class of anesthetic drug, often referred to as a *dissociative anesthetic.* Ketamine acts primarily as a strong N-methyl-D-aspartate (NMDA) receptor antagonist, blocking excitatory glutamatergic activity on neurons. In addition, ketamine is known to inhibit muscarinic, and less so nicotinic, acetylcholine receptors, while slightly potentiating GABA-A and voltage gated potassium channels (Alkire et al., 2008). Ketamine is favored strongly as an anesthetic drug utilized outside of human patients, with high usage in veterinary cases with its wide dosing safety ranges. Behaviorally, ketamine is known to cause sensory hallucinations and disordered conscious processing in its subjects in a dose-dependent fashion, and is sufficient to produce complete unconsciousness. In addition, and related to these effects, ketamine has also been used extensively for the creating of an animal model of schizophrenia (Alpert & Angrist, 2003; Frohlich & Horn, 2014; Gil-da-Costa, Stoner, Fung, & Albright, 2013). More recently, ketamine has gained popularity for its wide-spectrum use, in particular for treating refractory depression and suicidality via single, low-dose (0.5 mg/kg IV) infusions delivered over 40 minutes (Covvey, Crawford, & Lowe, 2012; Grady, Marsh, Tenhouse, & Klein, 2017; Sinyor et al., 2018). As clinical trials are successfully revealing for the power of ketamine to treat psychiatric disease, the shift to an intranasal formulation of ketamine highlights the possibilities of harnessing its mechanism of action to drive healthcare changes at scale (Lapidus et al., 2014; Singh, Gillespie, & Harvey, 2018). A neural systems level understanding of how the high-dose psychomimetic or dissociative anesthesia arises remains unclear. As a result, cellular and molecular explanations are attributed mechanistically to ketamine's novel mind-altering effects.

Inhaled General Anesthetic Agents

Both isoflurane and sevoflurane are inhalant anesthetics and not substantially different structurally than the earliest di-ethyl ethers (Figure 1-1, ether molecular structure: —O—). While sevoflurane has become increasingly the standard inhalant general anesthetic used (overtaking isoflurane), both drugs significantly potentiate GABA-A receptors and glycine receptors to enhance chloride-mediated inhibition. They both have generally similar inhibitory drive on both nicotinic and muscarinic receptors, as well as AMPA receptors. One notable difference is that isoflurane is a major potentiator of serotonin in the central nervous system. Sevoflurane, which lacks this property, is thus preferred as it can help reduce the risk of inducing serotonin syndrome in a patient undergoing a long procedure.

Nitrous oxide (N_2O), known colloquially as 'laughing gas', is another classical anesthetic used for medical and, in particular, dental procedures. Its euphoric, dissociative and analgesic effects arise at lower dose as a result of the network effects driven in part by nitrous oxide's potentiation of two-pore and inwardly-rectifying potassium channels, and inhibition of nicotinic acetylcholine, NMDA, serotonin, and kainite receptors. While all of these gas anesthetics have been around for some time, and resemble some of the chemical structures of the original ethers, the tight control parameters and fast mechanism of action keep these drugs relevant, especially in children where propofol is often avoided.

General Anesthetic Adjunct Agents

While the drugs referred to above can induce unconsciousness when used independently, there are other pharmacological agents that are traditionally supplemented to the GA cocktail to increase its efficacy. On their own, at least at clinically-used doses, GA adjunct agents cannot produce unconsciousness when used in isolation. They are more known to elicit sedation or analgesic effects when administered (or abused) independently. When added to intravenous or inhaled GA, they strongly reduce the doses required of the

other agents to induce and maintain unconsciousness (Gill, Shah, & Ogilvy, 2001; Smith et al., 1994).

Three such anesthesia adjunct drug classes used in common clinical practice are: opioids (e.g. fentanyl), benzodiazepines (e.g. midazolam), and α2 adrenergic receptor agonists (e.g. dexmedetomidine). Opioids primarily target the three principal μ-, k-, ∂-opioid receptors to deliver potent analgesic effects via a metabotropic pathway that enhances GABAergic inhibition. Also used regularly are benzodiazepines, which serve as a potent class of anxiolytics and hypnotics with variable half-life formulations. Benzodiazepines allosterically bind GABA-A receptors, an ionotropic chloride channel, in order to promote GABAergic inhibition (Haefely, 1989). The final group is the α2 adrenergic receptor agonists. Upon binding the α2 receptors, these drugs cause the inhibition of the release of pre-synaptic norepinephrine, the major arousal neurotransmitter in the brain. This class of drugs comes in the form of intravenous (dexmedetomidine HCl) and oral (clonidine), acting as pure sedation agents in isolation. Both induce a rousable, sleep-appearing state with sleep spindles measured on EEG and can invoke profound hypotension and bradycardia.

Beyond the cellular and molecular effects outlined here for these anesthetic agents, detailed metabolic and pharmacokinetic-pharmacodynamic models can accurately capture a drug's given physiological effects within the peripheral tissues and central compartments, including the brain (Ching, Purdon, Vijayan, Kopell, & Brown, 2012). As a result, the detailed molecular understanding has falsely given rise to the notion that we therefore understand the full extent of these drugs' production of unconsciousness. For example, the rate of an agent crossing the blood-brain-barrier is used as a surrogate in studies to understand how quickly a drug makes someone unconscious (Barr et al., 2001). Thus, despite the tremendous amount of work spanning the past century to characterize these drugs at the microscale, the findings do not intrinsically explain the higher order

mechanisms of these agents to disrupt complex neural systems and the network computations expressed in the awake, conscious state.

1.3 Network Theories of Unconsciousness

For centuries, philosophers have dissected and debated the nature of consciousness in an attempt to describe the unique experience of the mind. Until recently, it has remained difficult to escape largely theoretical discussions by applying testable hypotheses to the brain. General anesthesia provides a rigorous scientific approach to study questions surrounding the nature of conscious thought. The leading theories are listed below for proposed network schema that supporting consciousness and provide hypothesis for how they might breakdown in general anesthesia, as well as in sleep or pathological conditions such as coma.

The first group of theories focus on a key anatomical structure and its role in conscious processing to support its candidacy for a focal center of consciousness. Focal epilepsy (e.g. epileptiform electrographic activity giving rise to absence seizures) is notable for classically disrupting consciousness in stereotypic, recurrent, and fleeting patterns. While there often is a restricted locus of these seizures, they arise from epileptiform activity in many discrete cortical locations, most commonly within the medial temporal lobe or parietal cortex (Blumenfeld, 2014).

The most prominent singular anatomical location insinuated in wholly generating or coordinating consciousness is the claustrum (Chau, Salazar, Krueger, Cristofori, & Grafman, 2015; Yin, Terhune, Smythies, & Meck, 2016). The claustrum is a sheet-like structure intriguingly well-positioned between the basal ganglia and cortex and spanning the anterior-posterior neural axis. Beyond this anatomical convenience, the claustrum is

massively and reciprocally connected to much of cortex (Crick & Koch, 2005). It is from this unique structure that cortex-wide clinical experiments with electrical stimulation of unilateral claustrum in a patient caused temporary unconsciousness (Koubeissi, Bartolomei, Beltagy, & Picard, 2014; Kurada, Bayat, Joshi, & Koubeissi, 2019).

Another major anatomical focus in the control of consciousness is the thalamus, which is thought to have a switch-like role over conscious states. Consciousness may emerge from the integration of information in large-scale cortical networks coordinated via connections with the thalamus. Even better positioned as the relay center from the periphery, the thalamus is often referred to the gateway to the brain. However, there is much more to the thalamic nuclei other than the simple sensory relay nuclei. The pulvinar is a large, interconnected nuclei with strong recurrent connections between visual areas and those involved heavily in attention. Perhaps the most studied candidate for its role in consciousness is in the central thalamus, within the intralaminar nuclei (IL) (consisting of the central lateral nucleus (CL) and the centromedian/parafascicular complex). This region contains neurons with high firing rates that send excitatory activity alongside adrenergic fibers from the brainstem up to the superficial layers across cortex. Focal traumatic or ischemic injury to the intralaminar nuclei can cause coma. GABA when injected into IL induces unconsciousness (Alkire et al., 2008; Mashour & Alkire, 2013). One hypothesis is that during general anesthesia, anesthetic-sensitive cells in layer 5 of cortex actually project back down to brainstem arousal centers and functionally deafferent themselves. Electrical stimulation of this region in coma patients causes marked behavioral improvements (Schiff et al., 2007). The IL nuclei project predominantly to superficial layers of cortex and that way affect long-rang intercortical communication.

Some theories only emphasize the network effects without focusing on the exact anatomical substrates over which their process acts. Whether frontoparietal disconnection, hypersynchrony, or asynchrony, these processes can arise in any region to disrupt activities

needed for conscious processing. Like thalamic disruption, it is often thought that frontoparietal disconnection syndrome would arise from top down or bottom up network disturbances. These functional hypotheses necessarily overlap with the theories that place their dedicated importance on either the frontal or parietal cortex as sufficiently maintaining the key role for conscious processing. Hypersynchrony is also often thought of as a key driver in unconsciousness (Purdon et al., 2013). Here, entrained signals lose the number of bits that can be encoded and cannot reliably connect to other brain regions to share information. The degree of synchrony in general anesthesia measured on the EEG has demonstrated to predict instantaneous sensory encoding breakdown (Supp, Siegel, Hipp, & Engel, 2011). The same holds for asynchronous brain rhythms. In cortical fragmentation (Lewis et al., 2013, 2012), portions of the awake brain are unable to communicate because the neighboring or anatomically connected regions are in a quiescent off state. Recently, similar dynamics were discovered in sleeping humans, with delta waves varying in frequency, amplitude, and waveform shape across different regions of cortex (Bernardi et al., 2019). Interestingly, these slow wave features have been identified in mice, but only as a result of congenital callosal dysgenesis (Vyazovsky & Tobler, 2005). The anatomical-functional motifs across these forms of fragmented networks hint at general mechanisms that could disrupt the key aspects of neuronal communication that may be critically important for sustained processing and awareness of the external environment.

There is one thread woven through the often at-odds theories supporting the neural correlates of consciousness: rhythmic brain activity. Every single one of these hypotheses, either directly or indirectly, are tied to the central role of these neural oscillations. Even when the theories don't directly address it in their respective theories of conscious processing, a body of work indirectly or directly implies it. For example, in the focal anatomical-based theories placing key regions such as the claustrum or central thalamus

at the center of consciousness, extensive additional work finds these brain regions to be key drivers and hubs in coordinated, rhythmic corticocortical activity (Guillery & Sherman, 2002; Vidyasagar & Levichkina, 2019). As such, it is worth understanding the ways neural oscillations can facilitate processing in the awake brain before understanding the full extent of their causal or correlative role in unconscious brains and pathologic states.

1.4 Contents of Consciousness

The prominent motifs defining awake, conscious processing are essential to understand and properly frame a discussion of the systems-level changes that take place in general anesthesia. While there are many posited claims for how conscious processing arises and how it *could* be disrupted, one thing is clear: neural oscillations appear at the core of each of these theories and the manners in which they change across conscious states is the defining feature of this work.

Oscillatory dynamics in neural activity are central to these processes of awakeness, awareness, and perception. The collective transmembrane currents flowing from soma to synapse summate over cellular aggregates to generate fluctuating extracellular voltage potentials across the brain. These signals are readily detectable by intra- and extracranial electrophysiological recording methods, and have been related in their frequencies, magnitudes, and correlations to roles in cognition. The relationships between oscillations and behavior has one of its clearest relationships demonstrated in the rat, where neural spiking relationships to the hippocampal or entorhinal theta rhythms (6-10 Hz) encode the animal's physical location in space (Buzsáki & Moser, 2013; Hafting, Fyhn, Bonnevie, Moser, & Moser, 2008).

But the role for oscillations in behavior extends to functions more classically ascribed to conscious experience: working memory and attention. Phase-dependent coding of items remembered in working memory was discovered in monkeys (Siegel, Warden, & Miller, 2009). Extending from this finding, the strength of intercortical phase locking between prefrontal cortex and visual area V4 predicted the successful retrieval of items from working memory (Liebe, Hoerzer, Logothetis, & Rainer, 2012). Experiments on visual attention also reveal similar patterns, with long-distance spike-field coherence enhanced for actively attended items (Gregoriou, Gotts, Zhou, & Desimone, 2009). These type of long-range coherence changes during cognitive tasks illustrate that highly structured network synchronizations are important to communicating information across brain regions (Womelsdorf et al., 2007). This goes to say, the role of rhythms in guiding cognitive processes is omnipresent and minor adjustments to the frequencies and amplitudes of these oscillations can affect the temporal and rate coding of action potentials that certainly is fundamental to normal brain processing. Neurons occasionally contain relevant information in their burstiness or their inter-spike-intervals, both of which are susceptible to ongoing rhythmic activity (Insanally et al., 2019). The mechanisms of consciousness, as a result, are perhaps best investigated and contained within the framework where these ongoing oscillatory processes can be most strongly manipulated and disrupted: general anesthesia.

The ultimate goal of this work is to better understand the following questions: do different types of general anesthetic agents affect neural populations differently, do they converge on similar network mechanisms of unconsciousness, are specific anatomical structures involved more prominently in producing or eradicating the state of unconsciousness, and is there a principled approach we can use to take these findings to automatically control the generally anesthetized state?

Chapter 2

Propofol Anesthesia

The contents of this chapter are produced from Jacob A. Donoghue, Jorge G. Yanar, Simon J. Kornblith, Mikael Lundqvist, Jefferson E. Roy, Emery N. Brown, and Earl K. Miller, Thalamic stimulation defragments cortical networks and wakes up generally anesthetized monkeys (*in preparation*).

2.1 Abstract

General anesthesia reversibly interrupts conscious experience. GABAergic anesthetics at high doses produce profound silent (DOWN) states with active (UP) states occurring intermittently across the brain on electroencephalographic and intracortical recordings. It is unclear how local and global patterns of synchronous activity of emerge in general anesthesia, and how these relate to the breakdown in cortical functional connectivity and the processing of sensory information. In addition, the role of the thalamus in orchestrating activity in the anesthetized brain is unclear. To address this, we simultaneously recorded neuronal activity from cortical regions [ventral lateral prefrontal cortex (vlPFC), caudal (clPFC), posterior parietal cortex (PPC), auditory cortex (CPB)] and the central thalamus of monkeys receiving propofol general anesthesia. We found that synchronous

neural activity varies in local and global brain networks, is coupled to local cortical slow oscillations (<4 Hz), and that patterns of synchrony and fragmented asynchrony simultaneously emerge in the unconscious state. Slow oscillatory dynamics within the intralaminar nuclei (<4 Hz) coordinate these cortical activity patterns. Finally, we show that activating the intralaminar thalamus with electrical stimulation recovers awake-like cortical ignition and rapidly awakens monkeys from deep general anesthesia. Together, these results shed light on the network architecture and dynamical systems required to support cortical processing, cognition, and consciousness.

2.2 Introduction

In general anesthesia, oscillations dominate electrophysiological recordings. Following the administration of propofol in humans, a characteristic oscillatory frequency procession commences within the EEG, as low amplitude alpha rhythms (8-12 Hz) of the awake state give rise to a period of paradoxical excitation with faster, larger amplitude beta-rhythms (13-30 Hz). This period is followed by a slowing in beta frequency, but with an increase in amplitude, along with the rise of alpha and a delta (0-4 Hz) slow oscillation. As depth of anesthesia is increased, brain dynamics continue to slow and the delta oscillation dominates the EEG while the remaining alpha band signal moves from the occipital regions to the frontal regions. In the deepest stages of anesthesia, so-called burst-suppression emerges where longer periods of isoelectric activity are disrupted by paroxysmal high-amplitude alpha and beta frequency oscillations(Brown, Lydic, & Schiff, 2010). These changes have been associated in numerous studies at the macro-level with a breakdown in functional connectivity, measured as coherence changes and via directed-causal models, that could disrupt the normal cognitive architecture from properly integrating information (Boly et al., 2012; Purdon et al., 2013). An elegant study by Lewis

et al. used a single multielectrode array implanted in cortex of human epilepsy patients undergoing propofol anesthesia to advocate for the role of the slow oscillation (0.1-1Hz) in temporally restricting neural firing patterns (Lewis et al., 2012).

The spread of neural information across cortical networks is a feature of the conscious brain. The impairment of sensory experience in the unconscious brain, therefore, could result from processes that impair proper encoding, distribution, or decoding of sensory signals. Therefore, we recorded spiking and LFPs across connected brain areas to determine how sensory encoding could transform alongside the dynamic fluctuations in oscillatory and spiking activity in general anesthesia. Particular sensory inputs may be filtered before even reaching sensory cortex (e.g. thalamic interruption), improperly represented in cortex (e.g. neural code changes), or fail to spread to connected cortices despite proper encoding (e.g. oscillatory fragmentation of networks). Thus, we sought to explore how brain-state dynamics may explain single neuron activity in unconsciousness, and perhaps shed light on features of the neural code essential to consciousness.

2.3 Methods

2.3.1 Subjects and Anesthesia Task Paradigm

Two rhesus macaques (*Macaca mulatta*) aged 14 years (MJ, male, ~13.0 kg) and 8 years (Monkey LM, female, ~6.6 kg) participated in these experiments. Both animals were pair-housed on 12-hr day/night cycles and maintained in a temperature-controlled environment (80°F). Each monkey was surgically implanted with a subcutaneous vascular access port (Model CP-6, Norfolk Access Technologies, Skokie, IL) at the cervicothoracic junction of

the neck with the catheter tip reaching the termination of the superior vena cava via the external jugular vein.

Two additional monkeys were implanted with multicontact laminar probes placed in visual area 4 (V4), Superior Temporal Gyrus (caudal parabelt), parietal areas 7a/7b, ventrolateral prefrontal cortex (46v, vlPFC), and the frontal eye fields (FEF) and recorded under the identical GA infusion paradigm as monkey MJ. Firing rate and timeseries data were collected from cortical sites on these subjects to add additional brain areas to the relevant analyses.

On a given experimental session, monkeys were head-fixed via a titanium headpost and placed in noise isolation chambers with masking white noise (50 dB). On half of sessions, a passive behavior task was initiated at the onset of the recording session (during awake baseline). This task included randomly delivered a pure tone 2000Hz for 500 msec, following a period (15 - 90 minutes) of awake baseline electrophysiological recordings or preliminary behavioral tasks, propofol was intravenously infused via a computer-controlled syringe pump (PHD ULTRA 4400, Harvard Apparatus, Holliston, MA). The infusion protocol was stepped such that unconsciousness was induced via a higher rate infusion (285 µg/kg/min for monkey MJ; 580 µg/kg/min for monkey LM) for 15 minutes before dropping to a GA maintenance dose (142.5 µg/kg/min for monkey MJ; 320 µg/kg/min for monkey LM) for an additional 45-90 minutes. Heart rate and oxygen saturation were monitored continuously and recorded throughout all phases of experiments using clinical-grade pulse oximetry (Model 7500, Nonin Medical, Inc., Plymouth, MN). SpO_2 values were maintained at values above 93% for each of the recording sessions.

Infrared monitoring tracked facial movements and pupil size (Eyelink 1000 Plus, SR-Research, Ontario, CA) throughout the course of the experiments. Loss of

consciousness (LOC) was deemed by the timestamp of the moment of eyes-closing that persisted for the remainder of the infusion. Recovery of consciousness (ROC) was classified as the timestamp of the first to occur between eyes reopening or regaining of motor activity following drug infusion cessation. Animals regained consciousness after the maintenance infusion was terminated and were monitored for an additional task-free period or during the performance of a task before being returned to their cage. To ensure propofol clearance from tissues and physiological recovery, experiments were never repeated on subsequent days. All procedures followed the guidelines of the MIT Animal Care and Use Committee and the US National Institutes of Health.

For the determination of the timestamp for the loss of consciousness (LOC) and recovery of consciousness (ROC), similar criteria were utilized for assessing these with propofol-infusion onset and propofol infusion offset as in DBS-onset and DBS-offset. On sessions that included the passive puff-tone behavioral task, LOC was determined as the last time of the first missed puff not followed by additional puff responses. Otherwise, the reduction in suprascapular EMG recordings were used as a surrogate. ROC was identified as the first blink-induced EMG deflection following a series of missed puff response. For DBS trials, ROC was determined via the same criteria but with the first puff response coming with respect to the DBS stimulation on. LOC following each DBS trial was also calculated similarly to the awake state, but with reference to the end of electrical stimulation (not cessation of propofol).

2.3.2 Thalamic Targeting and Implantation

DBS is a well-established tool for recording and modulating pathological and normal circuits in both humans and monkeys (de Hemptinne et al., 2015; Malekmohammadi,

AuYong, Ricks-Oddie, Bordelon, & Pouratian, 2018; Schiff et al., 2007) We inserted two multilaminar probes (0.5 mm contacts with 0.5 mm intercontact-spacing, NuMed Inc, Hopkington, NY) bilaterally into the intralaminar thalamic nuclei, targeting the long axis of the central lateral nucleus and extending ventrally to reach the centromedian and parafasicular nuclei. To obtain this precise targeting, we developed a chamber-based stereotactic localization methodology combined with serial intraoperative MRI during electrode placement. Custom-reamed carbon PEEK recording chambers were affixed to the skull with acrylic and ceramic screws stereotaxically determined to target the central thalamus. Recording chamber grids with 1mm grid holes were inserted into the chambers, filled with sterile saline, and the monkey's head was then imaged by 3T MRI. Subsequent confirmation of the appropriate grid holes targeting the thalamic structures of interest, monkeys were generally anesthetized and brought to the operating facility, grid holes of interest were marked on the acrylic inside the chamber, and a small-bore craniotomy (<2mm) was performed at the grid hole markings. A fine-tipped thermal cautery device was used to rupture the dura in the craniotomy sites and cauterize neighboring vessels. The grid was replaced in the chamber and the monkey was transferred anesthetized to the imaging facility and administered Ablavar™ (gadofosveset trisodium) to highlight any vasculature obstructing the trajectory to thalamus (e.g. thalamostriate vein).

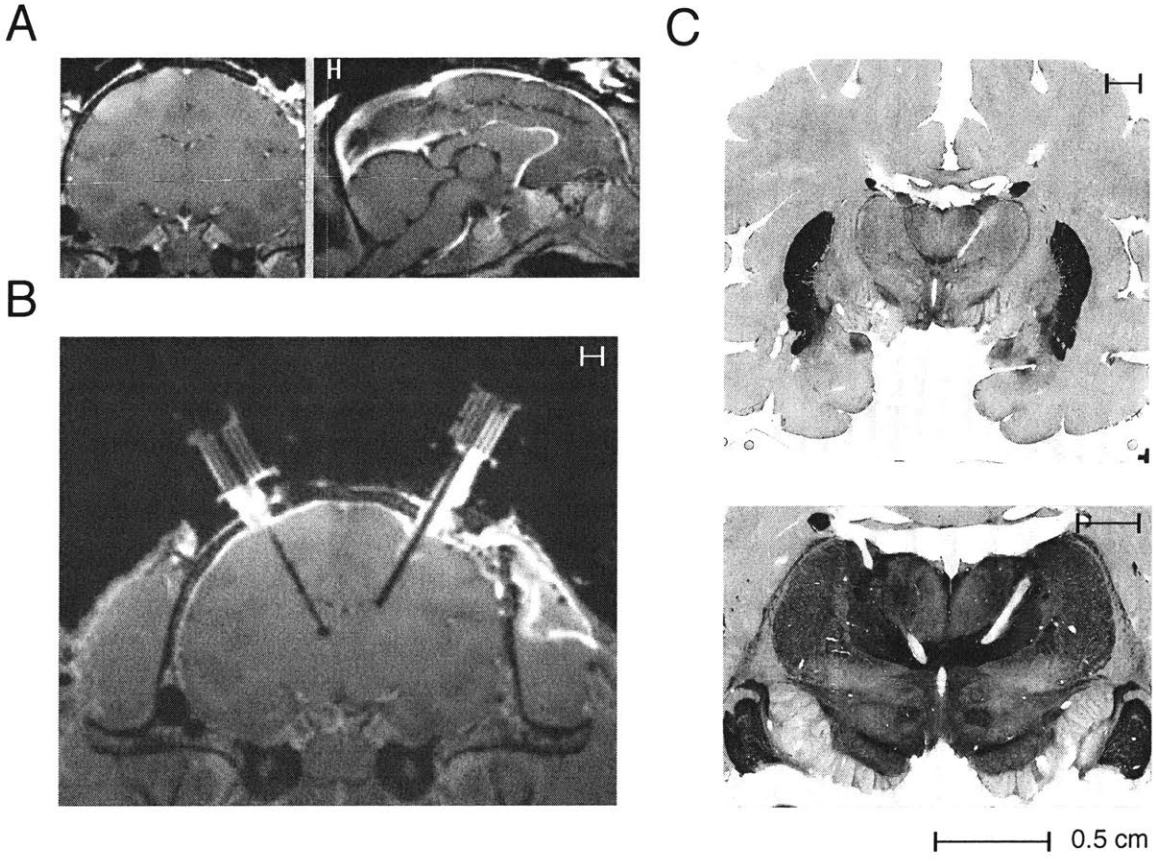

Figure 2–1: DBS implantation methodology. **A**, Gadolinium-based agent (Ablavar™) injected intravenously to highlight vasculature, in particular the venous return pathways abutting the lateral ventricles. **B,** Cannulae-stylettes targeting the thalamus. Carbon PEEK grids affixed to the skull are filled with saline to illuminate the grid holes and trajectories. Trajectories from planning from previous Ablavar scan known and adjusted given the saline-based scan. Cannulae-stylettes lowered toward the thalamus, and reimaged in place. Cannulae-stylettes withdrawn as needed so that when the cannulae reaches the edge of the thalamus, the stylettes is withdrawn, and the electrodes are inserted, reimaged, and lowered past cannulae tip into the thalamus. **C**, AChE stains highlight precision of our deep brain targeting method.

Just outside the MRI bore, stylette-cannulae were inserted into the relevant grid holes and lowered several mm into cortex and one set of 0.5 mm resolution images was

obtained. Upon confirmation of correct trajectory on MRI, the stylette-cannulae were lowered to their final position, with the tip approximating the thalamus. The stylettes were then removed, and electrodes of marked length lowered to the depth of the cannulae. Following another MRI-based measurement (scan 2) with the electrodes still in the cannulae, the electrodes were lowered to their final positions within the thalamus and reimaged (scan 3). Upon final assessment of correct localization, the probes were fixed in place and the chamber sealed with acrylic. Histological staining with acetylcholinesterase was used to confirm exact electrode contact locations within the central thalamus of both monkeys.

2.3.3 Electrophysiology Recordings

Both monkeys were chronically implanted with four 8x8 iridium-oxide contact microelectrode arrays (MultiPort: 1.0 mm shank length, Blackrock Microsystems, Salt Lake City, UT), for a total of 256 electrodes distributed in the prefrontal (46v and 8a), parietal (7a/b), and temporal (caudal parabelt) cortices. Specific anatomical targeting utilized structural MRIs of each animal and a macaque reference atlas, as well as visualization of key landmarks on surgical implantation (McLaren et al., 2009). LFPs were recorded at 30 kHz and filtered online via a lowpass 250Hz software filter and downsampled to 1 kHz. Spiking activity was recorded by sampling the raw analog signal at 30 kHz, bandpass filtered from 250Hz-5kHz

DBS generally produced artifacts that were highly correlated across channels. We removed these artifacts using ZCA-whitening (Eldar & Oppenheim, 2003). ZCA whitening is the linear whitening transformation that minimizes the mean squared error between the original and whitened signals. First, we applied a fourth-order Butterworth band-pass

filter to the raw, 30 kHz recorded signals between X and Y Hz. Next, we estimated the cross-channel covariance matrix Q from the filtered signals recorded during DBS stimulation. Finally, we multiplied the matrix of filtered signals by $Q^{-1/2}$ to yield the whitened signals. For computational efficiency, we computed the cross-channel covariance matrix using a subset of 100,000 randomly selected time points. From these whitened signals, we manually set voltage thresholds to capture high-frequency spikes and sorted these units using principal component analysis in commercially-available software (Offline Sorter v4, Plexon Inc., Dallas, TX).

2.3.4 Thalamic Stimulation

For electrical stimulation of DBS electrodes, we adapted electrical stimulation parameters previously shown to cause behavioral improvements in coma patients and awake, behaving monkeys (Baker et al., 2016; Schiff et al., 2007). We unilaterally delivered 180 Hz bipolar, biphasic, square wave pulses (1-3.2 milliAmps) between 6-8 contacts on monkey MJ and 6 contacts on monkey LM. Five minutes into the maintenance anesthesia dose (20 minutes from infusion start), 30-second "trials" of electrical stimulation were delivered as the propofol infusion continued. DBS trials were separated by 2 minutes intervals, except the 4^{th} and 5^{th} stimulation runs, which were separated by a 5-minute inter-trial interval. These DBS washout periods sufficiently allowed for reestablishment of the behaviorally-judged anesthetized state (e.g. loss of puff responses).

2.3.5 Firing Rate and Synchrony Analysis

To compute the running average firing rate, we binned the single unit spike trains with 200 msec bins for the length of entire recording session. For the global synchrony peak analysis, individual sorted units were binned into non-overlapping 10000 msec windows. The average correlation rho for the population of pairwise correlations was thus called the global peak to reflect the coordination in firing rates of neurons across the brain.

Power spectral densities were calculated in the fieldtrip toolbox using a multitaper method (K = 5, TW =3) for windows across the entire session. Pre-onset infusion of the drug was referred to as the awake baseline. Anesthesia epochs used for synchrony analyses were not evaluated near the time of LOC or the transition to the lower maintenance doses. Pairwise coherence was also computed for all electrodes on all of the array locations for these epochs. All of these analyses were replicated using the interval 'Pre-DBS Anesthesia': 15 seconds before DBS onset, DBS: 30 second stim trial, and 'post-DBS': 30 seconds post-DBS. For all of these epochs, we additionally computed Granger causality and pairwise phase consistency analyses, we first divided the continuous LFP data into 4-second windows with 2-second overlap and computed spectra for each time segment and cross-spectra pairwise for all channels. We subsequently used the ft_connectivityanalysis function from the *FieldTrip* toolbox to compute the respective connectivity functions on this output (Oostenveld, Fries, Maris, & Schoffelen, 2011). 95% confidence intervals in these figures capture the across-session variance and are computed as 1.96 * *standard error of the mean.*

2.4 Results

2.4.1 Slow Oscillations Emerge Across Cortical Areas

Propofol caused a shift to strong, slow, cortical rhythms that reduced spiking by entraining it. The decrease in spiking began with propofol infusion and was especially pronounced around LOC (Figure 4-1D, no different between cortical areas). After propofol, spiking steadily increased up to ROC but without quite reaching pre-LOC spike rates even 30 minutes post-ROC. As seen in human EEG, there was a shift from awake-state high-frequency, low-amplitude LFP power to low-frequency (1—4 Hz, delta band) high-amplitude power (with intermittent isoelectric activity characteristic of burst suppression) that became pronounced after LOC. It was followed by a return to the high frequency awake-like state after ROC (Figure 2-2A, 2-2B). LOC has been posited to result from hypersynchrony of cortical activity to the delta oscillations.

2.4.2 Spiking and Oscillatory Patterns in Propofol General Anesthesia

In general anesthesia, firing rates uniformly decreased across all brain areas recorded. Within single sessions, the mean firing rate of neurons from both sensory and higher order cortices remained at lower firing rates throughout periods of unconsciousness (Figure 2-2D). Baseline firing rates during sustained unconsciousness were not significantly different between prefrontal and sensory cortical areas ($t(9) = 0.602$, $SEM = 0.5365$, $p = 0.56$). After cessation of propofol infusion, firing rates significantly increased leading up to recovery of consciousness. Interestingly, pre-LOC firing rates were often not obtained within 30 minutes of ROC. While the overall rates of individual neurons were lower during GA, we next sought to explore the temporal relationships in spiking activity across all

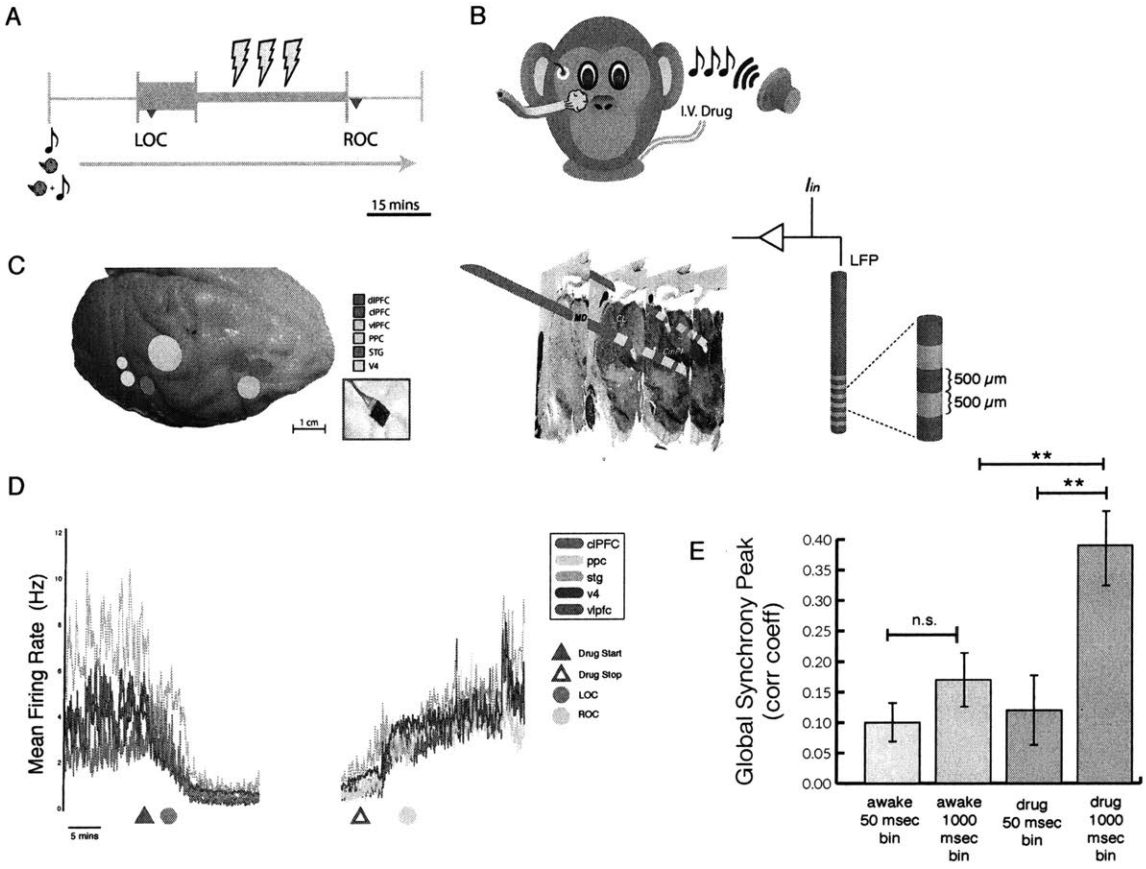

Figure 2–2: Propofol anesthesia and cortical synchrony. **A**, Session paradigm with 15-minute induction infusion (fast rate, thick orange bar) in the middle of recording session (blue), covering awake (pre-LOC) and generally anesthetized epochs, before switching to a halved rate propofol infusion for maintenance phase of experiment (narrow orange bar). 30-second DBS trials (yellow bolts) occur during lower-dosed maintenance phase of propofol infusion. LOC: Loss of consciousness, ROC: Recovery of consciousness. **B**, Task set up. One-half of sessions used the passive sensory paradigm utilizing puffs and tones to elicit sensory neural responses and assess level of consciousness (i.e. response to air-puff). **C**, Cortical recording locations (left) and central thalamic recording locations (right). dlPFC: dorsolateral prefrontal cortex; clPFC: caudal lateral PFC; vlPFC: ventrolateral PFC; PPC: posterior parietal cortex; STG: superior temporal gyrus; V4: visual area 4; MD: mediodorsal nucleus of the thalamus, CL: Central lateral nucleus (intralaminar); CmPf: centromedian/parafasicular complex. **D,** Spike rate for all recorded areas on a given propofol recording session. **E**, Global synchrony peak at different bins (50 vs. 1000 msec) compared at awake versus propofol conditions.

recorded single units. GA has been characterized by both hypersynchronous and asynchronous neural processes. We hypothesized that this discrepancy may arise for the evaluation of coordinated neural activity at different time scales. Pairwise correlations were computed for binned spike counts for well-isolated single units identified in all cortical regions (See Methods). We calculated the global synchrony peak by identifying the mean spike count correlation coefficient across all pairs of isolated single units, evaluated at multiple bin sizes (50 msec and 1000 msec) in different states of consciousness. In the awake state, global synchrony of spiking neurons was not dependent on the bin-size over which the firing rates were evaluated (Figure 2-1E, green bars). In general anesthesia, however, we found that at smaller bin sizes neurons were less coordinated in their spiking activity as synchrony values significantly decreased below the awake baseline. Interestingly, when spike count synchrony was evaluated over larger bin sizes the resulting global synchrony peak was substantially increased for the anesthesia epoch and elevated significantly above the awake baseline value (Figure 2- 1E, blue bars).

On pairwise coherence analyses, several patterns stood out. Neighboring regions of cortex were functionally disconnected by incoherent slow activity. Remarkably however, each of the two prefrontal regions was strongly coherent with the posterior parietal electrode array (Figure 2-3D). Beta coherent activity tended to follow these patterns as well, with the only exception being that it increased between PFC and PPC. The results of the Granger causality analysis are also presented in Figure 2-3E. Slow oscillatory activity significantly flowed in both directions between PFC an PPC. However, the slow oscillation tended not to flow bidirectionally across PFC. Instead, the slow oscillation from clPFC → vlPFC decreased.

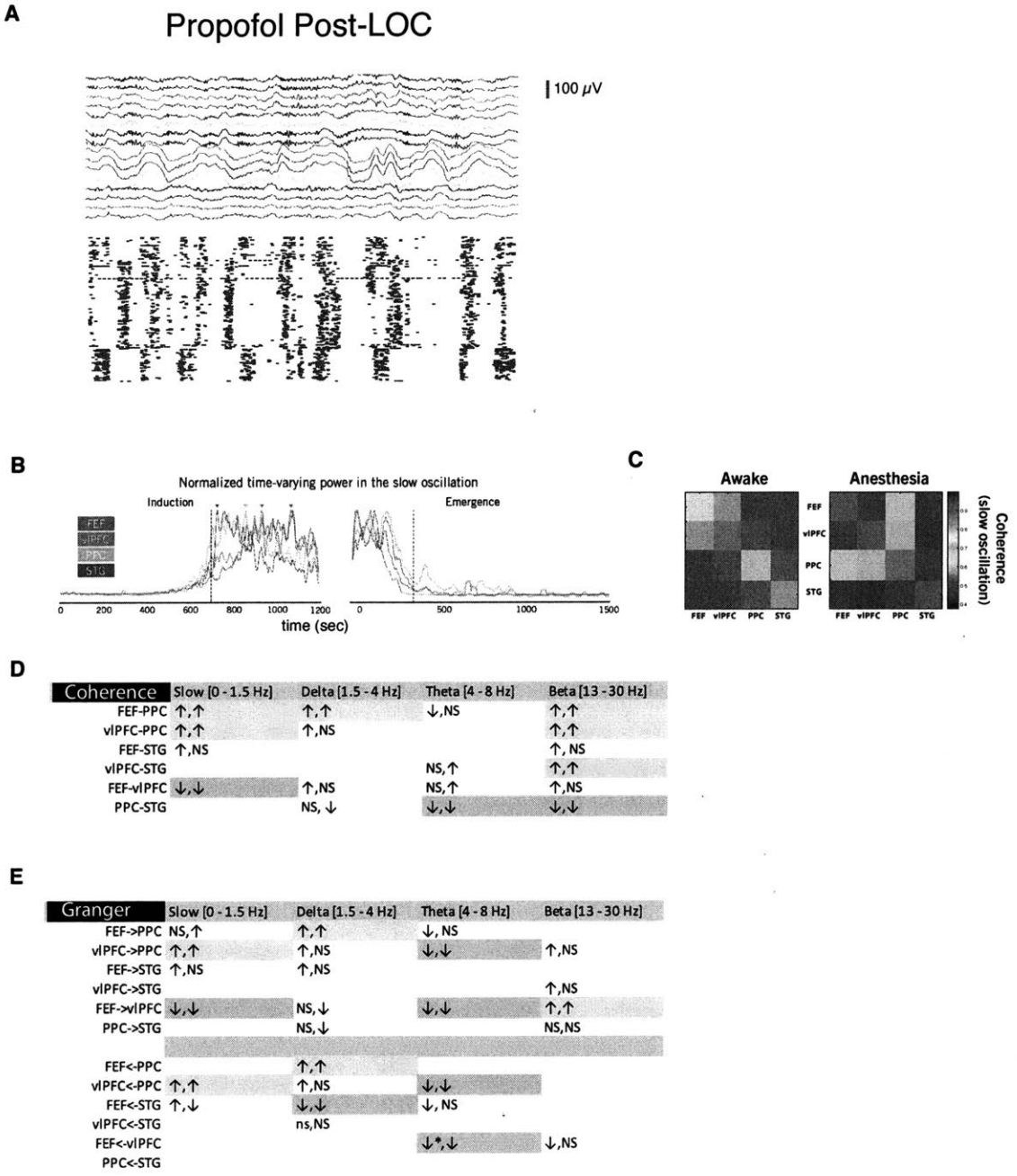

Figure 2–3: Spiking and synchrony changes with propofol. **A,** LFPs under propofol anesthesia, and the same single neurons below in anesthesia. **B,** Power changes across propofol session. **C**, Delta band coherence changes. **D, E** All significant coherence and Granger causality changes that occurred in both monkeys, green (increased) or red (decreased).

2.4.3 Electrical Stimulation Awakens Cortex and Anesthetized Monkeys

Mounting evidence suggests that the thalamus regulates cortical processing and rhythms. We simultaneously recorded thalamic LFPs from multilaminar probes (NuMed Inc, Hopkington, NY) in the intralaminar nuclei (ILN) and mediodorsal (MD) thalamus of two monkeys. The ILN has been associated with wakefulness and the MD is interconnected with the PFC. After LOC, the thalamus seemed to be "driving" cortex. Cortical delta oscillations phase-lagged behind those in the thalamus, suggesting thalamic influence over cortex. When awake, there was significant alpha/beta band influence of PFC LFPs over PPC LFPs, consistent with a cortical top-down influence from frontal to parietal cortex. However, after LOC, the thalamus lowered the frequency of this interaction and reversed it. MD thalamus exerted delta-band influence over the PPC, which then, in turn exerted delta-band influence over PFC.

This supports the hypothesis that thalamus regulates conscious cortical states, in this case causing LOC when it heterogeneously entrains cortex at slow rhythms. To directly test for a causal role of the thalamus, we aimed to "wake" the cortex via high-frequency electrical stimulation that activated the thalamus. After LOC, while propofol was still being infused, we applied 180 Hz, bipolar electrical stimulation across electrodes in the central thalamus for thirty second trials, administered every two to five minutes (Figure 2-4A and 2-1C, see Methods). Different combinations stimulation sites were tested; the only effective were those centered in the ILN, the nuclei most associated with consciousness.

Deep brain stimulation (DBS) largely reversed the effects of propofol (see methods). The animals' eyes opened (Figure 2-4B), they began to respond to sensory stimulation (Figure 2-4C), pupil diameter increased (Figure 2-4B), heart rate increased (Figure 2-4E), and they regained muscle tone and limb movement (e.g., Fig 2-4A). DBS also produced

an awake-like cortical state, reducing low frequency LFP power across cortex (Figure 2-4F), increased spike rates (Figure 2-4D), and decreased the global synchrony (Figure 2-4E). Figure 2-4A shows this shift in LFP power across frequencies and time. LFP power in lower vs higher frequencies decreased vs. increased during DBS. This awake-like state cortically and behaviorally persisted for several seconds to several minutes after DBS (Figure 2-4A).

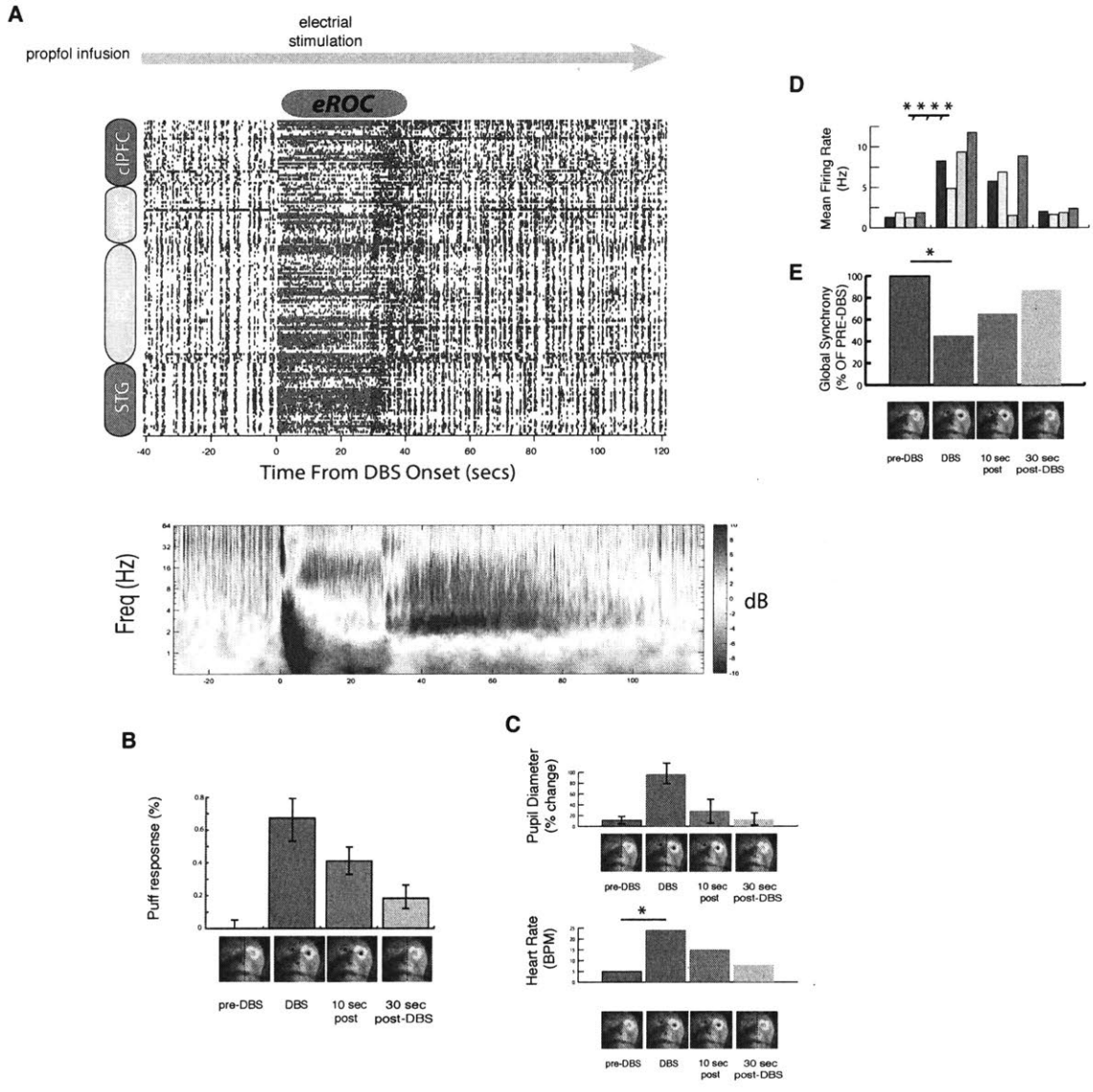

Figure 2–4: DBS wakes up anesthetized monkeys and reverses patterns of general anesthesia. **A**, visualization of a single trial with single units arranged in each row, yellow-shaded portion is DBS segment. Lower panel reflects average PFC spectrogram for DBS stimulation. **B**, Puff responses, **C**, Pupil diameter (upper) and (lower) heart rate (bpm). **D**, mean firing rate of single units within a cortical region. **E**, Global spiking synchrony, as a percentage of the PRE-DBS segment at 1000 msec bins.

2.5 Discussion

A convergence of theoretical and electrophysiological evidence has been presented to suggest that consciousness may emerge from the integration of information in finely tuned cortical networks coordinated exquisitely by connections with the thalamus. Our work here suggests that the thalamus can, in fact, take on a switch-like role to drive overwhelming inhibition and ignite the system back into the conscious state. We show that we can recruit large thalamocortical networks with thalamic DBS under general anesthesia, reinstate their natural dynamics, and restore cognitive behavior. There is substantial evidence suggesting the central thalamus has a special role in modulating conscious states. The intralaminar nuclei receive neuromodulatory projections from the arousal systems in the reticular formation of the brainstem. Neurons within the intralaminar nuclei project to the superficial layers of cortex and have high baseline firing rates that could help coordinate cortical activity (Alkire et al., 2008). Injection of GABA directly into these nuclei reduced behavioral arousal (Miller et al., 1990), while the addition of nicotine was able to revere sevoflurane anesthesia in the rat (Alkire et al., 2007). The strongest evidence to support our conclusions comes from human DBS studies in the minimally conscious state, a pathological state (here, induced by traumatic brain injury) where electrographic features resemble those of deep anesthesia (Brown et al., 2010). Researchers at Cornell University demonstrated that deep brain stimulation (DBS)

applied bilaterally to the central thalamus can recover cognitive function, as well as limb control and feeding behaviors (Schiff et al, 2007).

We provide substantial physiological evidence for the driving of the adrenergic arousal system with DBS (e.g. pupillary dilation, heart rate increase, etc.). It is entirely possible that this adrenergic drive is sufficient to restore the awake-like cortical state with restored thalamocortical coordination and enhanced information processing. It is known that adrenergic drive is sufficient to switch thalamic relay neurons from bursting to tonic mode, even in the presence of exogenous GABA (e.g. a situation like propofol general anesthesia) (Masson, Masson, Debay, & Bal, 2002). Importantly, this flip of thalamic projection neurons to relay mode increases thalamocortical spike transfer, which may support the fundamental awake state and allow normal cortical coding. This restored cortical processing could directly arise from DBS and explain a mechanism for the rapid reversal of behavioral and neurophysiological effects of general anesthesia.

We show that propofol induces the same structured changes in cortical dynamics in NHPs as humans. Beta power decreases in all cortical areas, however frontal areas are noticeable for having the strongest increases in beta-excitation as the anesthetic is first infusing (and leading up to the point of loss of consciousness (LOC). The transition from the awake to anesthetized state is characterized by a global increase in slow (<1 Hz) and delta oscillations (1-4 Hz) across all frontal, parietal, and temporal cortices, well as in the intralaminar nuclei of the thalamus. Beta power does increase in subsets of cortical electrodes during the deepest stages of anesthesia, occurring in long trains during the otherwise isoelectric period. It is of note that this beta power is also seen strongly in the thalamus, and may be a driver of the cortical beta rhythms under anesthesia. In addition, we see evidence of cortical fragmentation during deep anesthesia- however the patterns are novel. We see a breakdown in connectivity as measured by slow-oscillation coherence, across the prefrontal cortical network but with a concomitant strengthening of

frontoparietal connectivity in the same band. This is remarkable given the near proximity of the two prefrontal regions, and their monosynaptic connectivity, in contrast to the long-range connections to parietal cortex. This indicates unconsciousness may simultaneously arise from both cortical fragmentation and hyperconnectivity, pushing against the dogmatic theories that require all one or the other.

Chapter 3

Thalamocortical Dynamics in Ketamine Anesthesia

The contents of this chapter are produced from Marek Kowalski*, Jacob A. Donoghue*, Jorge G. Yanar, Meredith Mahnke, Jefferson E. Roy, Emery N. Brown, Nancy J. Kopell† and Earl K. Miller†, Thalamocortical dynamics under ketamine anesthesia (*in preparation*). *indicates co-first author, †indicates co-senior author.

3.1 Abstract

In sleep, general anesthesia or coma, unconsciousness is typically characterized by long periods of cortical quiescence that are interspersed with brief windows of excitability, severely restricting and depressing spiking. Paradoxically, however, the N-methyl-D-aspartate receptor antagonist ketamine produces unconsciousness while increasing high-frequency, gamma-band power (30-80 Hz). To determine how unconsciousness is possible with a seemingly active cortex, we recorded from four distinct areas of the primate neocortex (two prefrontal areas, parietal, and temporal) during ketamine anesthesia in rhesus macaques. Ketamine not only increased gamma power globally, it also induced

high levels of spiking and gamma that was locally hyper-coherent. In addition, gamma tended to flow upstream through cortical networks under ketamine anesthesia, from early sensory areas toward prefrontal cortex. In contrast, the awake state beta rhythms (12-30 Hz) that functionally connected parietal regions to other cortical regions, were entirely wiped out. Prefrontal cortical spiking activity uniquely entrained activity in the intralaminar thalamus, hijacking a major center for wakefulness and cortical integration. This suggests that unconsciousness can occur through a hyperexcited state, whereby local cortical interactions overwhelm long-range cortical interactions and thalamocortical flexibility is restricted.

3.2 Introduction

The unconscious brain is often one of a markedly decreased firing activity, as exemplified by sparsity of action potentials with general anesthesia (Kaneko, Koyanagi, Oi, & Kobayashi, 2016) and sleep (Watson, Levenstein, Greene, Gelinas, & Buzsáki, 2016), periods of electrical inactivity in coma (Young, 2000) and brain death (Szurhaj, Lamblin, Kaminska, & Sediri, 2015). However, recent findings from propofol anesthesia indicate that unconsciousness is possible even when spiking approaches wakefulness. It may be because spiking is confined to brief UP-states interspersed with quiescent DOWN-states (Lewis et al., 2012). Short bouts of spiking emerging at different times in different cortical areas could "fragment" the cortex, blocking cortical communication and the integration needed to support consciousness (Lewis et al., 2012) and NREM sleep (Nir et al., 2011).

By contrast, dissociative anesthesia, exemplified by ketamine, is characterized by catalepsy, increased muscle tone, open eye lids, and nystagmus (Domino, Chodoff, &

Corssen, 1965), as well as a prominent emergence delirium that may leave memories of hallucinations (Sklar, Zukin, & Reilly, 1981). It also increases cortical gamma, a frequency band associated with wakefulness greater than 30 Hz, a paradoxical phenomenon that has been reported ever since ketamine's initial discovery (Miyasaka & Domino, 1968). This has fueled speculation that ketamine anesthesia resembles REM dreaming, despite the fact that only a fraction of patients reports dreaming under high-dose ketamine (Sklar et al., 1981) and even those reports cannot be dissociated from a dream-like state during emergence delirium.

However, new details emerged from a recent analysis of frontal electroencephalogram (EEG) in humans anesthetized with ketamine (Akeju et al., 2016). Associated with periods of high levels of cortical activity were gamma oscillations (30-80 Hz with peak frequency between 30-50 Hz) that periodically fragmented into "bursts" by shorter duration OFF-states scattered across the scalp recordings. This suggests that ketamine may prevent normal local computations and also act by disrupting long-range cortical communication. If so, it would support theories that consciousness depends on coordinating cortical activity and integrating its information. We tested this in monkeys.

3.3 Methods

3.3.1 Electrophysiological Recordings

Two monkeys (*Macaca mulatta,* one male and one female) were each chronically implanted with four 8x8 iridium-oxide contact microelectrode arrays (MultiPort: 1.0 mm shank length, Blackrock Microsystems, Salt Lake City, UT), for a total of 256 electrodes distributed in the prefrontal (46v and 8a), parietal (7a/b), and temporal (caudal parabelt)

cortices. Specific anatomical targeting utilized structural MRIs of each animal and a standardized macaque reference atlas, as well as visualization of key landmarks on surgical implantation. For central thalamic recordings, six or eight contact leads were lowered into the central thalamus targeting the intralaminar nuclei via custom stereotactic equipment and intraoperative MRI guidance for confirmation of positioning.

3.3.2 Anesthesia Protocol

A single bolus injection (20 mg/kg) of ketamine hydrochloride was delivered intramuscularly to the proximal quadriceps of head-fixed monkeys. Animals were pre-dosed with an intramuscular injection of the anti-cholinergic drug glycopyrrolate (0.01 mg/kg) 15 minutes prior to ketamine administration in order to reduce secretions for airway stability. Unlike atropine, glycopyrrolate acts strictly peripherally, as it does not cross the blood-brain-barrier. Heart rate and oxygen saturation were monitored continuously and recorded throughout all phases of experiments using standard clinical pulse oximetry clasped to the dorsal aspect of the ear (Model 7500, Nonin Medical Inc, Plymouth, MN).

3.3.3 Data Preprocessing

Single units were sorted manually offline using principal component analysis with commercially available software (Offline Sorter v4, Plexon Inc., Dallas, TX). All other pre-processing and analyses were performed with Matlab (The Mathworks, Inc, Natick, MA). For analyses, we extracted task-free periods of awake and ketamine recordings from two animals: ~600 seconds of awake baseline and ~1200 seconds post-ketamine from n=5

recording sessions in Animal 1, and ~100 seconds of awake baseline and ~1200 seconds of post-ketamine from n=4 recording sessions in Animal 2. We. Define the post-ketamine epoch as the period of unconsciousness. Prior to all LFP analyses, we subtracted from all channels the mean LFP for their respective array in order to account for possible detection of a common field potential by the closely spaced channels.

3.3.4 Time-Frequency Analyses

Power spectral density was calculated with multitaper method in sliding, non-overlapping windows of 10 seconds (K=5 tapers for each window, TW=3) and subsequently log-transformed to convert to decibels. A representative resulting spectrogram is depicted in Figure 3-1C. To obtain power spectral densities for awake and ketamine anesthesia periods, we averaged over all time windows from respective condition, with the exclusion of a segment of 5 minutes immediately post-ketamine injection and prior to emergence of gamma power. For Figure 3-1B, we calculated the difference between awake and ketamine PSD by subtracting log-transformed power in the awake state from log-transformed power under ketamine. Spectrograms were generated to capture both temporal and frequency structure of gamma bursts using multitaper power spectral analysis in 0.5-second windows sliding by 0.1-second increments. We restricted this analysis to frequencies between 30-80 Hz as guided by estimates of ketamine gamma range from Figures 3-1B and 3-1C.

To extract specifically the slow oscillation that modulates gamma power (waxing and waning of gamma bursts), we first used Matlab 'filtfilt' function to band-pass the raw signals between 30-80 Hz with a 100th-order filter (built using Matlab 'fir1' function). We then Hilbert-transformed this signal (Matlab function 'Hilbert') and took its absolute

value to represent the slow modulation of instantaneous power of gamma. We performed coherence analysis described below on the resulting time series to create Figure 3-1D.

We computed classical coherence between any all pairs of electrodes in this study in non-overlapping 10-second sliding windows, excluding the first 5 minutes after IM administration of ketamine to allow for emergence of gamma oscillations. We averaged over all windows from respective condition to obtain final estimates.

For Granger causality and pairwise phase consistency analyses, we first divided the continuous LFP data into 4-second windows with 2-second overlap and computed spectra for each time segment and cross-spectra pairwise for all channels. We subsequently used the ft_connectivityanalysis function from the *FieldTrip* toolbox to compute the respective connectivity functions on this output (Oostenveld, Fries, Maris, & Schoffelen, 2011). 95% confidence intervals in these figures capture the across-session variance and are computed as 1.96 * *standard error of the mean.*

3.3.5 Confidence Intervals

We computed 95% confidence intervals around the mean difference between baseline awake and ketamine power spectral densities and coherence by resampling estimates from all non-overlapping windows pooled from all recording sessions for each animal. We took a difference between these two condition estimates, repeated these 10,000 times, and computed 95% confidence intervals from the resulting distribution. Percent change in Figures 3-1E, 3-1F, and 3-2D is a single descriptive number calculated by subtracting mean awake coherence from mean ketamine coherence and included only where the confidence interval around the difference between ketamine and awake condition did not include zero.

3.3.6 Spiking Analyses

To transform sums of spike trains into continuous time series, we first added sorted single unit spike trains independently for each cortical area. Spike trains were time series binned in 1 msec that included zeros and ones, with a one representing a millisecond bin where a spike occurred. We subsequently convolved the resulting sum with a Gaussian kernel of either 1000 or 10 msec duration using Matlab function 'conv'.

We used the k-means algorithm (Matlab 'kmeans' function) with the assumption of two clusters to isolate periods of high and low firing activity (UP- and DOWN-states) from periods of ketamine anesthesia, beginning 5 minutes post-ketamine injection. Awake baseline firing rates were not included for cluster separation. Of the two isolated clusters from anesthesia period, we marked the one with higher mean firing rate as an UP-state and the other one as DOWN-state. We computed mean firing rates during respective states by averaging the convolved spike rate function from Figure 3-2C during UP-states only. We also summed the number of timestamps spent in each UP- or DOWN-state and compared these sums to determine which of the two states accounted for more of the anesthesia time.

Cross-correlation of cortical firing and thalamic LFP. Cross-correlation analysis for temporal precedence was performed for convolved mean firing rates (Figure 3-4C) and band-passed slow (0.1-0.8 Hz) and fast (30-80 Hz) activity as previously described (Adhikari, Sigurdsson, Topiwala, & Gordon, 2010). Briefly, sum of spike trains for each cortical area was convolved with Gaussian kernel of 1000 msec duration using Matlab 'conv' function and thalamic LFPs were band-passed in respective frequency ranges using Matlab function 'filtfilt' and 100th-order bandpass filter build with Matlab function 'fir1'.

Cross-correlation was calculated in sliding windows of 10 sec duration using Matlab function 'xcorr' on each consecutive 10-s window.

3.4 Results

3.4.1 Frequency-specific Effects in Cortical Oscillatory Activity

Subtraction of the awake, baseline power spectral density (PSD) from that under ketamine anesthesia (Figure 3-1B) revealed a similar marked increase in gamma (30-80 Hz) and slow-delta (< 5 Hz), as well as a drop of beta power (15-30 Hz), that mirrors the spectral changes seen in EEG in humans administered ketamine (Akeju et al., 2016). There was a consistent temporal order to these changes: awake beta power dropped shortly after intramuscular (IM) injection of ketamine, followed shortly thereafter by a decrease in slow-delta power, and an increase in gamma power several few minutes later (Figure 3-1C, representative spectrogram).

Under ketamine anesthesia, there were increases in gamma bursting in every patch of macaque cortex we tested (Figure 3-1D), expanding upon previous reports from only frontal EEG leads in humans (Akeju et al., 2016). We concentrated our analysis on frequencies in the gamma range of 30-80 Hz. This enabled us to use short time windows for a temporally resolved spectrogram of gamma power changes. Because segments of fast activity in raw LFP traces averaged approximately 1 second in duration, we analyzed power in 0.5-second epochs in order to capture onsets and offsets of gamma bursts in the resulting spectrograms for each area (Figure 3-1D). Of note, power spectrograms in Figure 3-1D are averages across all channels within each 3.2 x 3.2 mm array per cortical area, yet are qualitatively indistinguishable from a spectrogram of a single channel. This

suggests that the temporal structure of gamma bursts is highly consistent across all channels within small patches of the cortex.

Furthermore, examination of the high-frequency spectral data (Figure 3-1D) suggested that ketamine gamma bursts often appear and disappear simultaneously– even in distant cortical areas. To quantify the correlation of waxing and waning of gamma burst episodes, we band-passed filtered the raw LFP signal between 30-80 Hz, performed a Hilbert-transform, and took the absolute value of the resulting Hilbert transform, creating a time series that represents the instantaneous gamma amplitude at each time point (Adhikari et al., 2010). We then performed coherence analysis between the resulting signals in the frequency band below 1 Hz (0.1-0.8 Hz) and instantaneous gamma amplitude to capture waxing-and-waning of gamma bursts, which happened less frequently than once per second.

This revealed that ketamine increased the correlation of gamma bursting between and, in particular, within cortical areas (Figure 3-1E). The exception was a decrease in correlation of gamma episodes between PPC and STG, evident in both monkeys individually (Figure 3-1E). Ketamine also increased slow-timescale coordination between the gamma oscillations, but it was more local than the fast-timescale gamma episode correlations. Gamma oscillations became more coherent within individual cortical areas, but there was little change between areas (Figure 3-1F).

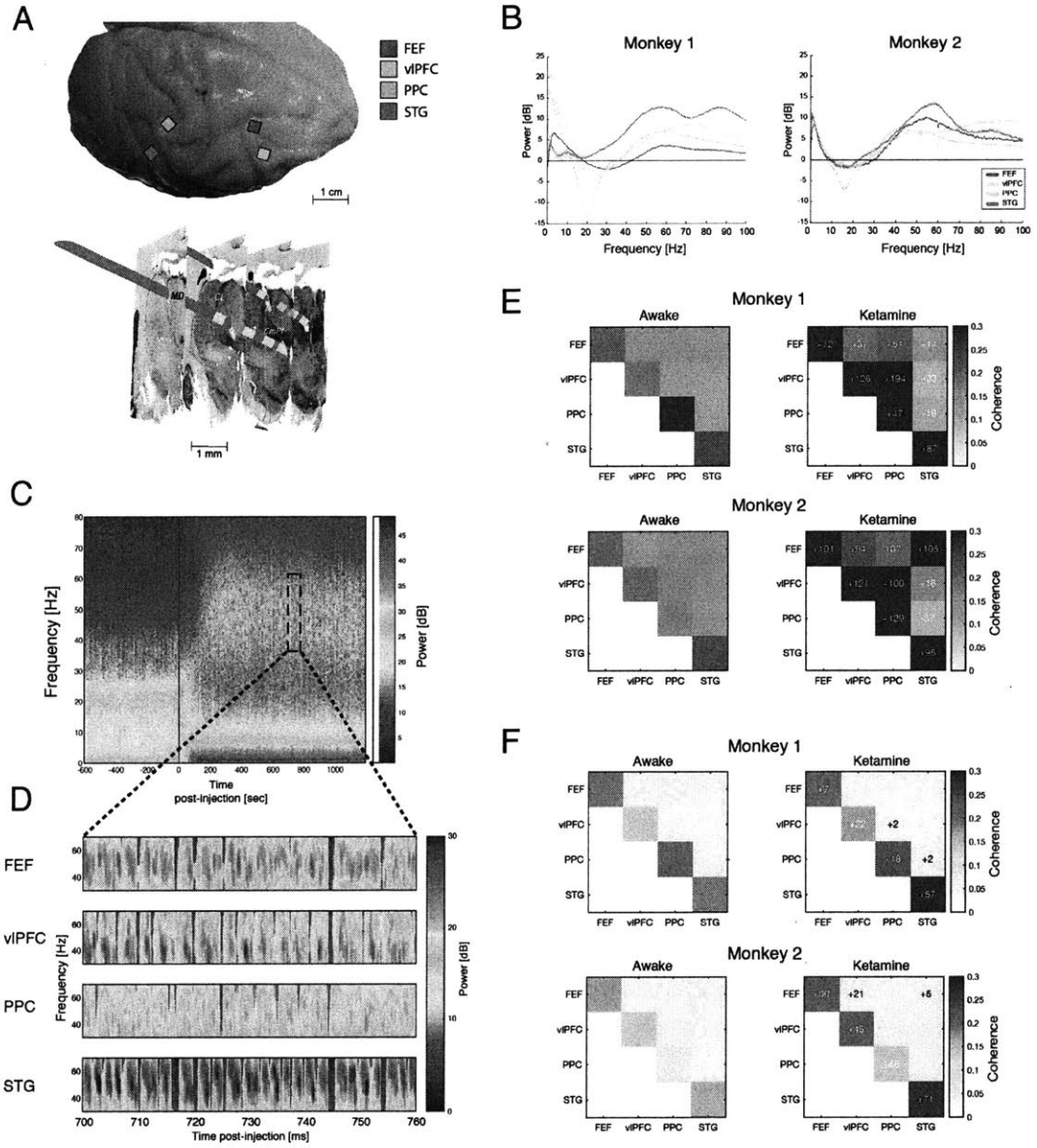

Figure 3–1 A, Recording setup with four cortical microelectrode arrays and intralaminar thalamic electrodes. FEF: frontal eye fields; vlPFC: ventrolateral PFC; PPC: posterior parietal cortex; STG: superior temporal gyrus. Thalamic intralaminar nuclei: CL (centrolateral) and CmPf (centromedian/parafascicular). **B,** Difference of power spectral density (PSD) between ketamine anesthesia and awake states (ketamine – awake). **C,** Representative average spectrogram from one cortical area (PPC) for a single session. **D,** Gamma-band spectrograms for the four cortical areas. **E,** Gamma burst coordination demonstrated via average coherence of slow (0.1-0.8 Hz) modulation of gamma amplitude for awake and ketamine periods. **F,** Coherence in gamma frequencies (30-80 Hz) within and between cortical areas. **E and F,** Overlaid numbers represent percent change of mean coherence with respect to awake baseline when confidence intervals did not include zero.

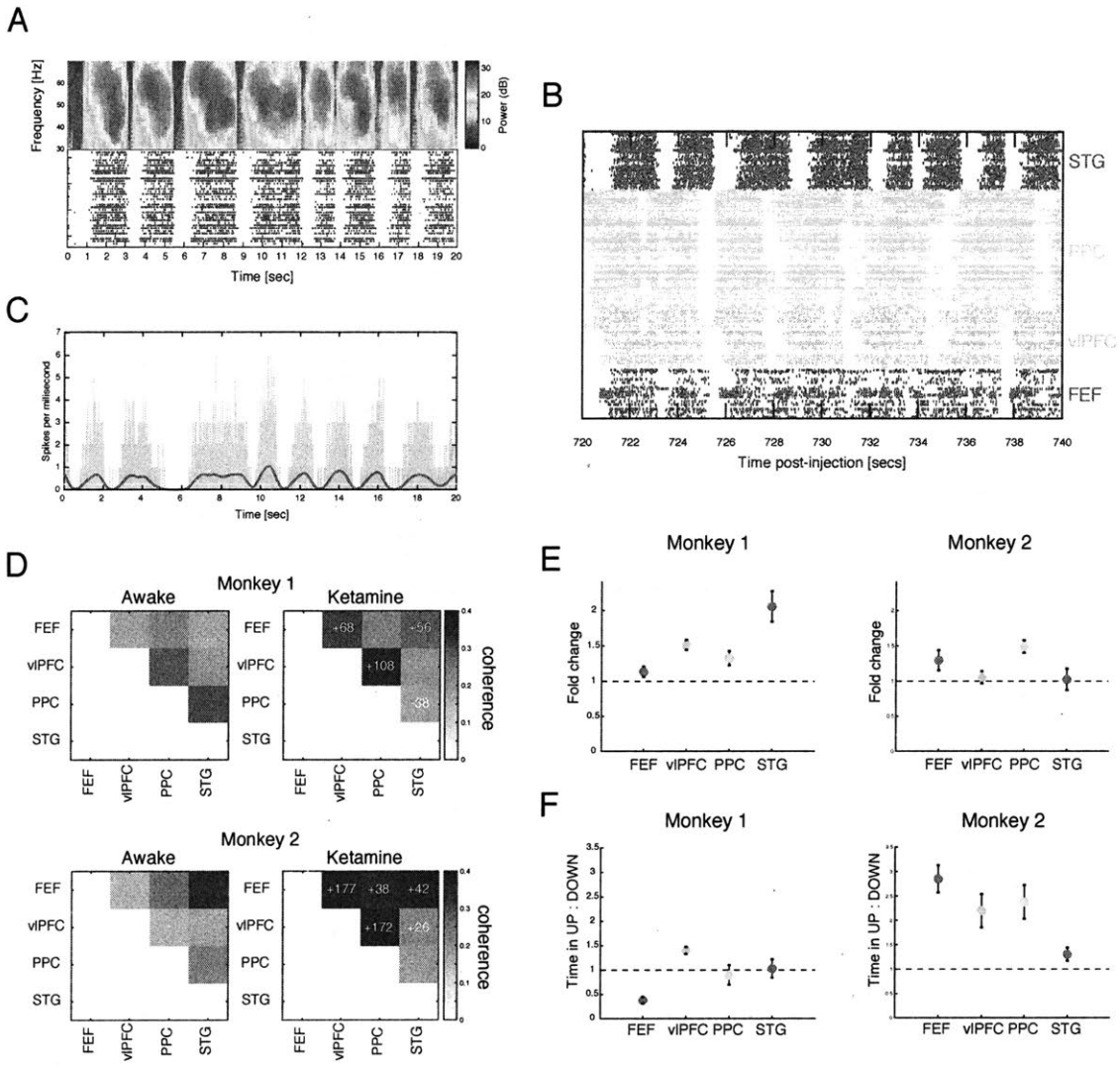

Figure 3–2: **A**, Area-average spectrogram of gamma bursts aligned with rasters of all isolated single units from same cortical region (here, STG). Every gamma burst corresponds to exactly one cortical period of high firing activity, surrounded by quiescence. **B**, Up-down states are present throughout all four cortical areas. **C,** Sample multiunit histogram from cortical area in ketamine anesthesia with smooth firing rates (red) and up-states (yellow) overlaid. **D**, Coherence between time series equivalent to the red curve in **C**, obtained for each cortical area as a surrogate for slow (0.1-0.8 Hz) modulation of spiking activity. Overlaid numbers equal percent change of mean coherence from baseline where confidence interval did not include zero. **E**, Fold-change of mean firing rates across all up-states (yellow in **C**), with respect to awake mean firing rate for each cortical area. Dashed line marks no change from baseline. **F**, Ratio of total time spent in UP- vs. DOWN-states during ketamine anesthesia. In **E, F**, error bars are standard deviations of the mean.

3.4.2 Ketamine Changes the Directional Flow of Cortical Rhythms

To examine whether disappearance of beta power could be implicated in abnormal information transfer between cortical areas, we computed the directional Granger causality measure between all cortical areas we recorded (Figure 3-3). Strikingly, there was a prominent peak in beta (12-30 Hz) Granger causality specifically in the direction from PPC to all other cortical areas. This was consistent for both animals. Beta power was also highest at baseline in PPC and therefore experienced the most prominent drop going into ketamine anesthesia (Figure 3-2). The information encoded in the beta oscillation under baseline conditions was lost with the complete disappearance of beta power under ketamine and a concomitant drop in Granger causality.

To determine if the powerful gamma bursts observed in ketamine anesthesia propagated through any particular network, we next evaluated the Granger causality metrics between all cortical areas. We found that gamma oscillations were directed up the cortical hierarchy from sensory areas toward more anterior prefrontal areas (Figure 3-3). Gamma granger causality went significantly from the superior temporal lobe to FEF, and then from FEF to vlPFC. The power and frequency of the gamma power tracked this flow of information such that across this network the amplitude and frequency of the gamma was highest in STG, lower in FEF, and lowest vlPFC.

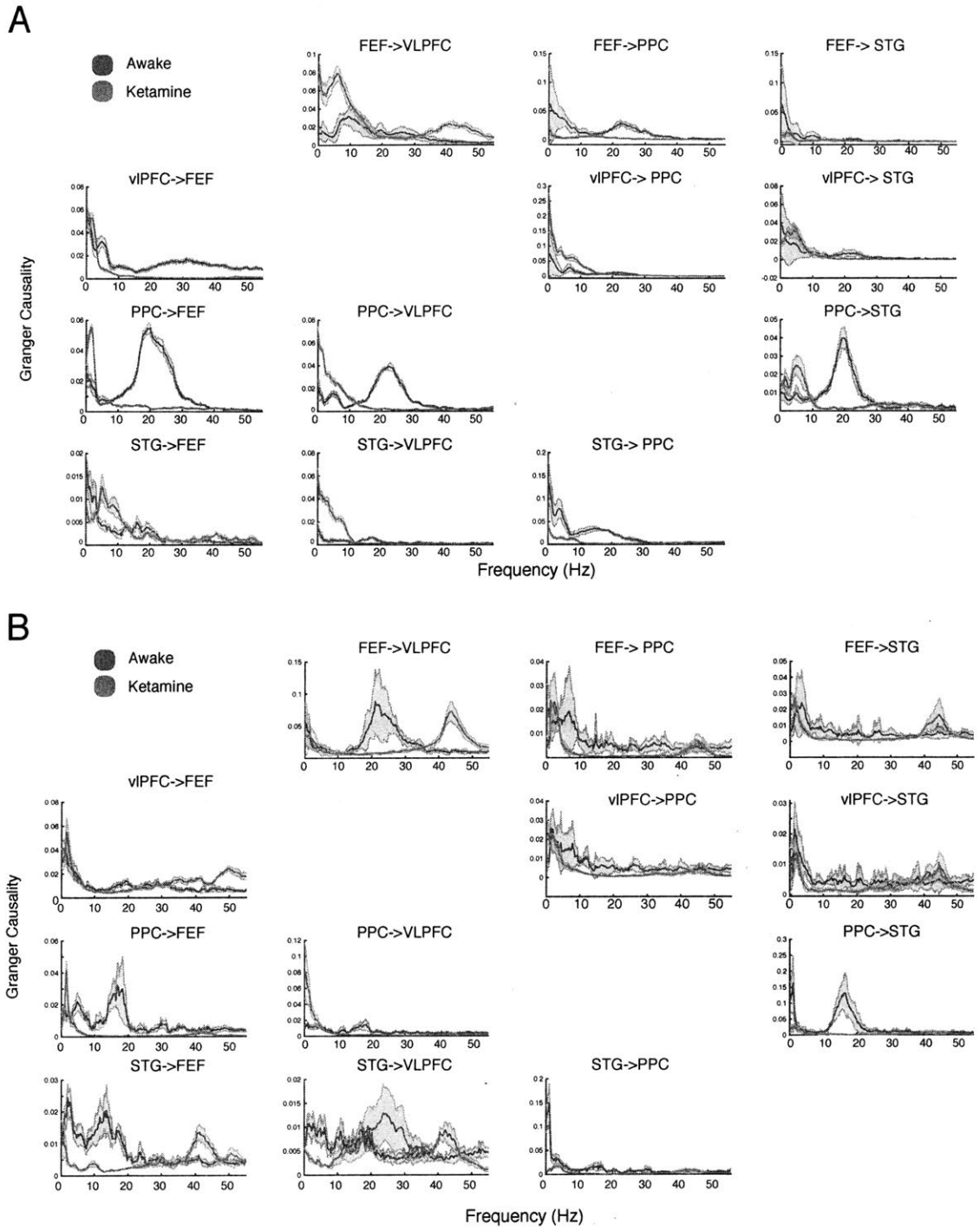

Figure 3–3. Directional rhythmic flow between cortical areas in awake baseline (blue) and ketamine anesthesia (red) evaluated via Granger causality. **A,** data from monkey 1 and **B**, data from monkey 2. 95% confidence intervals computed as 1.96 * *standard error of the mean.*

3.4.3 Hyperactive Spiking and Increased Coordination Between Cortical UP-States

Ketamine and other similar NMDA blockers have been found to disinhibit pyramidal cells via NMDA antagonism at fast-spiking (FS) interneurons (Homayoun & Moghaddam, 2007). To test for elevated spiking under during ketamine up-states, we isolated up-states by using a k-means algorithm that clustered periods of high and low firing activity in the smoothed signals (convolved with 1000-ms Gaussian kernel and marked in red in Figure 3-2C; the up-states isolated using this method are marked in yellow in Figure 3-2C). We then computed the mean spike rate during the periods of high spiking and compared that to baseline (Figure 3-2E). Spike rates were increased in most or all cortices in both animals during ketamine up-states. Furthermore, the sum of duration of all up-states was greater than that of down-states in on monkey across all areas and varied by region in the second monkey. This demonstrated that individual regions of cortex under ketamine anesthesia can be hyperactive the majority of the time (Figure 3-2F).

At the spiking level, gamma bursts corresponded to classically defined UP-states, or periods of high firing activity of individual neurons surrounded by quiescent DOWN-states (Figure 3-2A). Like gamma bursts, distinct UP-DOWN states were present in all of the sampled neocortex (Figure 3-2B) and were coordinated (Figure 3-2E). To capture their coordination in the slow (< 1 Hz) timescales, we first convolved the sum of all spikes in each cortical area with a Gaussian kernel of 1000 msec duration. We then used the resulting continuous time series to compute coordination between spiking states. As suggested by the analysis of gamma, ketamine increased coordination between UP and DOWN states, especially within areas. The only exception to this, yet again, was a consistent coordination decrease found between PPC and STG (Figure 3-2E).

3.4.4 Central Thalamus (CMT) is Entrained by Frontal Activity

The central thalamus is known to modulate cortical states across the entire spectrum of wakefulness (Saalmann, 2014). Thus, we recorded LFP from multilaminar probes within CMT (Figure 3-1A) to characterized the thalamic and thalamocortical contributions to the anesthetized state. The predominant spectral changes in CMT LFPs under ketamine anesthesia was an increase in slow-delta power (<5Hz) (Figure 3-3A). Broadband gamma power was increased, but less substantially than the increase of cortical gamma power under ketamine (Figure 3-3B; 3-1B). However, even within single sessions, a clear temporal relationship was evident between the slow thalamic LFP and the waxing and waning of cortical spiking (Figure 3-3C).

We used cross-correlation to test to explore temporal relationships between cortical spiking and CMT LFPs. We found there to be a highly consistent correlation between frontal cortical spiking and centromedial thalamic LFPs. The cortical spiking from Area 8A and vlPFC was left-shifted in the time domain with respect to the thalamus by 25-50 msec (Figure 3-3D, first two panels). This was specific to prefrontal cortical areas. Between them, Area 8A led the thalamus earlier than did vlPFC. PPC spiking and thalamic oscillatory activity correlated centered at zero lag whereas the envelope of spiking in STG bore no relationship to the shape of thalamic LFP. Thus, it appeared that the increased frontal spiking under ketamine entrained central thalamic LFPs, and likely PPC LFPs, which did not occur in the awake state.

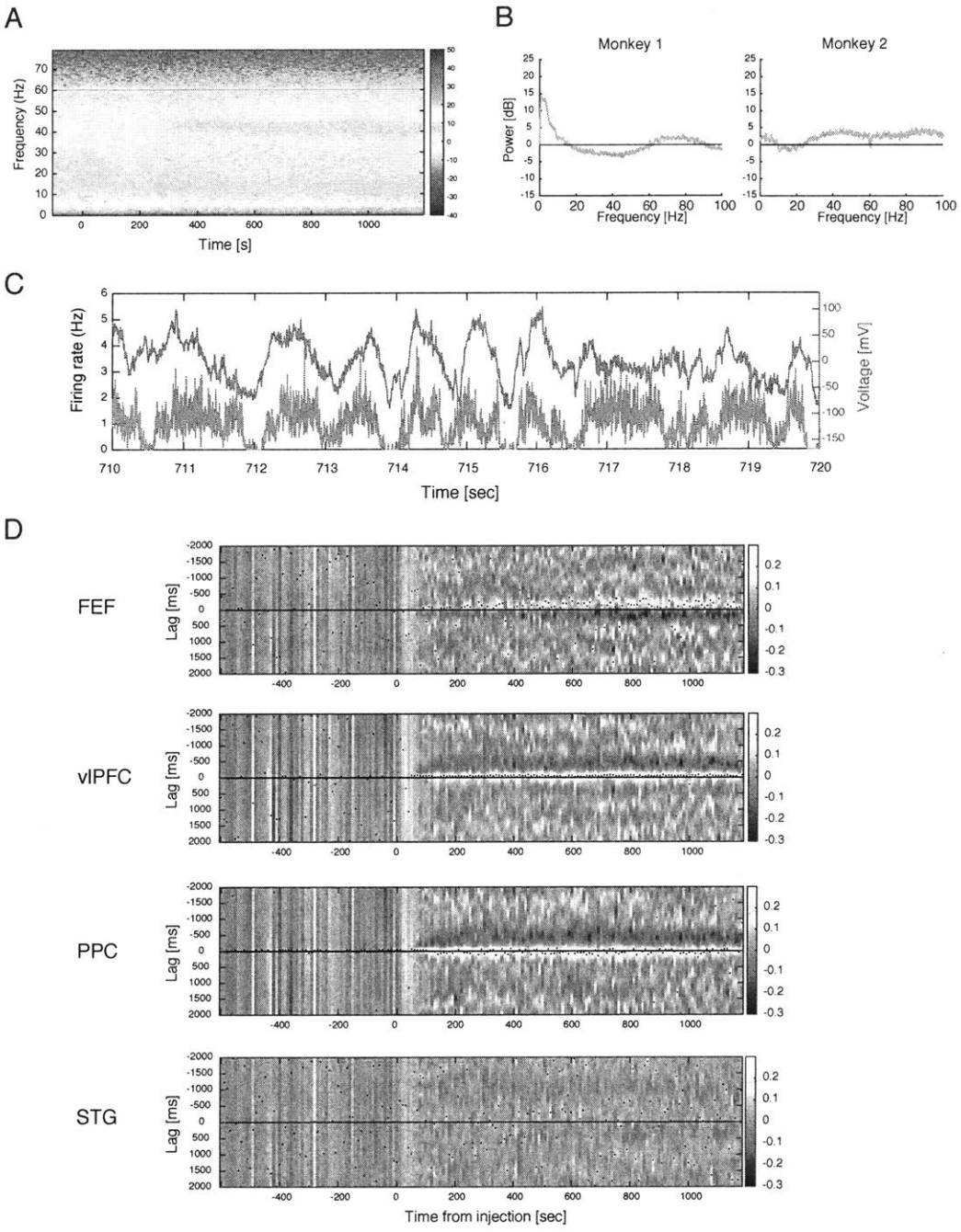

Figure 3–4: Cortical spiking entrains local field potentials of central thalamus. **A**, Representative spectrogram of intralaminar thalamic LFP. **B,** Average PSD difference, (ketamine) – (awake), from intralaminar thalamus. **C,** Comparison of sum of cortical spikes in vlPFC (gray) and central thalamic LFP (orange). **D**, Cross-correlation of cortical spiking and thalamic LFP computed at different lags (y-axis) and across time (x-axis) reveals significant correlation under ketamine (cross-correlation peak per bin shown as block dot). Negative lag (up) indicates cortex leads.

3.5 Discussion

Our findings show that unconsciousness may be possible despite abundant and coordinated firing across most of the cortex. We propose that, apart from brevity and misalignment of spiking UP-states in sleep (Nir et al., 2011) and general anesthesia (Lewis et al., 2012), there might exist other means of disrupting the cortical activity that supports conscious processing. One contender that emerges from our work is local hypercoherence in specific, stereotyped frequencies such as gamma.

In ketamine anesthesia, each cortical area appears to be a hypersynchronized "hub" whose gamma oscillation is not coherent with that of other areas, even if elevated gamma power appears in all of them at the same time. Aberrant information processing due to hypersynchrony is a known phenomenon in other global states of the brain, such as Parkinson's disease (Cole et al., 2017) and epilepsy (Tóth et al., 2018). This adds further support to the possibility that locally hypercoherent gamma oscillations in our data block normal intra- and inter-cortical communication under ketamine. Our results also suggest that PPC may be a beta-generating center that communicates information to other brain areas using this particular frequency band in the awake state. Ketamine disrupts this rhythm strongly, and thereby the causal directionality of beta oscillations outward from PPC is eliminated. Additionally, massive prefrontal cortical spiking seems to entrain at least one major subcortical center for wakefulness, the centromedial thalamus (CMT). Both FEF and vlPFC revealed the highest correlation with cortical spiking preceding thalamic LFP changes on the order of 25-50 msec. If cortex remains in a globally hyperexcited state for the duration of ketamine anesthesia, and this hyperexcited state

also dictates the excitability of CMT neurons, it is unlikely that CMT stimulation[2], as was performed in rodents in sleep (Gent, Bandarabadi, Herrera, & Adamantidis, 2018), could lead to awakening from ketamine. This may partly explain why cortex under ketamine is unarousable until the anesthetic w ears off and cortex may once again be modulated by subcortical structures.

One incidental finding from our data shows that, despite generally coordinated activity across frontal-most cortices, slow modulation of firing and gamma activity between PPC and STG was consistently lower in ketamine compared to wakefulness (Figure 3-1D and 3-2D) This finding warrants further investigation in additional subjects. Integration across the temporoparietal junction (TPJ), which separates our PPC and STG arrays, is critical to attention (Pedrazzini & Ptak, 2019), awareness (Graziano, 2018), and the theory of mind (Saxe & Kanwisher, 2003). If decreased coupling of firing activity between PPC and STG reflects the loss of integration at the TPJ, it could be an additional explanatory factor for altered consciousness brought on by ketamine.

Perhaps most surprisingly, our study directly undermines comparisons of ketamine anesthesia to a dream-like state such as REM sleep. Among other findings, this comparison has been used to deny ketamine the status of a general anesthetic that induces true unconsciousness (Darracq et al., 2018), in spite of the fact that other anesthetics, too, induce dream-like experiences (Radek et al., 2018). Now, our present work shows that gamma coherence between distant cortical areas in ketamine anesthesia remains unchanged from wakefulness, but does show a prominent increase locally. This stands in opposition to what has been observed in subanesthetic ketamine (Castro-Zaballa et al.,

[2] Single session experiments in monkey MJ indicated that central thalamic DBS protocol that reversed propofol anesthesia did not succeed in ketamine anesthesia to restore normal appearing behavior or cortical dynamics. Experiment not extensively repeated due to extreme increase in sympathetic response caused by the DBS.

2019), where broad decreases in gamma coherence resemble what occurs in REM sleep. While subanesthetic ketamine is, in fact, an accepted model of psychosis (e.g. schizophrenia) that may resemble vivid dreaming, our data invalidate comparisons of UP-states in ketamine anesthesia to psychosis or REM sleep based on the measure of gamma activity alone. Frankly, as we show via the discovery of local hypercoherence, gamma in ketamine anesthesia may be more of a facilitator of true unconsciousness rather than a signature of any conscious activity. Furthermore, since previous studies indicate that transient spiking structures during up-states of sleep and general anesthesia may resemble those from normal wakefulness (Destexhe, Hughes, Rudolph, & Crunelli, 2007), hyperexcited and hypercoherent ketamine UP-states may be the furthest of all anesthetics from resembling a wakeful baseline. Thus, the neural dynamics of ketamine anesthesia reflect an alternative, excitatory-based means to produce disrupted conscious processing and point to distinct systems-level mechanisms for pharmacologically induced unconsciousness.

Chapter 4

Closed-Loop Control of Conscious States in Non-human Primates

The contents of this chapter are produced from Jacob A. Donoghue*, Souresh Chakravarty*, Meredith K. Mahnke, Jefferson E. Roy, Roman F. Loonis, Earl K. Miller**, and Emery N. Brown**, Closed-loop control of general anesthesia in non-human primates (*in preparation*). * indicates co-first author; ** indicates co-senior author

4.1 Abstract

General anesthesia (GA) is a pharmacologically-induced, reversible state characterized by unconsciousness, analgesia, amnesia and akinesia along with maintenance of physiological stability. Anesthesiologists most strongly rely on observable features (e.g. patient movement or responsiveness) and cardiovascular and respiratory vital signs for gauging depth of anesthesia. The variability in individual responses to GA can make it challenging to avoid under- or oversedating a patient. Monitoring of electroencephalographic (EEG)

activity during GA can help prevent this. Here, we sought to automate the control of anesthetized states by developing a closed-loop anesthesia delivery (CLAD) system using propofol in non-human primates. From intracranial recordings of local field potentials (LFPs) and spikes, we identified a spectral marker for sedation and GA sensitive to changes in the infusion rate. We validated a pharmacokinetic-pharmacodynamic (PK-PD) modeling paradigm for the dose-effect relationship between propofol infusion and brain activity in a subject-specific manner. We established a Linear Quadratic Regulator (LQR) paradigm for an optimal control framework whereby a subject's anesthetic level was established from the LFP and the drug dose was automatically adjusted to achieve a target marker value. We validated our CLAD schema both *in silico* and *in vivo* and stably regulated the marker about the target value over a prolonged period of time. This paradigm opens up the framework for CLAD systems that automatically control anesthesia in human patients.

4.2 Introduction

General anesthesia (GA) can be defined as a drug-induced reversible state characterized by unconsciousness, analgesia, amnesia and akinesia along with maintenance of physiological stability. (Brown, Purdon, & Dort, 2011). In clinical applications of GA, such as surgery, the brain's neuronal circuitry responsible for cognitive functions is pharmacologically perturbed by anesthetic drugs to induce the state of unconsciousness. In prolonged surgeries it is essential to maintain a desired level of unconsciousness in the patient for an extended period of time, often exceeding multiple hours. This is usually achieved by manual control of the anesthetic drug dosage within an allowable range. Undersedating patients can result in intraoperative awareness, a traumatic situation in which an individual becomes conscious, often while still paralyzed, during a surgical

procedure. On the other hand, oversedating individuals can result in physiological instability or lead to prolonged and dangerous emergence from anesthesia. Another important concern with GA is the post-operative cognitive dysfunction that may arise in the elderly population, possibly linked to the type and dosing of chosen anesthetics (Rohan et al., 2005). Modern technology may help achieve refined and safer control on the state of unconsciousness under GA by monitoring the anesthetic state and adjusting the drug dosage in real time.

Different anesthetic states (sedation, GA, medically-induced coma) can be accurately monitored by viewing the brain's electrical activity via electroencephalogram (EEG) measurements over time. This emerges from the characteristic patterns and progression of EEG waveforms at the different depths of anesthesia. In the case of GA in humans, the EEG spectral power can be tracked visually to monitor the anesthetic state on be commercially available frontal EEG (Purdon et al., 2013; Schwender et al., 1996). The Bispectral Index (BIS) is the most prominent EEG biomarker and is used clinically to gauge general anesthesia depth, relating a proportion of higher frequency oscillations to the slower ones. Closed-loop anesthesia delivery (CLAD) systems have been developed from these principles in an attempt to control and maintain particular anesthetic states defined by these types of biomarkers (Gentilini et al., 2001).

One of the clearest brain states to define from EEG recordings is that of burst suppression, which arises in deep GA or in the etiologies giving rise to coma (e.g. anoxic brain injury, trauma, metabolic toxicity, etc.). While it is not necessarily identical across individuals, burst suppression is characterized by prominent isoelectric periods that can be more easily be identified and quantified, for example, by integrating the length of the isoelectric period or the duration of the high-frequency bursts on EEG (Brown et al., 2011; Ching et al., 2012). Medically-induced coma traditionally refers to intentionally driving a patient into this burst suppressive state. Furthermore, regulating the appropriate level of

sedation for critical care patients can significantly complicate patient management and negative affect patient outcomes. Most CLADs work has focused on modeling and implementing single-state automated control of medically-induced coma using the clear EEG signal markers present with burst suppression. Specifically, CLAD approaches have been developed for humans to control therapeutic medically-induced coma by tracking the burst suppression probability from EEG and have been validated extensively on rodents (Ching et al., 2013; Liberman, Ching, Chemali, & Brown, 2013; Shanechi, Chemali, Liberman, Solt, & Brown, 2013; Westover et al., 2015).

The neural dynamics that emerge before burst-suppression emerges in GA are less easily demarcated and exhibit more subject-to-subject variability (Brown et al., 2011). Controlling these states, ranging from light sedation to deep anesthesia, in a subject-specific manner does not inherently translate from PK-PD models (Absalom, Mani, Smet, & Struys, 2009). Unsurprisingly, the systems designed for automatically regulating burst suppression do not generally translate to a multi-state control paradigm with variable neural dynamics (Ching et al., 2013; Liberman et al., 2013; Shanechi et al., 2013; Westover et al., 2015; Yang & Shanechi, 2016). Early work simply used quantitative EEG to target median EEG frequency values for specific bands (e.g. 2-3 Hz) by closed-loop alteration of propofol (Schwilden, Stoeckel, & Schüttler, 1989). More complex control regimes focused on manipulating physiological biomarkers derived from other spectral properties of the EEG have shown more promise in non-burst suppressive states. Anthony Absalom and colleagues have used proportional integral derivative (PID) control in their CLAD systems (Absalom & Kenny, 2003). Ngai Liu and co-workers have developed control systems that can co-administer propofol and remifentanil using a PID controller (Liu, 2017; Liu et al., 2011; Liu & Rinehart, 2016). Dumont and colleagues have developed a robust PID paradigm and have tested it in human studies (Dumont, 2012; Dumont, Martinez, & Ansermino, 2009). Recently, a multicenter study of a CLAD system based on a PID

control scheme and the BIS marker was developed (Liu & Rinehart, 2016; Puri, et al., 2016; Puri, Kumar, & Aveek, 2007). While significant limitations still prevent these paradigms from safe implementation on human patients, control design is an iterative process requiring detailed numerical studies and appropriate animal experiments (Mage, et al., 2017; Karnik, 2017). With these scientific and technological foundations, we have developed a novel electrophysiological signal-guided CLAD system for GA with special emphasis on testing this paradigm on non-human primates.

Since a human brain shares more homologous features with a macaque brain than with a rodent brain (Hutchison & Everling, 2012), the non-human primate model is ideal to validate the CLAD system prior to prospective testing on humans. Human-based anesthesia monitoring, such as with the BIS, is thought to predominantly reflect the activity in the prefrontal cortex of humans, as the standard setup involves a set of electrodes placed on the forehead of a patient. The expansion of prefrontal cortex is prominent in primates, as opposed to in rodents or other common experimental model animals. In macaques, the expanded prefrontal cortex has been shown to display diverse features that support higher cognition like in humans, and provides an ideal surrogate target location to study the breakdown in processes that drive awareness and working memory (Miller & Cohen, 2001). As meaningfully, the anatomy of the thalamocortical loops implicated mechanistically in propofol-mediated loss of consciousness is unique to primates (e.g. parvocellular mediodorsal thalamus projections to the lateral prefrontal cortex) (Vijayan, Ching, Purdon, Brown, & Kopell, 2013).

Here, we validated the first CLAD system for GA in non-human primates (rhesus macaques). The CLAD system's core algorithm operated in a cyclic manner whereby the system iteratively analyzed a short duration segment of local field potential (LFP) data recorded from electrodes implanted within prefrontal cortex (PFC). From the power spectral density of the signal in this time window, the state descriptor indicative of the

anesthetic drug concentration in the brain was estimated using a Kalman filter (Kalman, 1960; Faragher, 2012). Then, a stochastic control algorithm compared this estimate with an operator-prescribed target that was deemed safe and determined the infusion rate for the next time increment. The updated infusion rate information was communicated to the actuator (syringe pump) that drove the propofol-filled syringe, thus completing a single iteration of the loop. A schematic of the flow of information within our CLAD system is illustrated in Figure 4-1.

In this work, we demonstrate:

1. A **spectral marker for sedation and GA** for propofol anesthesia. The marker is found to be sensitive to infusion rate changes.
2. A **pharmacokinetic-pharmacodynamic (PK-PD) modeling paradigm** that describe the dose-effect relationship between propofol infusion and brain activity observed via EEG or LFP. A deterministic parameter estimation scheme is developed to calculate the parameters of this PK-PD model. This modality can be useful in determining subject-specific parameters from electrophysiological recording from anesthesia sessions.
3. An **optimal control framework**, designed with robustness considerations, that automatically gauged the subject's anesthetic level from the LFP recording and automatically adjusted the drug dose to achieve a target value of the marker.
4. **Experimental validation of CLAD in macaques**. In our initial validation experiments of our CLAD scheme, we regulated the marker about target value in a stable manner and over a prolonged period of time.

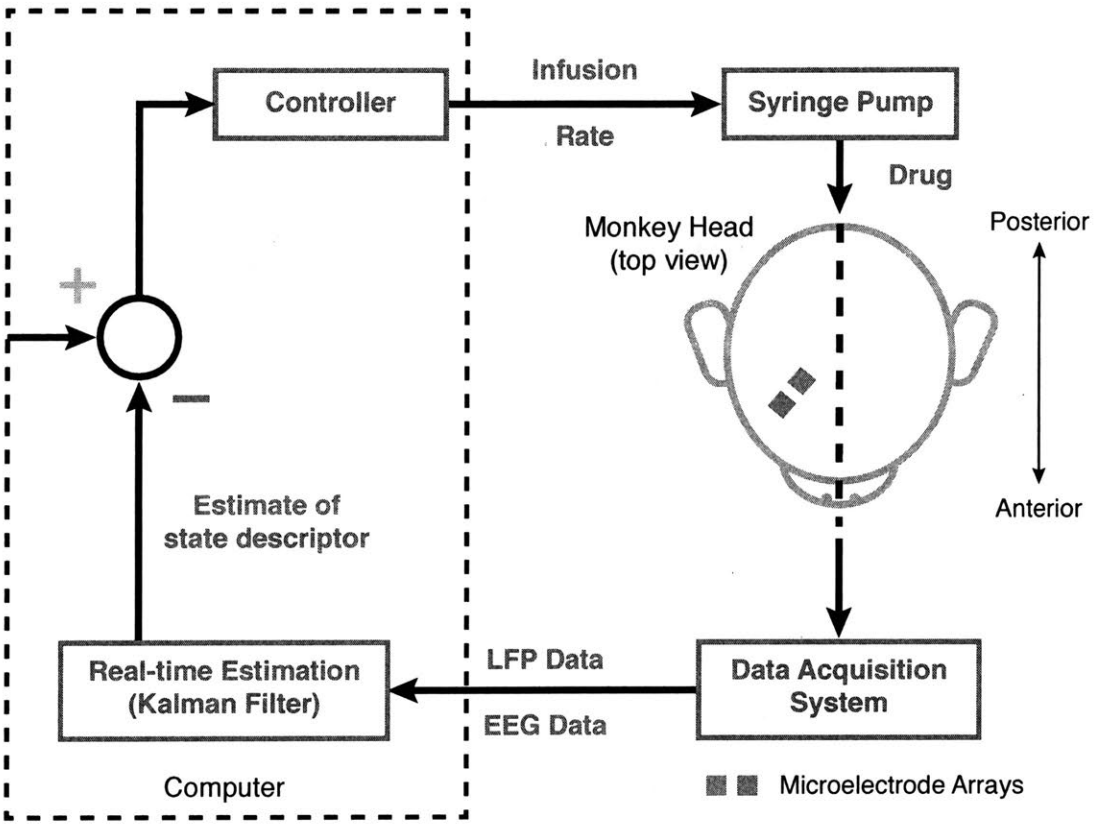

Figure 4–1 Illustration of the CLADS framework for macaque model.

4.3 Methods

4.3.1 Electrophysiological Recordings

Three rhesus macaques (*Macaca mulatta*) were chronically implanted with multielectrode arrays (MultiPort Utah Array, Blackrock Microsystems, Salt Lake City, UT) placed in prefrontal cortex (Subject A (Male, 17 years old): Area 8a, Supplemental Eye Fields (SEF), and dorsolateral PFC (46d); Subjects B (Male, 16 years old) and C (Female, 8 years old): Area 8a and ventrolateral PFC (vlPFC)). Spiking activity was recorded by sampling the raw analog signal at 30 kHz, bandpass filtered from 250Hz-5kHz, and high-frequency events were isolated that crossed manually-set thresholds on individual electrodes. Spikes were manually sorted into single units using commercially-available software (Offline Sorter v4, Plexon Inc., Dallas, TX). LFPs were recorded at 30 kHz and filtered online via a lowpass 250Hz software filter and downsampled to 1 kHz.

4.3.2 General Anesthesia Paradigm

Propofol requires intravascular administration to be effective and is the route of delivery in human patients. Monkeys were head-fixed via an implanted titanium headpost and placed in noise-isolation chambers with masking white noise (50 dB), upon where vascular access was percutaneously established. Monkey A was cannulated in the marginal ear vein prior to experiments. Monkeys B and C were each implanted with a vascular access port (Model CP-6, Norfolk Access Technologies, Skokie, IL) residing in the scapular region of the back, with the catheter tip reaching the termination of the superior vena cava via the external jugular vein. After a period of awake baseline recordings (median = 19 mins, inter-quartile range = 9.5 mins, minimum = 0 mins, maximum = 27 mins, across 12 recording sessions), propofol was infused via a computer-controlled syringe pump

(PHDULTRA4400 and PHD2000, Harvard Apparatus, Holliston, MA). In the closed-loop sessions (utilizing PHD2000), the flow rates were updated in real-time via a custom-written code communicating with the pump through a serial port using functionalities from Matlab's Instrument Control Toolbox (The Mathworks, Inc, Natick, MA). Heart rate and oxygen saturation was monitored for the duration of the experiment (Model 7500, Nonin Medical, Inc., Plymouth, MN), with SpO2 values maintained above 93 percent.

Infrared monitoring tracked facial movements and pupil size (Eyelink 1000 Plus, SR-Research, Ontario, CA) throughout the course of the experiments. Loss of consciousness (LOC) was deemed by the timestamp of the moment of eyes-closing that persisted for the remainder of the infusion. Recovery of consciousness (ROC) was classified as the timestamp of the first to occur between eyes reopening or regaining of motor activity following drug infusion cessation.

Several infusion protocols were utilized. In the initial open-loop experiments, we used a fixed step-up and step-down dosing scheme to assess subject-specific response variability across sessions. In these sessions, the propofol infusion rate was increased in 5 steps up to a maximum of 0.2850 mg/kg/min and decreased down the same steps while holding each rate for 9 min (Figure 4-4C (subject A, 5 sessions), Figure 4-5 (subject B, Session 1)). To analyze the variability of the candidate marker with changes in drug dosing, we implemented the following dosing regimen in subject A: 0.3 mg/kg/min for 20 min, 0.001 mg/kg/min for 3 minutes, 0.2 mg/kg/min for 15 minutes, 0.001 mg/kg/min for 3 minutes, 0.1 mg/kg/min for 15 minutes, and finally 0.25 mg/kg/min for 15 minutes (Figure 4-5, Session A6). In each of the closed-loop sessions, the initial open-loop infusion was held between a constant value between 0.25 to 0.3 mg/kg/min and maintained for 30 to 40 minutes to permit LOC, the spO_2 and heart rate stabilization, and placing the candidate marker within a controllable regime. The propofol infusion during closed-loop sessions was adjusted in real-time according to the difference in marker estimate derived

from the PK-PD model with respect to the target marker (see Equation 16). The maximum dose infusion rate during the closed-loop session was enforced to be 0.4 mg/kg/min.

4.3.3 Anesthetic Signatures from the LFP

To characterize the oscillatory dynamics of the LFPs across the GA sessions and obtain power spectral densities, multitaper spectral analysis was performed (Bokil, Andrews, Kulkarni, Mehta, & Mitra, 2010). The multitaper spectrogram was obtained at a resolution h (minutes) followed by calculation of the band-wise power using the definitions of bands per recent literature on analysis of LFP from macaque cortex under propofol anesthesia (Ishizawa, et al., 2016). The parameters for the multitaper spectral analyses used stationary time windows in the interval of 10 to 30 seconds without overlap, time-halfbandwidth product of ~ 4 and number of tapers ~ 3. We took the ratio of the power (calculated from spectral estimation) in $0.1 - 4$ Hz to that in $14{-}30$ Hz and then converted this quantity to the decibel scale.

The controller update rate was set to be the same as the stationary time window for the marker analysis. This leads to the practical practical constraint that the pump update rate could not be arbitrarily small because of the presence of a short transient period before the flow stabilized to the prescribed flow rate. In benchtop flow rate calibration experiments with water, we found this transient period to be on the order of 5 seconds. As a result, our controller update rate was constrained to be in the range of 10 to 30 seconds and was sufficient to capture the dominant trend in the spectral estimates. Note that water has lower viscosity relative to oil-in-water emulsions such as propofol, further justifying the selection of the longer window selection of 10-30 seconds (Baker & Naguib, 2005).

For the logarithm of band-wise power estimates and the ratio calculated as above, discrete-time filtered estimates were determined by using the following state space estimation paradigm,

$$x_k = Ax_{k-1} + w_k \tag{1}$$

$$y_k = Cx_k + v_k \text{ , where } v_k \sim N(0, \sigma_y^2) \tag{2}$$

$$w_k \sim N(0, Q) \tag{3}$$

$$x_0 \sim N(\mu_0, \Sigma_0) \tag{4}$$

In our study we utilized two different versions of state space models. In the first version we assumed a first-order random walk model where, A=1, C = 1, $Q = \sigma_x^2$ is a scalar, and $\sigma^2{}_y$ is the variance of the observation noise. The reduced complexity of this model allowed for real-time implementation. To perform statistical comparisons, we required a model which had smoothness constraints in the first and second time derivatives of the marker estimate. In this second version, we used a *constant jerk* state space model (Bar-Shalom, Li, & Kirubarajan, 2004) which comprises a scaling parameter, $\sigma^2{}_x$, and a 3rd order process variable, $x_k = [p_k \ , \ d_k \ , \ a_k \ ]^T$, where p_k, d_k and a_k can be regarded as position, velocity and acceleration quantities inspired from kinematic equations of motion, and

$$A = \begin{bmatrix} 1 & h & 0.5h^2 \\ 0 & 1 & h \\ 0 & 0 & 1 \end{bmatrix}, \quad Q = \begin{bmatrix} \frac{h^5}{20} & \frac{h^4}{8} & \frac{h^3}{6} \\ \frac{h^4}{8} & \frac{h^3}{3} & \frac{h^2}{2} \\ \frac{h^3}{6} & \frac{h^2}{2} & \Delta \end{bmatrix} \sigma_x^2, \quad C = [1,0,0] \tag{5}$$

The *constant jerk* model assumes that the second order time derivative of a scalar state variable follows a random walk resulting in smoothly varying filtered estimates. The results from this model are shown Figures 4-2, 4-3, 4-6, and 4-7.

We identified a biomarker, here referred to as the *ratio marker*, to track the anesthetic state of the monkey during a propofol anesthesia session from a single channel LFP recording. This ratio marker was calculated as the Kalman filtered estimate of the ratio of power in 0.1−4 Hz band to that in the 14−30 Hz band (Shumway & Stoffer, 2000). The closed loop implementation of regulating this ratio marker is discussed in subsequent sections (see Methods 4.3.6) for both *in silico* and *in vivo* experiments.

For both state space models, we set the variance of the observation noise, $\sigma^2{}_y$, equal to variance of the first few (~5) minutes of data, under the no drug condition. The scaling parameter, $\sigma^2{}_x$, in the process noise covariance matrix was set to $0.1\sigma_y$ so that the estimate was dominated by the process dynamics instead of the observation dynamics resulting in a more continuous trajectory. For the *constant jerk* state space model, we followed the steps below to initialize the model parameters. The mean μ_0 of the initial estimate was calculated as the coefficients of a quadratic function fitted to the first 20 points in the segment and $\sum_0$ was arbitrarily set as Q. This arbitrary initialization was based on the premise that the initial state parameters would not influence estimates farther into the recording session and the estimate trajectory would primarily be dictated by the observations and the choice of the σ_x/σ_y ratio (Bar-Shalom, Li, & Kirubarajan, 2002)

4.3.4 Estimating the Ensemble Spiking Activity

As the monkey became unconscious under propofol induction, the average spiking activity across all the electrodes in each electrode array reduced and the opposite trend was observed when the monkey regained consciousness. To track this gradual depression in ensemble spiking activity over a time scale h, we used a state space framework. At any

given time-window h, we let there be r_i number of spiking activities identified per channel for the i-th channel where $i \in \{1, 2, ..., n_c\}$[3]. The maximum number possible spikes that can be recorded at any given time bin of size h was n_s for a given channel. Therefore, for the entire ensemble, at the k-th time bin the total number of spiking events across all channels was given by $r_k = \sum_{i=1}^{n_c} r_i^{(k)}$ which can take a maximum allowable value of $N = n_c n_s$. We assumed that this count is a realization from a non-stationary binomial distribution as,

$$\Pr(r_k|N, p_k) = \binom{N}{r_k} p_k^{r_k}(1 - p_k)^{N-r_k} \tag{6}$$

where, p_k is the probability of occurrence of a spiking event on any of the channels within the k-th time bin. Although we sacrificed temporal correlation in spiking activity at a finer resolution (less than h), the p_k estimated over this coarse timescale was able to track gradual changes in the ensemble spiking activity. For a smooth estimate of p_k, we linked it to a real-valued scalar state x_k via a logistic function,

$$p_k = \frac{\exp(x_k)}{1+\exp(x_k)} \tag{7}$$

where, x_k evolves as a first-order Markov continuous-valued process in discrete time,

$$x_k = x_{k-1} + \varepsilon_k \tag{8}$$

where $x_0 \sim N(\mu_o, \sigma_0^2)$ and $\varepsilon_k \sim N(0, \sigma_p^2)$. This allowed us to use an existing algorithmic framework to estimate an optimal $\hat{p}_k$ from a data sequence of $\{r_k\}_{k=1}^{K}$ (Chemali, Ching, Purdon, Solt, & Brown, 2013).

[3] The scope of all mathematical symbols defined here are confined to this section only; only exception being p and h

4.3.5 Pharmacodynamic Modeling of Drug-effect Relationship

We used a second-order model inspired by a two-compartment pharmacokinetic model, such that

$$\dot{b}_i(t) = \lambda_i b_i(t) + u(t) \tag{9}$$

where u denotes the infusion rate (mg/min) and λ_1 and λ_2 are assumed to be real and distinct eigenvalues of the rate-constant matrix such that $\lambda_2 < \lambda_1 < 0$. The effect site kinetics are given by $x(t) = b_1(t) - b_2(t)$, which equals the drug amount in the second compartment of a mamillary two-compartment model after multiplying by a constant factor (Schwilden, 1981). Here, the chosen biomarker in the operating range showed a polyphasic pattern and demonstrated piecewise continuous and monotonic segments with non-zero, non-decreasing drug infusion rates. In each of the continuous segments, the marker trajectory in terms of the effect site kinetics could be described as,

$$y_m(t) = E_0 + \text{ß}E_{max}\left(\frac{\left(\frac{x}{x_{50}}\right)^{\gamma}}{1+\left(\frac{x}{x_{50}}\right)^{\gamma}}\right) \tag{10}$$

where, ß takes user-prescribed values of -1 (or +1) depending on whether the segment corresponded to monotonically decreasing (or increasing) trends for non-decreasing infusion rates.

For each of the phases, the parameters were estimated from the data by minimizing the squared residual between the model and observation. The optimization was performed in an alternating manner. First, starting with an initial guess of λ_1 and λ_2, we searched over the parameters of the sigmoid function,

$$\{E_0^*, E_{max}^*, x_{50}^*, \gamma^*\} = argmin\ 100\left(\frac{\Sigma_{t\,\epsilon\{\Delta,2\Delta,\ldots\}}(y_m(t)-y(t))^2}{\Sigma_{t\,\epsilon\{\Delta,2\Delta,\ldots\}}(y(t))^2}\right) \tag{11}$$

Then, using the optimum value of the parameters, we solved another optimization problem to identify a candidate λ_1 and λ_2.

$$\{\lambda_1^*, \lambda_2^*\} = argmin\ 100\left(\frac{\sum_{t\,\epsilon\{\Delta,2\Delta,\ldots\}}(y_m(t)-y(t))^2}{\sum_{t\,\epsilon\{\Delta,2\Delta,\ldots\}}(y(t))^2}\right) \tag{12}$$

This sequence of two optimizations was iterated until either the termination conditions prescribed in terms of convergence on the objective function or maximum iterations was satisfied. Importantly, the initial condition of $x(t)$ and relevant initial guesses required to commence the optimization for all of the piecewise discontinuous segments (except for the first) were derived from the result of the optimization on the previous segment. For the monkey data analyzed here, three segments were sufficient to capture the polyphasic dynamics. The aforementioned optimization problems were solved using the *fmincon*() function present in Matlab's Optimization Toolbox.

4.3.6 Optimal Control Design

We developed a feedback control paradigm to regulate the ratio marker by real-time adjustment of the propofol infusion rate. In order to employ a discrete time closed-loop control strategy, we used a Linear Quadratic Regulator (LQR) paradigm as it is well-established for optimal control. In this framework, we sought to determine a sequence of infusion rates that minimized a loss function. This loss function was posed as a sum (over all discrete time points) of weighted contributions of quadratic forms described on the deviation of latent state variables and infusion rates from their respective nominal or target values. The optimal control signal was a linear function of the estimate of the state variables.

We assumed that the infusion rate remained constant in time between two consecutive control inputs. Since the observation is inherently noisy and the initial condition (state estimate where the auto-pilot is activated) is uncertain, we used a stochastic estimation technique to filter the signal and calculate the state estimate. The corresponding estimates of the hidden state variable, representing a measure of anesthetic amounts in the effect compartment, came directly from directly from the PK-PD model (Equations 9, 10, 11, 12). As the observation model and state models were nonlinear, we used a Kalman Filter to estimate the states of the linearized model (where linearization is affected about the prescribed values of the target and corresponding steady state). This permitted determination of the best estimate to minimize the estimation error covariance.

From these observation and state modes, we developed the control scheme. We represented the dynamic equations in discrete time with zero-order hold over a sampling interval of h,

$$\delta b_k = A\delta b_{k-1} + B\delta u_{k-1} + w_k \tag{13}$$

$$\delta y_k = C\left[\delta b_{1,k}, \delta b_{2,k}\right]^T + v_k \tag{14}$$

where, $\delta(x) = x - x_0$, where x_0 denotes the target response of from the nominal model, A is the state transition matrix, B is the input scaling matrix, and C is the latent state scaling matrix. The system matrices were as follows,

$$A = \begin{bmatrix} e^{h\lambda_1} & 0 \\ 0 & e^{h\lambda_2} \end{bmatrix};\ B = \begin{bmatrix} \frac{e^{h\lambda_1}-1}{-\lambda_1} \\ \frac{e^{h\lambda_2}-1}{-\lambda_2} \end{bmatrix};\ C = [c_{11}, c_{12}] \tag{15}$$

We assumed w_k and v_k to be zero-mean Gaussian white noise with covariances W and V, respectively. We considered a state-feedback based control action of the following form,

$$u_k = u_o - K_c[\hat{b}_{k|k} - b_0] \tag{16}$$

where K_c denotes the control gain and u denotes the infusion rate (mg/min). The states b_k were estimated using an observer such that the filtered estimate $b_{k|k}$ is given by,

$$\delta\hat{b}_{k|k} = \delta\hat{b}_{k|k-1} + K_e(\delta y_k - C\delta\hat{b}_{k|k-1}) \tag{17}$$

where K_e denotes the Kalman gain matrix. The control gain K_c is the linear quadratic regulator (LQR) gain that minimizes the quadratic performance metric,

$$\sum_{k=1}^{\infty} \delta\hat{b}_{k|k}^T Q\delta\hat{b}_{k|k} + \rho\delta u_k^2 \tag{18}$$

Therefore, the control problem was parameterized by both the parameters characterizing the Kalman filter (W, V) and the LQR control scheme (Q, ρ). The estimator and control gains were evaluated using Matlab functions *dare()* for solving the discrete algebraic Riccatti equation necessary for subsequent Kalman gain calculation and *lqr()* for generating LQR gains. This framework ensured that the simulation studies preceding *in vivo* experiments would properly establish the properties of the controller for a given animal.

4.4 Results

4.4.1 Dynamic Changes in Power and Spiking Rate in Prefrontal Cortex During Propofol Anesthesia

We found characteristic dynamics of propofol GA reflected in the spectrograms and spectral power estimates from the LFP as well as in the ensemble neural spiking activity (Figure 4-2). As previously reported, ensemble firing rates decreased during propofol GA,

reaching lowest baseline rates between LOC and ROC (Lewis, et al., 2012; Ishizawa, et al., 2016). The onset of propofol infusion triggered an elevation in broad beta (12-25 Hz) LFP power, along with an increase in lower frequency slow and delta oscillations (0.1-0.5 Hz and 0.5-4 Hz, respectively). In addition, the higher frequency gamma oscillations (25-34 Hz) decreased throughout propofol anesthesia. These trends reversed upon the cessation of propofol infusion and before ROC. These frequency-specific power changes are broken down in Figure 4-2B.

We next analyzed the changes in the ratio marker juxtaposed with the propofol infusion trajectory and the ensemble spiking activity (see methods section 4.3.3 and 4.3.4). The ratio marker displayed consistent dynamics across sessions that were robust to the power fluctuations in individual frequency bands as well as across-session variability in noise and baseline power values (Figure 4-2B, bottom row). We also verified that the time-trace patterns were consistent across multiple channels of a given multielectrode array. Furthermore, the LFP power changes were sufficiently similar across both prefrontal arrays (Figure 4-3, left vs. right columns), allowing for any particular channel to be selected to calculate the effective ratio marker to characterize the states of GA.

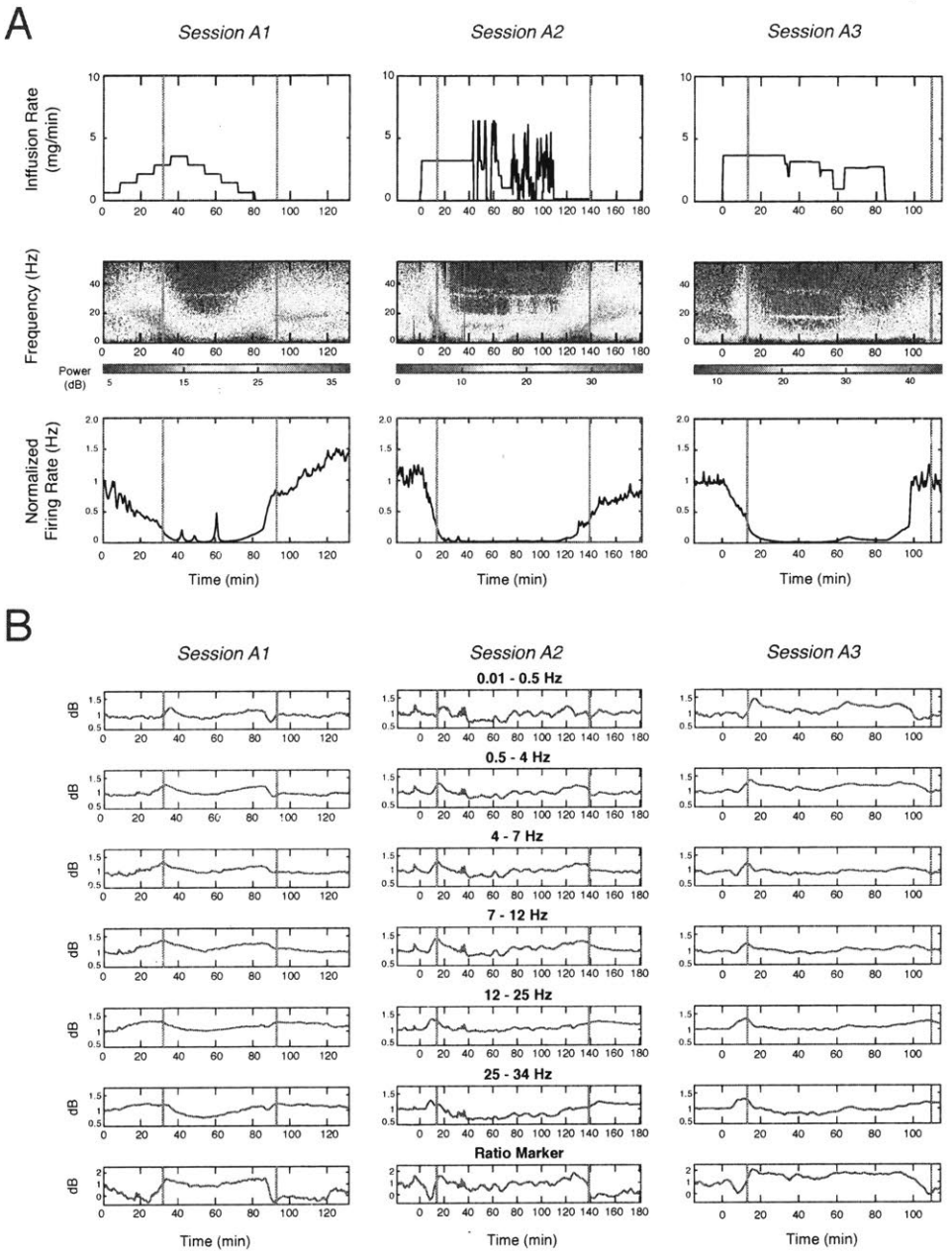

Figure 4–2: A, Neural dynamics across propofol anesthesia sessions. Each column indicates a single session in subject A (A1, A2, A3) under a given infusion protocol (top row), demonstrating single channel LFP spectral responses (middle row) and baseline normalized ensemble spiking rates (third row). **B**, Frequency specific spectral and ratio marker changes for each session (same columns as above). Upper rows show baseline normalized power in frequency bands: <0.5 Hz, 0.5-4 Hz, 4-7 Hz, 7-12 Hz, 12-25 Hz, and 25-34 Hz. The last row is the ratio marker. LOC and ROC are respectively marked by magenta and red solid vertical lines.

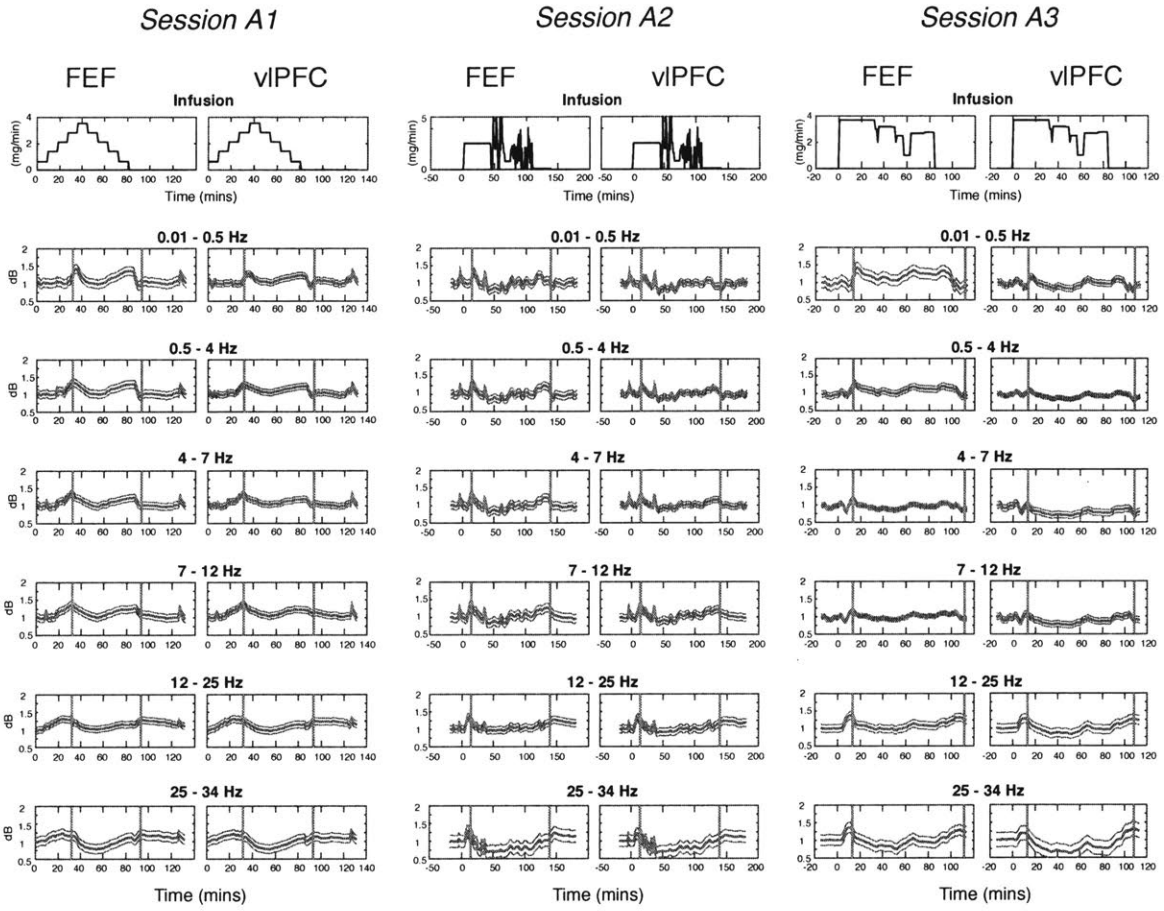

Figure 4–3: LFP power from FEF and vlPFC compared in three anesthesia sessions in Subject A. For each session, band-wise spectral activity shown for an electrode in FEF (left column) and vlPFC (right column). The first row presents the drug infusion protocol in mg/min. Subsequent rows trace the average (across all channels) baseline-normalized power in frequency bands, <0.5 Hz, 0.5-4 Hz, 4-7 Hz, 7-12 Hz, 12-25 Hz and 25-34 Hz. Confidence bounds (red lines) equal the mean ± standard deviation. LOC and ROC are respectively marked by magenta and red solid vertical lines.

4.4.2 Ratio Marker Demonstrates Polyphasic Trends

The ratio marker demonstrated a wide dynamic range as it modulated across individual sessions of propofol GA. Most prominently, the ratio marker exhibited polyphasic trends whereby the increasing drug infusion caused the marker to switch directions. In all subjects, the ratio marker displayed an initial decrease at low doses and then rose with increasing dose until a saturation point was attained. This polyphasic marker pattern was consistent across multiple monkeys and multiple sessions for a given monkey for which an identical stepped-dosing regimen is employed (Figure 4-4).

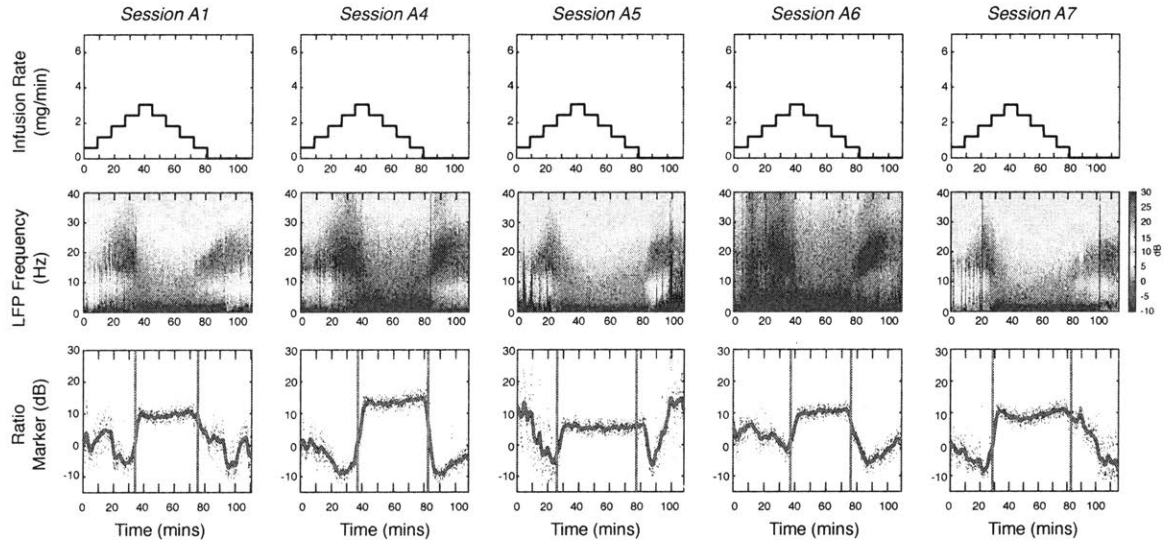

Figure 4–4: Robust polyphasic features of the ratio marker across sessions in subject A. Displayed for each session are the infusion rate (top row), a multitaper spectrogram from a single channel from within FEF (middle row), and a fixed-interval smoothed ratio marker estimate (blue solid line) atop the raw marker data (blue dots) (bottom row). LOC and ROC are respectively marked by magenta and red solid vertical lines in the ratio marker plots.

The polyphasic nature of the ratio marker was not dependent on the increasing, fixed-stepped dosing regimens of propofol. When the dosing regimen was altered to constant fixed-rate infusions, irregularly stepped dosing regimens (e.g. variable fixed rate

infusions), or even instantaneously-variable open or closed-loop infusion paradigms, the ratio marker retained the same polyphasic characteristics (Figure 4-5). Thus, no matter no infusion settings, the marker appeared to decrease below the baseline values before increasing after the animal lost consciousness. Similarly, the inverse trend appeared after drug cessation irrespective of the preceding dosing regimen.

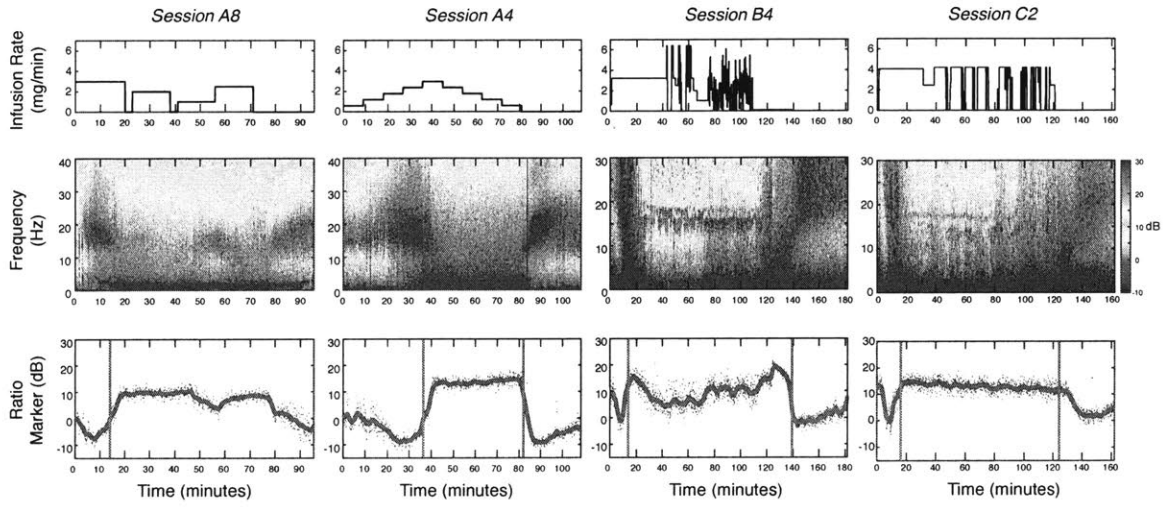

Figure 4–5: Polyphasic features of anesthetic marker during induction phase across subjects and dosing schemes. Displayed for each session (columns) are the infusion rate (top row), a multitaper spectrogram from a single channel from within FEF (middle row), and a fixed-interval smoothed ratio marker estimate (blue solid line) atop the raw marker data (blue dots) (bottom row). The left and right vertical magenta-colored dashed lines overlaid on the marker data indicate the time points for LOC and ROC, respectively.

To analyze the polyphasic nature of this marker across individuals, we calculated the filtered estimate $\hat{x}_{k|k}$ using the procedure described in section 4.3.3 for 10 general anesthesia sessions (Figure 4-6). We calculated the dynamic difference estimate, $\hat{x}_{k|k}\ \hat{x}_r$, where $\hat{x}_r$ represents the estimate of the marker during the awake baseline phase. The baseline mean μ_r and variance values σ_r^2 were determined by averaging the mean and variance from all time points less than or equal to h, where h was the time-resolution at

which the spectral markers are calculated. In each session, we identified a time-point t_1 corresponding to the minimum value of this difference estimate across all the time-points in the epoch 5 minutes after drug start. We identified a second time point t_2 corresponding to the maximum value of this difference estimate across all the time-points in the portion of the same epoch that exceeds t_1.

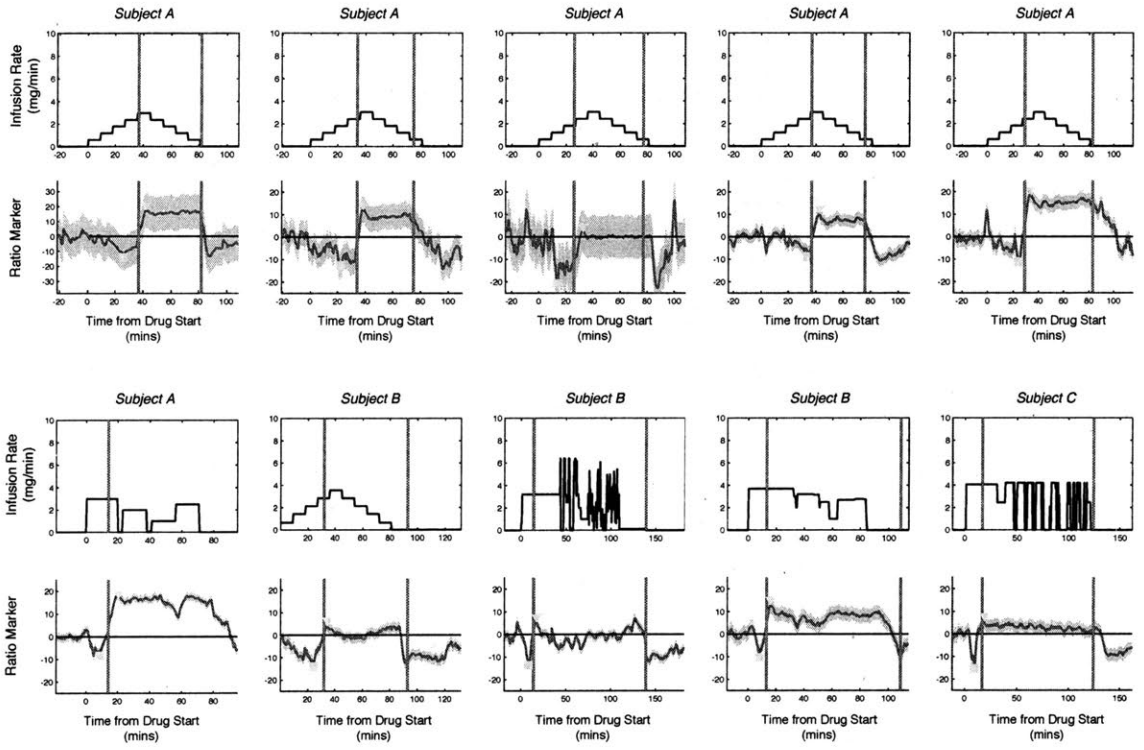

Figure 4–6: Marker data from ten sessions in three subjects. Each subfigure comprises a top and a bottom panel illustrating the time-trace of the infusion protocol and of the difference between the filtered estimate and its baseline value along with the associated 95% confidence interval. For each session, time points t_1 and t_2 are represented as a solid turquoise square and triangle, respectively, on the difference marker estimate curve. LOC and ROC time points indicated by the magenta and red colored solid vertical lines, respectively.

The ratio marker necessarily centered around a value of 0 in the early portion of the awake state. The difference between the marker estimates and the baseline value corresponding to t_1 and t_2 across 10 recording sessions. Across all sessions and subjects,

the marker significantly decreased and then increased across the two interval segments as the animal progressed into unconsciousness ($p < 0.00017$, two-sided Wilcoxin Rank Sum Test; Figure 4-7A). We next asked if the time of LOC always occurred during the polyphasic inflection point in the marker. By comparing t_1 and t_2 values with the corresponding LOC time-point across 10 sessions we concluded that the interval (t_1, t_2) includes the behavioral time-point t_{LOC} ($p < 0.00018$, two-sided Wilcoxin Rank Sum Test; Figure 4-7B). In other words, t_1 and t_2 defined the piecewise time interval within which LOC occurred. Together, these analyses demonstrate that before LOC the marker decreased below the awake baseline and then continued to rise, through LOC, and ultimately increased higher than the marker values during the awake state.

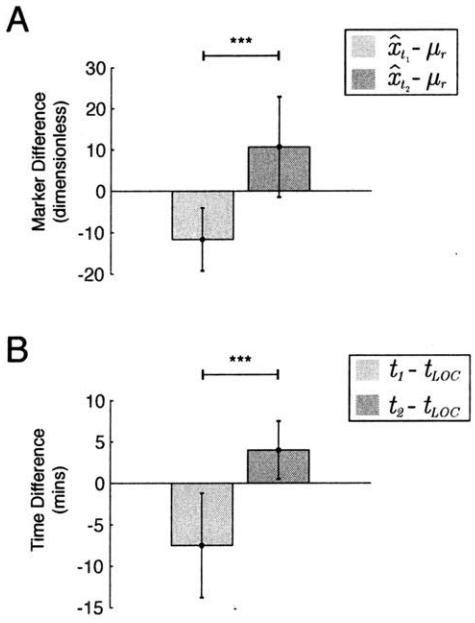

Figure 4–7: Polyphasic flip in the ratio marker around LOC. Bar plots with 95% confidence intervals showing **A** $\hat{x}_t$ - μ_r for the marker difference from baseline before LOC (green) and post-LOC (orange), and **B** $t - t_{LOC}$ for the time difference from LOC to marker minimum (green) and maximum (orange). Asterisks indicate significant pairwise difference ($p < 0.0001$, Two-Sided Wilcoxin Rank Sum Test).

4.4.3 Pharmacodynamic Modeling of Single Channel LFP

A state space model (SSM), essential for subsequent control design, was used to develop a mathematical description relating the evolution of the ratio marker to the drug dynamics. The logical sequence used to develop the model is outlined in Figure 4-8. The state equations were based on a two-compartment mammillary pharmacokinetic model (Figure 4-8A). The central compartment received the drug infusion u_k with the drug and functioned to clear the drug (e.g. hepatic clearance, the primary mechanism of propofol breakdown). The central compartment was reciprocally connected to a second compartment to simulate diffusion across the blood-brain-barrier. The second compartment dynamics were modeled as the drug state in the brain (Struys, et al., 2000). The estimated model thus reflected the following relationship: the gradually increasing value of effect site drug amount, x_k, was a consequence of the constant non-decreasing drug infusion, u_k, in the induction time range considered and the assumption of a linear dynamical system (the two-compartment pharmacokinetic model).

In order to fully capture the polyphasic marker dynamics of general anesthesia, we utilized multiple independent functions to fit the ratio marker. The associated pharmacodynamic estimate comprised three piecewise continuous and monotonic sigmoidal functions fitted to the ratio marker observation. These functions modelled the marker for these particular state equations (Figure 4-8D). A key benefit of such models was that the parameters provided session-specific summary statistics for further analysis. The combined PK-PD model when fit to ratio marker data across multiple sessions (as shown in Figure 4-9) yielded both an estimate of the plausible drug dynamics in the brain (effect site dynamics) as well as an approximation of the nonlinear dynamics of the ratio marker under a non-decreasing propofol induction (refer to section 4.3.5 for methodological details). In all subjects and sessions, the model fits across multiple sessions

of propofol anesthesia captured the true underlying dynamics (Figure 4-9). The effect site drug concentration (dashed pink line in Figure 4-8C, Figure 4-9) increased as the ratio marker displayed polyphasic features during the induction epoch. Thus, even as the marker changed its directionality in the course of general anesthesia, the PK-PD model was robust to such fluctuations.

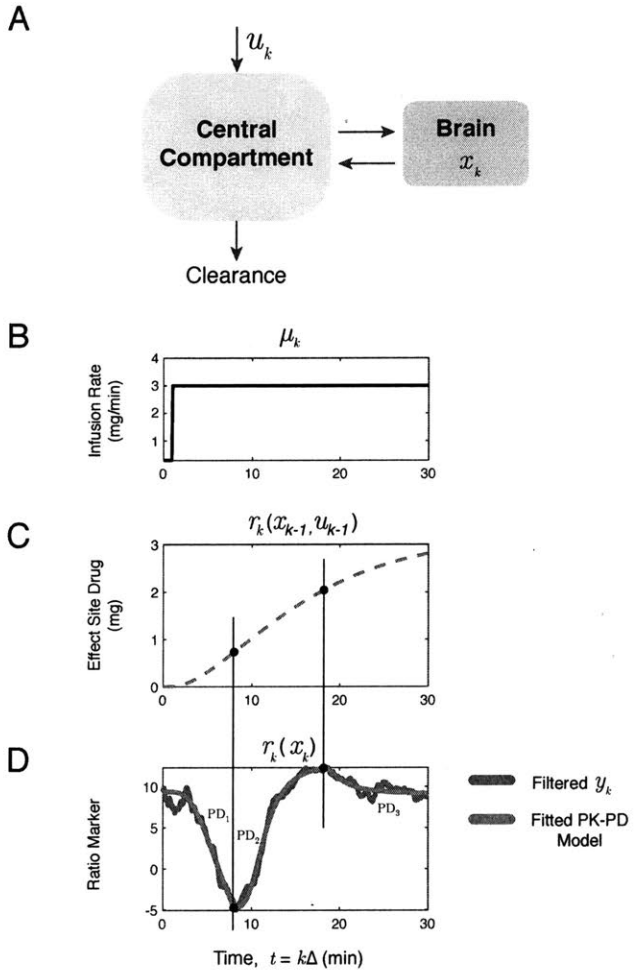

Figure 4–8: Illustration of modeling scheme. **A** two-compartment PK-PD model with infusion rate u_k and hidden state-variable x_k. **B** Propofol infusion rate over experiment session. **C** Effect site drug amount (mg). **D** PK-PD model fit (red solid line) and the hidden state variable x_k map to the filtered ratio marker y_k (solid blue line) via three piece-wise continuous sigmoid functions (PD_1, PD_2, PD_3).

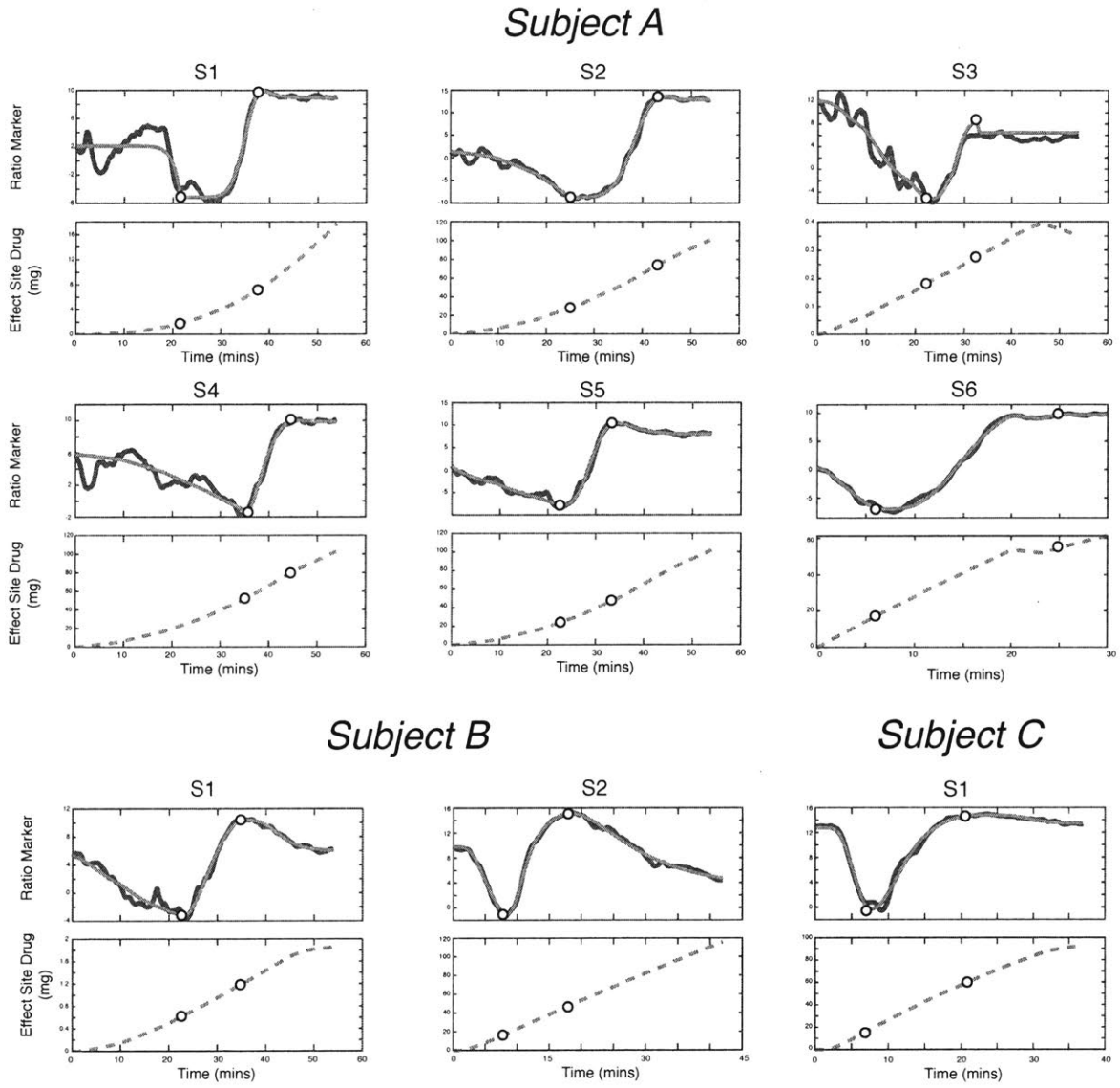

Figure 4–9: PK-PD model for marker dynamics during induction of general anesthesia. In the top panels, the smoothed PK-PD model (red solid line) is displayed atop the measured ratio marker (blue solid line), starting at the time of drug infusion. The segments in the triphasic model are marked as yellow circles on each plot. In the corresponding lower panels, the effect site drug amounts are shown as the dashed pink lines for same time interval.

4.4.4 Closed-loop Control of the Ratio Marker

Given the PK-PD stability and generalizability displayed across sessions and subjects, we hypothesized that we could modulate the model parameters to automatically control the level of general anesthesia via the spectral ratio marker. Thus, we used the PK-PD model estimates to build a nominal model for control design (Figure 4-10; Methods 4.3.5, 4.3.6).

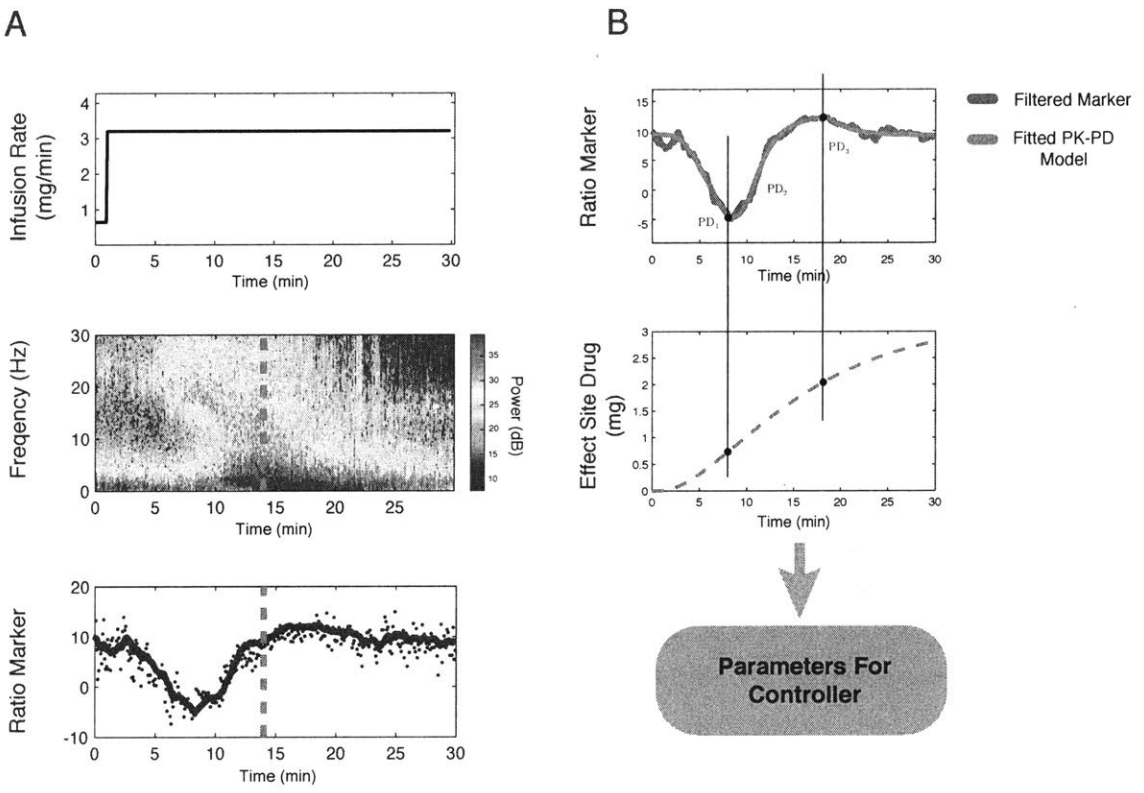

Figure 4–10: Parameter estimation using experimental data and computer simulation of control. Subfigure (numbered from top to bottom) **A**, top to bottom: pre-planned infusion rate programmed into the syringe pump, spectrogram from a single FEF channel LFP recording, and the observed marker (blue dots) and the smoothed estimate (solid blue line) **B**, System Identification. PK-PD model from the ratio marker provided an estimate of the hidden state variable (effect site anesthetic amount, pink dashed line) and output the set of model parameters used by the controller. PD_1, PD_2, PD_3 refer to the 3 piecewise continuous and monotonic sigmoidal functions fitted.

Using the PK-PD model estimated from the non-human primate experiments, we next sought to validate in silico implementation of the CLAD system (Figure 4-11). The CLAD system was implemented using a linear quadratic regulator strategy, with the ratio marker value of 10 known *a posteriori* to define the post-induction unconscious state. Following an induction period with open loop control (fixed rate infusion), closed-loop control was engaged to restore the ratio marker to the target value (10) and maintain the unconscious state for a period of 60 minutes. We found that the model successfully controlled the marker to reach the target state. Interestingly, the model initially turned off the drug entirely for several minutes to drive down the effect site propofol and raise the ratio marker. Shortly thereafter, real-time manipulation of the infusion rate took over to facilitate target marker approximation. The difference between the ratio marker and the target followed a linear trend, decreasing over the course of the closed-loop control (Linear Model, $R2 = 0.711$, $F(1,848) = 2089.75$, $p < 6.73e\text{-}231$). Thus, the infusion rate was modulated such that over time the ratio marker significantly converged to the target marker and maintained about this value for the duration of the experiment. The infusion rate fluctuations permitted this convergence even as the effect site drug amount continued to decrease. These results established the feasibility of implementing a subject-specific CLAD system for successful anesthetic state control, whereby the drug infusion is driven by the model for the physiological ratio marker and not simply the effect-site pharmacokinetics.

Next, we sought to demonstrate that this closed-loop regime could accurately and safely be implemented in living subjects with propofol anesthesia. We successfully deployed this control scheme in actual closed-loop experiments on an otherwise healthy rhesus macaque. The results from a session of closed-loop anesthesia control session are presented in Figure 4-12. Following an open-loop period of fixed rate propofol infusion,

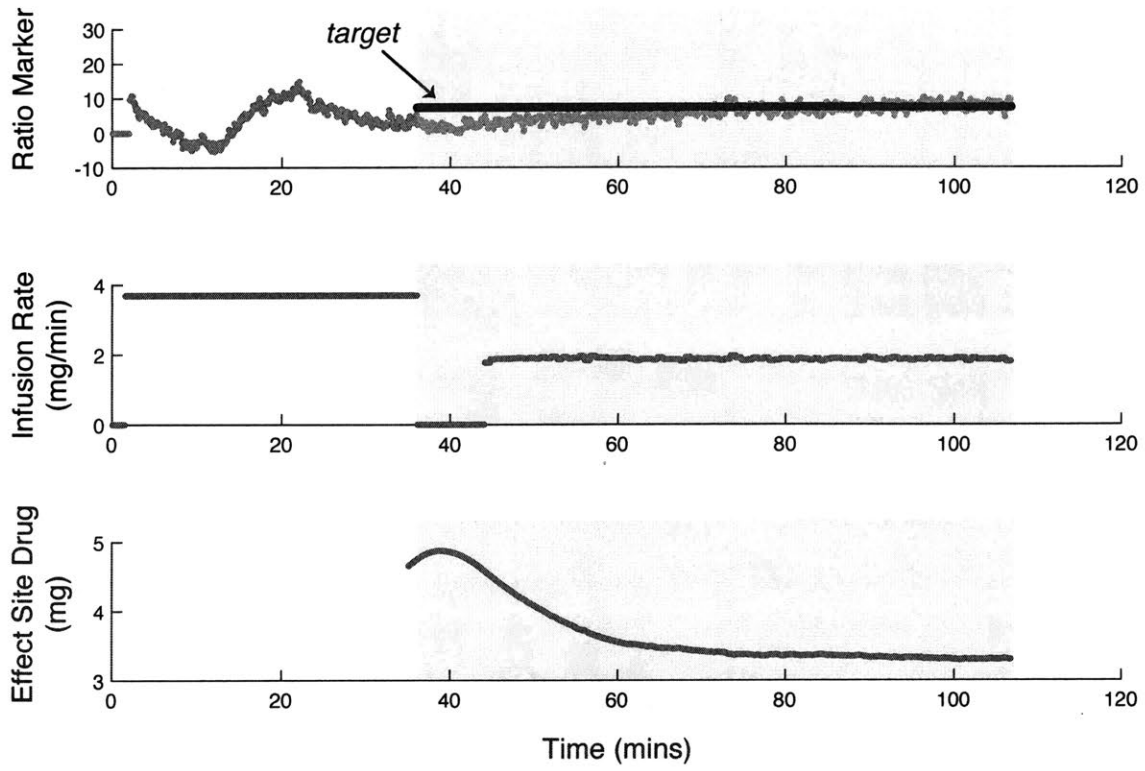

Figure 4–11: *In silico* CLAD simulation example with closed-loop control period (shaded yellow epoch). Top panel: simulated ratio marker (red line) tracks the target ratio marker (black solid line). Middle panel: Infusion rate (blue solid line) is fixed in open loop mode and fluctuates during CLAD. Bottom Panel: effect site drug concentration (blue solid line) during simulated CLAD.

the monkey lost consciousness and cardiovascular stability was maintained. The closed-loop portion of the experiment followed subsequently, with the ratio marker target set to a fixed value for maintained unconsciousness. During the CLAD epoch, the ratio marker significantly approximated the target (Figure 4-12A) through rapid adjustments of the propofol infusion rate (Figure 4-12B). The infusion rate modulation was sufficient to both undershoot and overshoot the target marker value as the model state was updated. Nonetheless, the ratio marker converged to the target marker and unconsciousness and physiological stability was safely and steadily maintained. To quantify the CLAD system's

ability to approximate the ratio marker, we explored the instantaneous difference from the actual marker to the target value. For the period of closed-loop control, we calculated the relative tracking error, the instantaneous marker difference normalized by the target marker value. The 95th percentile of the absolute value of the relative tracking error for the *in vivo* CLADS session was 0.1290, which implies that 95% of the time the relative error was within 12.9% of the target. Over this epoch, the population mean of the error distribution did not significantly different from 0 (Figure 4-12C, empirical probability density function with mean = 0.0496, standard deviation = 0.0556), indicating that the CLAD system significantly tracked the target marker.

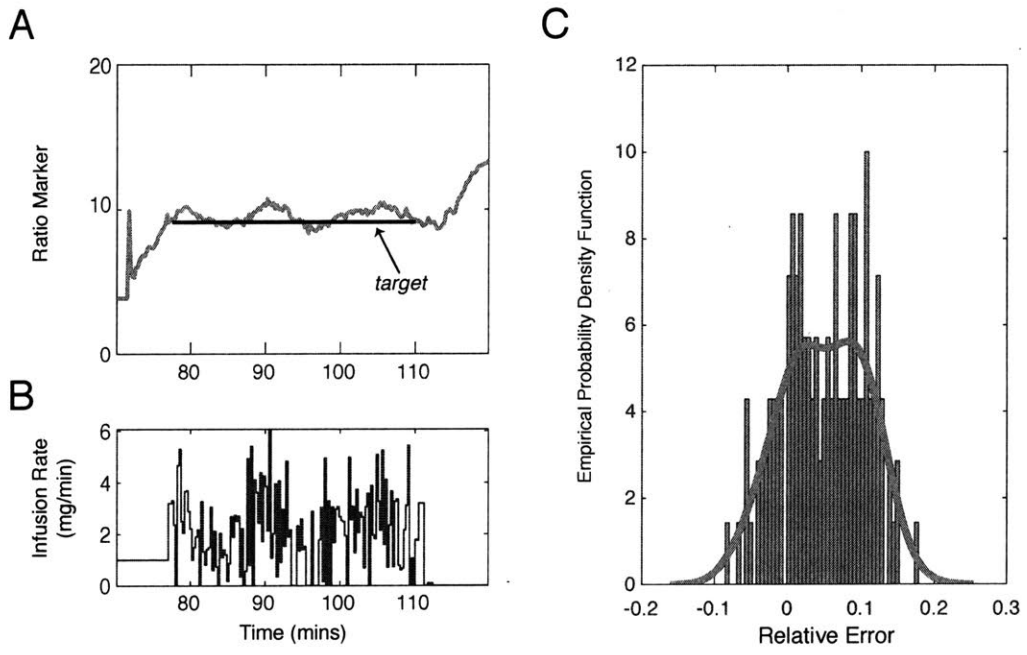

Figure 4–12: Data from CLAD session in Subject B. **A**, Marker trajectory (red line) and the target value to track (black line). **B**, Drug infusion rate during closed-loop control mode. **C**, Empirical probability distribution histogram with 50 msec bins (green) with overlaid kernel density plot (red solid line) of the relative tracking error, (Marker - Target)/Target.

4.5 Discussion

We developed a theoretical framework and practical methodologies to formally evaluate and deploy a system for closed-loop control of general anesthesia in primates. To support our framework, we first quantified the spectral properties of prefrontal neural activity in multiple infusion protocols with propofol general anesthesia. In the recorded LFPs, higher frequency oscillations (14-30 Hz) first increased after drug administration, before decreasing later into the infusion. Low frequency oscillations (< 4 Hz) on the other hand, increased with propofol. Together, the ratio of power in $0.1-4$ Hz band to that in $14-30$ Hz band captured the dynamics at each of the different stages of propofol anesthesia. Next, we showed that a Kalman Filter of this instantaneous power ratio provides a smoothed estimation of the hidden state and provides a reliable biomarker of sedation level. This filtered estimate, the ratio marker, provided an ideal target for optimal control via an LQR strategy. Through both *in silico* and *in vivo* macaque experiments, we validated the stable regulation of the ratio marker about a setpoint and successfully demonstrated closed-loop control of GA in a primate model. The strength of our non-human primate CLADS model ultimately arose synergistically from the spectral properties of the neural dynamics observed under GA, the identification of a successful biomarker target, and the proper control paradigm.

The choice of the relevant signals for the characterization and control of unconscious states has not always been entirely obvious in CLAD system development. Detailed pharmacokinetic and pharmacodynamic modelling has not proved sufficient on its own to support successful CLAD systems capable of use in routine clinical care (Liu & Rinehart, 2016; Shafer & Gregg, 1992). Much of the work in the field continues to focus on maintaining closed-loop control of serum drug levels in humans or monkeys (Mage, et al., 2017; Karnik, 2017; Hom, et al., 1999). It is, after all, the first measurable and most

accurately titrated metric. Maintaining specific target serum concentrations is especially useful in pharmacological use cases whereby infused agents are intended to penetrate tissues in an appropriate therapeutic range that maximizes efficacy and minimizes toxicity (e.g. antibiotics or chemotherapy drugs). In these cases, the circulating serum concentration values recorded are either the desired end-target or a reliable proxy for the concentrations of an agent in a connected compartment (e.g. kidney, liver, bone, etc.). The approaches used in these types of studies, while increasingly efficacious and technically rigorous, are less reliable in translating to the regulation of physiological functions in general. For controlling complex neurophysiological states of consciousness, they are insufficient. To effectively link PK-PD models to neurophysiological states, a focus is emerging on recording neural activity patterns using EEG to better define the drug-effect relationships.

The selection of the proper target marker has encumbered CLADs work to date. EEG provides feasibility and an optimal route to obtain real-time information on levels of sedation and unconsciousness directly from the target organ. Yet, the activity patterns observed, while profoundly altered with anesthesia, do not give rise to an obvious target biomarker. As a result, spectral indices from the EEG have been employed as physiological biomarkers to characterize unconsciousness states with the monitoring markers like spectral entropy, 90% spectral edge frequency, median frequency, and alpha and beta frequency power parameters in propofol infusion (Mahon, Greene, Greene, Boylan, & Shorten, 2008; Schwilden et al., 1989; Tonner & Bein, 2006). The most widespread and utilized indices of unconsciousness are the bipspectral indices used in commercial products such as the BIS monitor (Medtronic plc, Minneapolis, MN) or the SedLine monitor (Masimo, Irvine, CA). These algorithms report a metric of consciousness on a scale of zero to one-hundred, integrating a proprietary ratio of high to low frequency algorithms. While these devices are commonplace in operating rooms across the globe, the

bispectral index notoriously can give rise to values that do not reflect the true physiological state of sedation or unconsciousness (Dahaba, 2005).

Our PK-PD model successfully characterized the drug-effect relationship through our robust ratio marker, which dynamically characterizes the relationship of high and low frequency oscillations across the different epochs of propofol anesthesia. In our approach, a Kalman filtered estimate of the 0.1−4 Hz band to the 14−30 Hz band LFP served as a robust biomarker of sedation level with distinct characteristics at different levels of sedation. Since the ratio-marker was sensitive to the drug-dose fluctuations, we could analyze this biomarker using pharmacokinetics-inspired second-order state space models where the observation is given by a nonlinear sigmoidal function. We fitted this model to the time-series data of biomarker and drug infusion from each anesthesia session. This importantly established our paradigm to be stable across individual sessions and across different monkeys, permitting variability in both signal and noise differences. One reason this is particularly critical is because specific models are often required for specific age ranges, perhaps due to pharmacodynamic differences between different aged individuals (Chakravarty et al., 2017; Marsh, White, Morton, & Kenny, 1991; Schnider et al., 1999). Our method avoids this. Using initial estimates from prior data, we learned the model parameters from an initial segment of the ratio marker during a single session. Whereas most CLAD models restrict and standardize parameters across individual sessions, our session-specific model was used in the closed-loop anesthesia control for the session from which it was built. While LFP is not equivalent to EEG recordings, it is unlikely that our paradigm generalizes because the ratio marker derives from high resolution estimates of the electrical fields from within the parenchyma of cortex. The frequencies of neural activity we used for our ratio marker are commonly observed in superficial EEG recordings, unlike high gamma activity (>80 Hz) which is not reliably obtained from

outside of the skull. The success of our system was more likely bolstered by the strength of our real-time control scheme to allow for inter-subject reliability.

The control scheme that we developed was an LQR with states estimated from data via a Kalman Filter was able to track the sedation state in real-time and control the hidden state with minimal latency. In traditional CLAD systems, it often takes substantial time to analyze and report the ongoing state, making neuromonitoring challenging for both rapid manipulations of level of sedation as well as accurate forecasting of a patient's state based on a delayed marker reading (Kreuzer et al., 2012; Pilge et al., 2006; Zanner, Pilge, Kochs, Kreuzer, & Schneider, 2009). In our system, we consistently converged on the target marker value because we penalized the deviation of the drug infusion about a steady state value and allowed our drug infusion rate to change a very fast rate. Furthermore, it is well known in literature that the discrete time LQR with the application of the Kalman Filter on the linearized model leads to a beneficial situation where the design of the controller and the estimator can be separated by virtue of the separation theorem. The implication is that when we attach the controller that is optimal with respect to the deterministic model in sequence with a Kalman estimator, the combined stochastic control problem is still optimal in the sense that it minimizes the ensemble average of the loss function used in the LQR strategy. In other words, unlike in commonly used proportional integral controllers, we could optimize the tradeoff between the competing costs of target tracking and actuation to provide stable feedback control. Furthermore, the principled design paradigm developed for the single input single output (SISO) case here can be generalized to the multi-input multi-output (MIMO) case to extend the current CLAD design paradigm to simultaneous administration of multiple drugs and multiple physiological observations. Opioids, benzodiazepines, ketamine, and dexmedetomidine have each been shown to have distinct spectral characteristics in EEG,

suggesting they could be independently controlled in an automatic manner through our LQR scheme (Akeju et al., 2016; Billard, Gambus, Chamoun, Stanski, & Shafer, 1997).

To our knowledge, we have implemented the first closed-loop propofol anesthesia study in monkeys. We created a PK-PD model to relate the drug infusion rate to the dynamics in the LFP band-specific power for rhesus macaques without the need of PK parameters from a separate pharmacokinetic study. In prior CLAD models for humans, the PK parameters are derived from systematic pharmacokinetic studies where the plasma or blood samples are collected over multiple time points after the administration of a bolus dose. Similarly, the most detailed pharmacokinetics study of propofol in non-human primates had previously been a single study evaluating the effects of a single a single propofol bolus. A macaque CLADS model now enables us to repeat experiments and obtain replicable data, an impossible task to perform in human patients. It is simply not tractable and is unethical to explore the broad parameter space for CLAD systems on a single human patient, let alone at scale. Additionally, macaques permit the flexibility of acquiring population neural activity data in the form of LFPs and spiking activity from numerous microelectrode arrays surgically implanted at multiple sites in cortex. This expanded recording setup allows sampling distinct neuronal subpopulations that could give rise to features without contamination from volume-conducted field potentials from neighboring regions. Moreover, the LFP features at the microscale were sufficiently uniform to sample from any particular electrode within of PFC and still get stable closed-loop control. The fact that prefrontal LFP from a random recording site can support CLADs further solidifies the significance of the monkey model for closed-loop GA.

Future steps to improve the control paradigm can drive better performance with tighter tracking of the target setpoints and guaranteed stability robustness. One likely way to accomplish this would be to adapt the control design to utilize a two-degree of freedom controller with integral action. The ratio marker derivation can also be modified,

perhaps with a new variable added to the model, with updates reflecting the discovery that a 17 Hz beta band emerges in propofol GA in monkeys. Accomplishing this will enhance the translation to humans, which have the prominent alpha oscillation in the same stage of GA. Furthermore, more complex control schemas can be more confidently developed with different dosing levels and earlier closed-loop control takeover in the procedure. Because the ratio marker consistently dipped and then increased above baseline following propofol administration, LOC can likely be detected and even predicted as the marker takes on a polyphasic shape. Ensuing experiments could begin surgical interventions after this time point, predicted fully by the ratio marker. This would serve as the ultimate test of safe and sufficient GA control before bringing a complete solution to the human operating room or intensive care unit.

The main motivation of closed-loop anesthesia delivery (CLAD) systems is to automatically titrate the drug to maintain the desired plane of anesthesia required for a given medical or surgical procedure. These automated systems aim to provide dynamic, patient-specific titration without inappropriate and dangerous oversedation or undersedation. As a result, clinical CLAD systems would enable anesthesiologists to focus on higher-level tasks with the same level of efficiency over a prolonged surgical procedure (Dussaussoy et al., 2014). Furthermore, the incorporation of such systems in clinical practice could lead to the standardization of anesthetic administration across multiple clinical sites and dramatically improve patient morbidity and mortality (Puri et al., 2016). Overall, our research here serves the dual purpose of advancing the existing CLAD technology toward these collective goals and of establishing a non-human primate model for testing CLAD systems prior to use in patients. While our studies here were developed with a focus on monkey LFP dynamics in propofol anesthesia, the modular steps and principled sequential approach directly translates this design paradigm for use in humans and in the automatic control of other anesthetic drugs.

Chapter 5

Conclusion

5.1 Summary of Results

We investigated the effects of different anesthetic agents on the at the scale of neural networks. The major findings are reviewed in Table 5.1. In Chapter 2, we explored the mechanisms of propofol general anesthesia. We found that slow oscillatory (< 4 Hz) power increased across cortical regions after monkeys lost consciousness. Despite that large slow oscillations emerged across brain regions, the slow oscillations were not globally coherent. In fact, we saw a unique mixture of synchrony and asynchrony on our electrodes: spike rates were more correlated of longer time scales than shorter ones. But rather than global cortical hypersynchrony, there was a heterogeneous mixture of increased and decreased synchrony that frequently fragmented cortex into a mosaic of areas that were "on" and "off" at different times. In the awake state, delta-band coherence between recording sites was weak and based on anatomical proximity: Stronger within an area or between neighboring regions (i.e. FEF–vlPFC, Figure 2-2C left, diagonal squares, mean pairwise coherence between electrodes). After LOC, there was a significant increase in delta-band coherence within areas but a heterogeneity across areas that defied anatomical

proximity. Electrical stimulation of the central thalamus immediately and continuously reversed the behavioral and physiological effects of GA. We attribute this to the arousal system being engaged via thalamic stimulation.[4]

In Chapter 3, we found that ketamine anesthesia brings upon a hyperexcited brain state characterized by gamma bursts and intermittent DOWN-states. This gamma rhythm flows upstream through cortical networks under ketamine anesthesia, from early sensory areas toward prefrontal cortex. In contrast, the awake state beta rhythms (12-30 Hz) that functionally connected parietal regions to other cortical regions, were entirely wiped out by ketamine anesthesia. Prefrontal cortical spiking activity uniquely entrained activity in the intralaminar thalamus, a major hub in the arousal pathways.

In chapter 4, we developed a principled PK-PD model in which we use a Kalman filtered estimate of a biomarker recorded from the LFPs of macaque PFC to track depth of general anesthesia. We successfully were able to model these parameters in silico linked to a closed-loop controller regime to demonstrate the utility of our biomarker in CLAD systems. We ultimately linked our algorithmic framework to a drug-pump and a living macaque to perform closed-loop CLAD experiments whereby the depth of anesthesia of was automatically controlled.

Finding	Figure
In propofol GA, LFP low frequency power increases and high frequency power decreases cortex-wide	2-2
In propofol GA, slow oscillations are fragmented across cortex such that they are incoherent across PFC while synchronized between PFC and PPC.	2-2
In propofol GA, spike rates decrease and are less globally correlated across brain areas with smaller time windows.	2-2D

[4] We utilized this knowledge of the power of the adrenergic arousal system to search for novel pharmaceutical agents that could reverse general anesthesia. We successfully discovered one such agent and are developing it for human use. See Appendix C for patent application: *Methods For Evaluating Treatments and Physiology in Human Patients Using Intravenous Alpha-2 Adrenergic Antagonist Agents.*

In propofol GA, electrical stimulation of the central thalamus immediately reverses the behavioral and neurophysiological effects of GA.	2-4
Ketamine increases global cortical gamma power and spiking and local coherence	3-1
Ketamine gamma rhythms flow from sensory areas toward PFC	3-2
Ketamine causes PFC spiking to entrain central thalamic oscillatory activity	3-4
Closed-Loop Control in a living rhesus macaque	4-12

Table 5-1: Summary of major findings.

	Slow/Delta (0.1 – 4 Hz)		**Beta** (13 – 25 Hz)		**Gamma** (35 - 80 Hz)	
	Propofol	**Ketamine**	**Propofol**	**Ketamine**	**Propofol**	**Ketamine**
FEF	↑	↑	N/C*	↓	↓	↑
vlPFC	↑	↑	N/C*	↓	↓	↑
PPC	↑	↑	↓	↓	↓	↑
STG	↑	↑	N/C*	↓	↓	↑

Table 5-2: LFP power changes in different types of anesthetic drug administration at the stabilized portion following of consciousness. Note, these affects are known to be different at the initial stages of GA before LOC (e.g. paradoxical beta increase with propofol) and appear to have sub-frequency band specific trends (e.g. 17 Hz beta rhythm in propofol is prominent). N/C: no consistent change across monkeys.

5.2 Human General Anesthesia Mechanisms in Monkeys

Beyond the explicit scientific findings that emerged from these works, together they highlight the feasibility and preferability of a macaque model for studying network

mechanisms for different anesthetic agents. The oscillatory activity changes we measured in LFPs from macaque prefrontal cortex resembled many of the stereotypic patterns observed in human frontal EEG that characterize GA. Across species, awake brain activity is often characterized by relative peaks in the beta and gamma frequency bands in both EEG and LFP power spectral densities. In ketamine, it was nearly identical to human experiments at surface level (Akeju et al., 2016), with gamma bursts alternating into cortex-wide on and off states. Just as in human EEG, we found that propofol induced the paradoxical increase in beta oscillations before producing large elevations in slow and delta oscillations and dampening high frequency gamma activity around the time of LOC (Figure 4-2). Microelectrode array recordings from within the prefrontal cortical locations in our monkeys, while not necessarily unsurprising, appear to provide a high-resolution window into the dynamics commonly seen on the frontal scalp recordings in humans receiving anesthesia. However, one finding stands in suspicious contrast to the human literature. The monkeys lacked the prominent increase in the alpha oscillations (8-12 Hz) that characteristically tracks unconsciousness in human GA using propofol (Purdon et al., 2013). Without additional consideration, the absence of this propofol trademark would cast substantial doubt on the feasibility of rhesus macaques as serving as ideal models for human CLAD models and perhaps anesthesia mechanism research in general.

Further examination of our monkey data reveals some intriguing insights into this seemingly anomalous finding. As previously stated, the alpha band power remained relatively unchanged across the recording session. The beta power did not follow the trend of gamma as substantially as one might have expected with higher frequency oscillations; gamma power dropped off sharply with unconsciousness while beta power did not demonstrate a prominent decrease (Figure 4-2B). In fact, there is a relative stabilization of beta power back to near-baseline awake levels (as opposed to gamma frequencies, which dropped below awake baseline).

A closer look into the beta oscillations during propofol GA in the monkeys reveals a profound and narrow peak in the power spectral density centered around 17 Hz that persists throughout the period of unconsciousness. Spectrograms with sufficient resolution (e.g. Figure 4-2A session A2) in these monkeys appear much like frequency-shifted analogs of those from EEG in humans receiving high-dose propofol. Thus, these prominent beta waves in monkeys appear to be the equivalent of the human propofol alpha oscillation.[5] One explanation for this frequency discrepancy is that the filtering of the skull in humans may serve as a low-pass filter down-shifting a faster intracranial rhythm. On the other hand, the brains of non-human animal models are known to simply run faster; characteristic oscillations in other species are often shifted to higher frequencies (Jacobs, 2013; Sederberg, Kahana, Howard, Donner, & Madsen, 2003). Regardless, the activity recorded in the monkeys for different frequency bands distinctly varied such that the anesthetized states could be uniquely defined and would otherwise be missed if evaluating frequency-specific changes over large, or even standard, frequency ranges. These findings provided the basis for our marker identification for the CLAD system we developed and validate the framework for use in humans and automatic management of additional drug classes (e.g. adrenergic, opioid, glutamatergic, etc.).

5.3 Future Work

The efforts to understand both the conscious and unconscious brain cannot be accomplished in one research program, despite our best efforts. We have employed different recording techniques (e.g. multielectrode arrays, laminar probes, DBS probes), different brain areas recorded (e.g. FEF, vlPFC, STG, V4, MD thalamus, CL thalamus,

[5] See Appendix A for supplemental materials outlining preliminary findings on the distinct beta oscillations observed during the deeply anesthetized states of propofol GA in rhesus macaques.

etc.) with different drugs (e.g. propofol, ketamine, dexmedetomidine), different sensory manipulations (e.g. auditory stimuli, air-puffs, light flashes, DBS pulse trains, etc.), all in monkeys that were previously, explicitly, or otherwise trained on cognitive tasks (e.g. multi-interval delayed saccade, interhemispheric memory transfer, rule-task, visual search, etc. Our diverse array of experiments and pilot studies set the stage for another generation of hypothesis-driven analyses to be performed utilizing the datasets created over the course of this work (see Appendix B).

This work and the forthcoming analyses must answer several outstanding questions. Foremost, what is the nature of sensory encoding in the generally anesthetized brain? Our data contains some of the answers, buried temporarily, on how sensory encoding might transform with anesthesia. Particular sensory inputs may be filtered before even reaching sensory cortex (e.g. thalamic interruption), improperly represented in cortex (e.g. neural code changes), or fail to spread to connected cortices despite proper encoding (e.g. oscillatory fragmentation of networks). Either way, future work will determine how brain-state dynamics explain single neuron activity in unconsciousness, and perhaps illuminate features of the neural code essential to consciousness.

One especially intriguing path will be to investigate the single-trial sensory data (e.g. air puff, sound, visual flash) across conscious states and across different anesthetics. It is readily apparent from our data that the ON and OFF states scatter throughout the brain in a mosaic that patterns cortex in ways that did not overlap with the functional maps of cognition (Figure 4-2). The important question that arises is, what happens to sensory information *beyond* primary sensory cortex? Here, history has long demonstrated certain forms of anesthesia maintain sufficient signal encoding (Hubel, 1963, 1982). Specifically, when sensory information reaches secondary sensory cortices, does the ON or OFF state of the cortex receiving the signal dictate how the information will be processed and whether it can be sufficiently relayed to higher-order areas or recurrently fed backwards? Perhaps information is not routed appropriately or does not sufficiently

activate enough neurons fast enough to trigger an ignition process to cascade through cortex (van Vugt et al., 2018). Or, as been considered by some, perhaps corticothalamic UP-states are true fragments of wakefulness (Destexhe, Hughes, Rudolph, & Crunelli, 2007). This should be investigated at every stage of the cortical hierarchy for different types of stimuli and will reveal key insights into corticocortical transmission in general and the latent connections that are masked or unmasked with general anesthesia. We would not be surprised in the thalamus had a major role in the likelihood of this normal or aberrant feedforward of feedback routing. Furthermore, these pursuits would directly align with the follow-up studies comparing GA to sleep, another state where regional slow waves and spindles have been shown to fragment cortex of sort (Latchoumane, Ngo, Born, & Shin, 2017; Nir et al., 2011).

From our perspective, the ultimate demonstration of a deep understanding of the neural dynamics of GA is through control paradigms. Automatically tracking and controlling the level of consciousness requires sufficient feature-space exploration and rigorous analysis to ensure robust control. Our next steps will be threefold. First, our non-human primate CLADs paradigm should be tested at a much larger scale on a number of different monkeys of different ages and weights to capture population variability. Secondly, for these systems to be useful clinically they must tolerate the environmental and physiological factors of being tested in an operating room on a monkey receiving noxious stimuli, such as surgery. Lastly, as human patients commonly receive multiple anesthetic agents for a given procedure, future work will have to simultaneously evaluate the robustness of our marker and CLAD system to other anesthetics and their combinations.

Collectively, this work highlights the diverse mechanisms that give rise to unconscious states. We have attempted, hopefully successfully, to demonstrate the power of general anesthesia as a tool for better understanding the functional connectivity of not just the anesthetized brain, but the awake brain as well. It is curious and potentially

meaningful that conscious processing can be disrupted from converging directions with profound inhibition (e.g. propofol) or overwhelming excitation (e.g. ketamine) to both (over)synchronize local neural populations. Furthermore, identifying the central thalamus as an excitatory hub capable of switching on an anesthetized cortex bathed in propofol reveals new windows into functions and capabilities of thalamocortical networks. Importantly, experiments like these do not simply describe how anesthetized neural networks behave. The anesthetized brain uncovers the relationships that are either masked by other processes in the awake brain. While conscious, these anatomical and functional networks exist; just with adjustments like altered synaptic weights, changed functional connectivity strengths and directionalities, and latency dissimilarities for temporal and rate coding. Thus, in thinking about how to best further investigate the neural correlates of consciousness and the holy grail of cognitive neuroscience, the question to ask first may just be: *so, what else causes unconsciousness?*

Appendix A

"Monkey Alpha": The Beta Oscillations of Propofol Anesthesia

Work by Jacob A. Donoghue, Jorge G. Yanar, Andre M. Bastos, and Earl K. Miller.

The following appendix contains the supplementary studies and analyses investigating the presence, distribution, shape, and functional connectivity of the ~17 Hz beta oscillation that dominates intracranial recordings from macaque cortex. The laminar distribution of this distinctive rhythm was characterized via additional recording sessions in two monkeys using 16-channel V and U probes (Plexon Inc., Dallas, Tx). Current source density analysis was used to isolate the beta rhythm to putative cortical layers. Visual evoked potentials were characterized across conscious states of awake and propofol general anesthesia via an established protocol for defining laminar structures (Bastos, Loonis, Kornblith, Lundqvist, & Miller, 2018) Following loss of consciousness, eyelids of the two animals were maintained open using ophthalmological surgical instruments with regular flushing of the cornea using sterile saline. The additional findings are explained in the figures below.

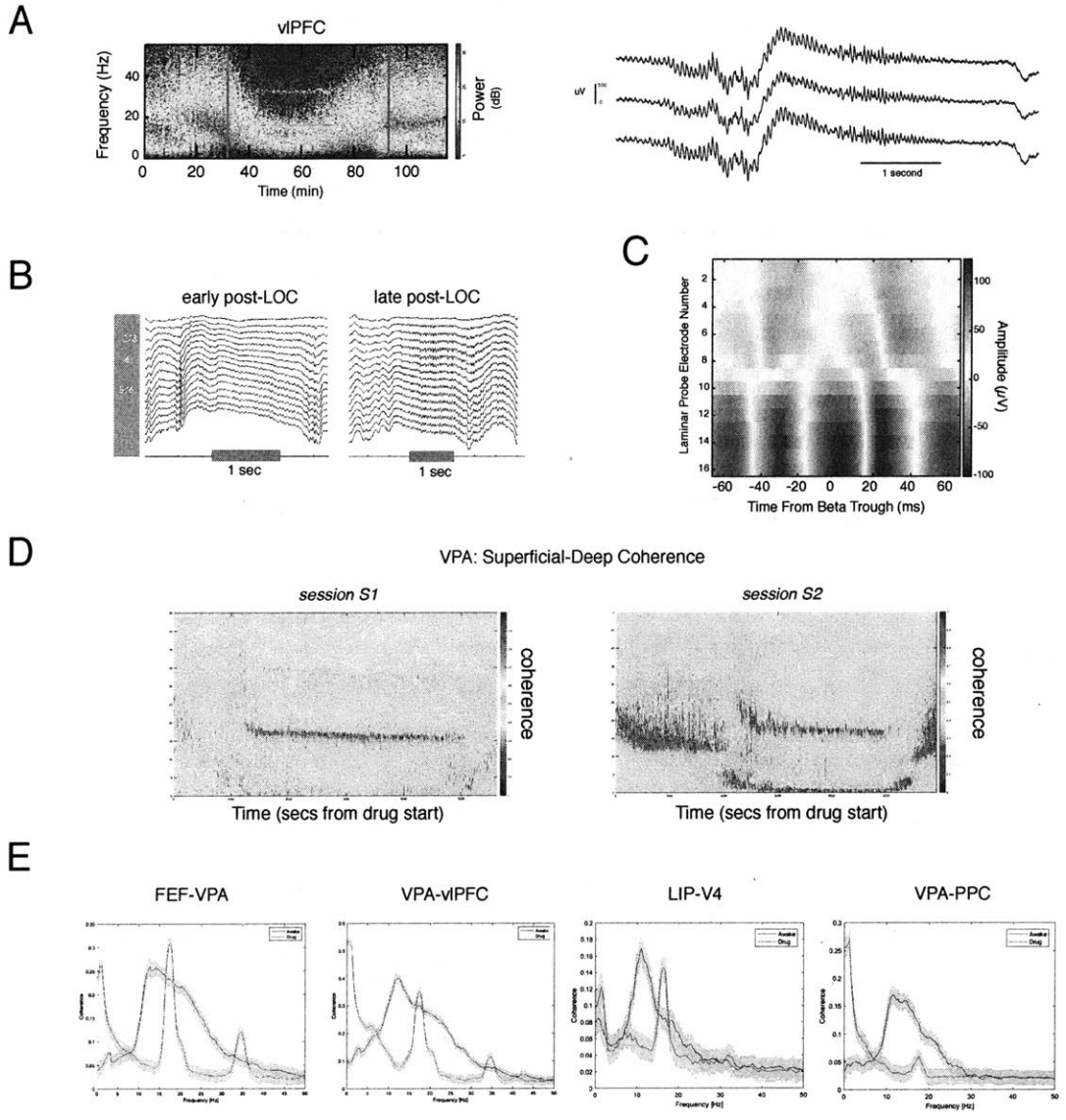

Figure A–1: 17 Hz beta oscillation across layers and areas in propofol anesthesia. **A**, Left, prominent narrow-band beta oscillation appearing between LOC (first vertical red line) and ROC (second red line). Right, beta appears in bursts across electrodes in PFC. **B**, Laminar LFP differences in PFC beta oscillations in early and late GA. **C**, Phase-shifted beta across cortical layers. Band-passed (15-25Hz) LFP troughs were detected on the deepest electrode via Matlab function *findpeaks()*. Deeper (higher number) electrodes were phase-locked to the deep beta rhythm. Superficial layers were phase shifted in their beta amplitude. **D**, Coherograms for two GA sessions. Pairwaise multitaper coherence computed between superficial and deep contacts of laminar probes within PFC. **E,** Pairwise coherence for (from L:R) FEF-VPA, VPA-vlPFC, LIP-V4, VPA-PPC. Beta coherence is strong across prefrontal circuits, but is also present across other areas (LIP-V4) and minimally present in others (VPA-PPC).

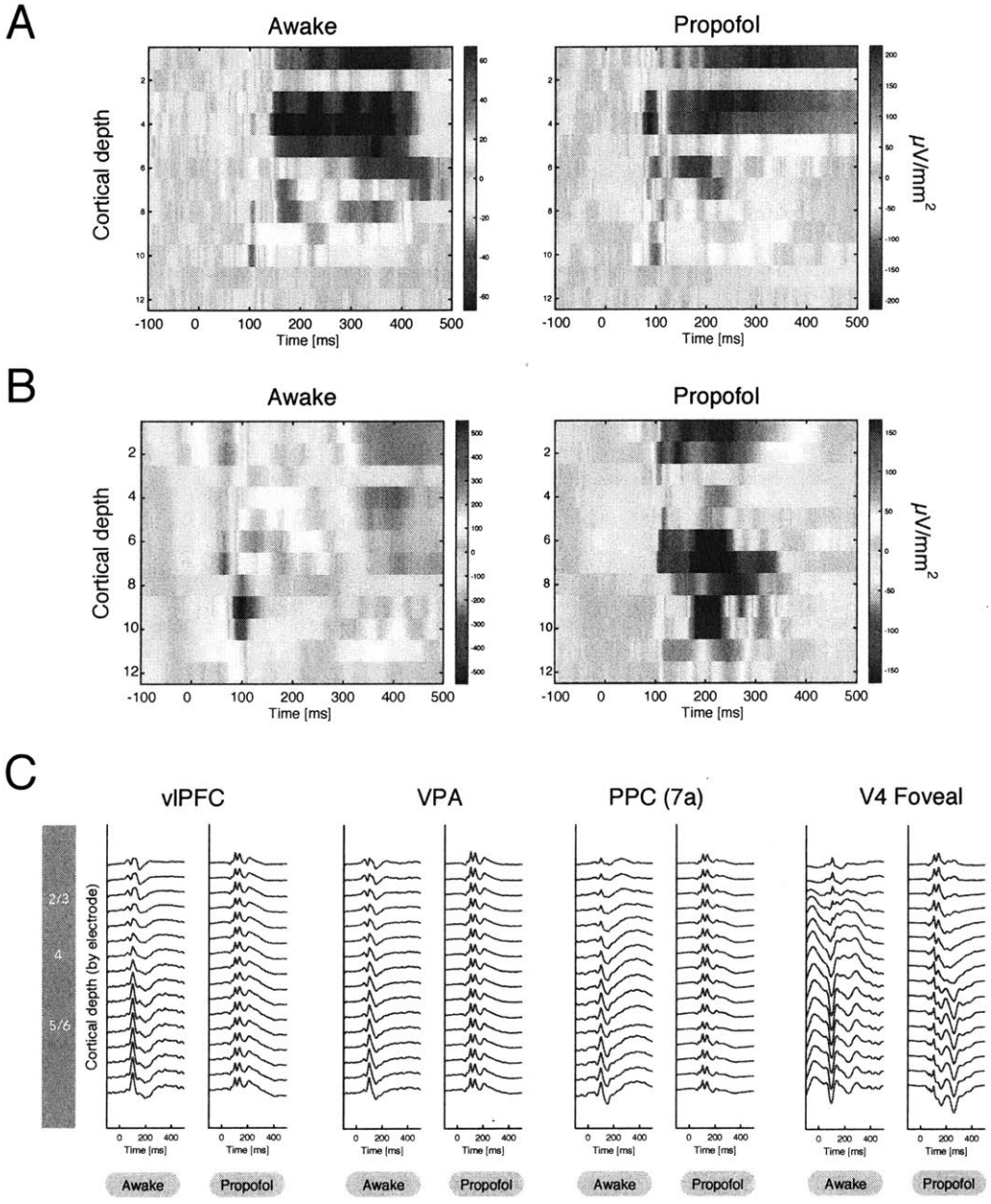

Figure A–2: Current source density (CSD) analyses to identify laminar effects of propofol general anesthesia. CSDs were computed with respect to the onset of a 100msec flash to elicit a visually-evoked potential (VEP). **A**, PFC and **B**, Foveal area V4 show sink and source dynamics in the awake (left) and generally anesthetized state (right). **C**, Laminar LFP differences in VEPs in all cortical regions between awake (left) and GA (right).

Appendix B

Neural Codes in Unconscious Cortex

The work presented in this appendix comes from *Interhemispheric Interactions in Working Memory* by Jacob A. Donoghue*, Scott L. Brincat*, and Earl K. Miller (in preparation). * these authors contributed equally to this work.

In this work, two rhesus macaques (one male, one female) were trained to perform a complex working memory task that occasionally required a shift in fixation point during the delay period, forcing the items presented to one visual field to be tested for similarity in the contralateral visual field (Figure B-1A). The memory fields of prefrontal cortex have been shown to have lateralized features (Rainer, Asaad, & Miller, 1998). This experiment explicitly tested whether an otherwise disengaged prefrontal cortex can receive task relevant information when swapping into the contralateral hemifield or whether these processes are automatic (e.g. occur upon saccade or bilateral representation of unilateral objects in a new task setting at sample). Two 8x8 microelectrode arrays (MultiPort: 1.0 mm electrode length, Blackrock Microsystems, Salt Lake City, UT) were implanted bilaterally into ventrolateral prefrontal cortex and dorsolateral prefrontal cortex, for a total of 256 recording sites. Receptive field (RF) mapping was performed to evaluate the

memory fields versus the. disengaged RFs during passive fixation and determine post-hoc if any of the test locations fell within a restricted RF. Monkey T performed 39,903 correct trials at 85.5% correct overall and Monkey E performed 25,123 correct trials at 83.9% correct overall. The initial results of these experiments evaluating the conscious or unconscious contributions to unified working memory are shown in this supplementary appendix.

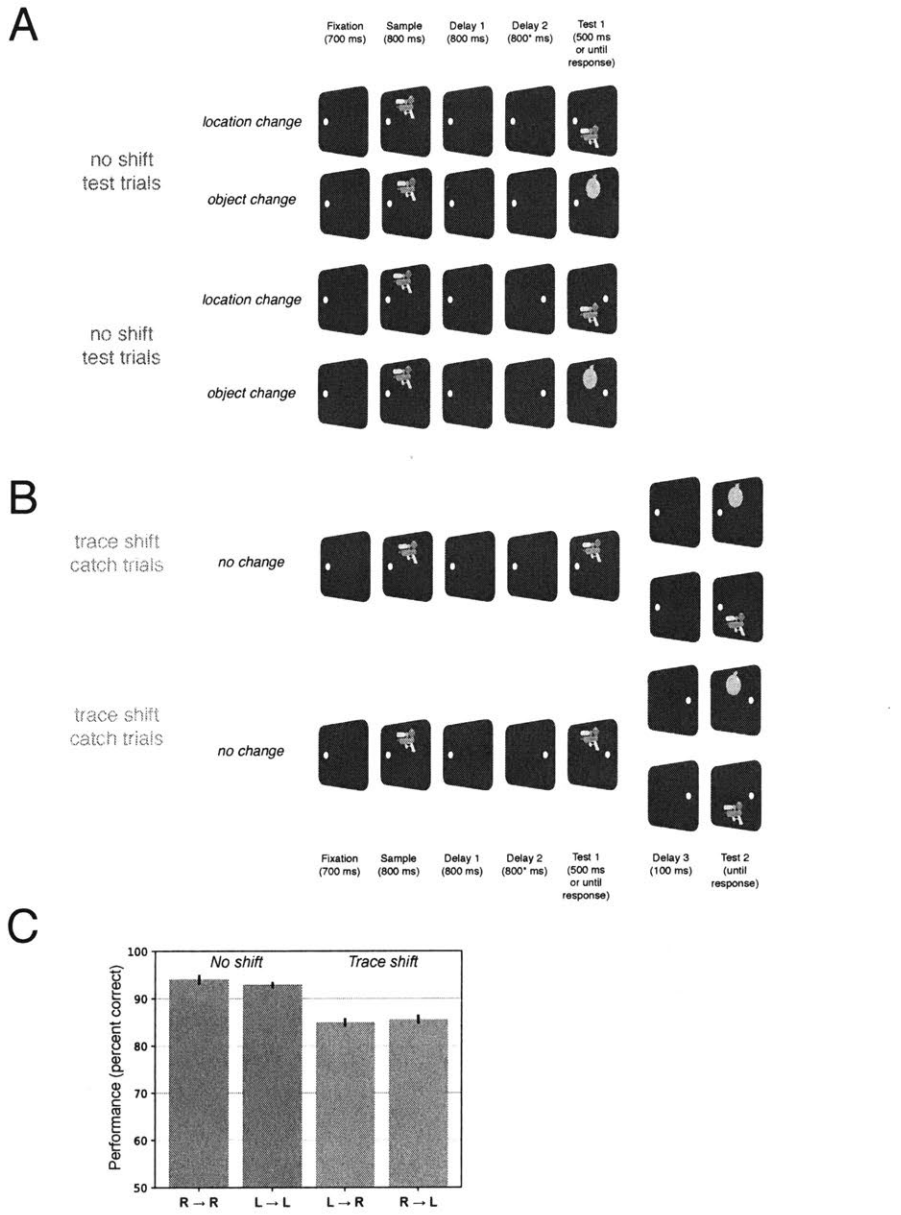

Figure B–1: A, Outline of task structure. Example conditions shown for left-starting fixation point. Trials could either shift the fixation point or not during the delay period (following delay period 1) and at test screen change in either object location or object identity. **B**, Other half of trials were catch trials, whereby the object identity or location did not change at test 1 (but always changed following a shorter Delay 3 epoch). Note (*), delay on trace shift trials permitted 100 ms for monkey to reacquire fixation for the start of Delay 2. **C**, behavioral performance across no shift and shift conditions. Note, an image of face of researcher (JAD) was use an object for the last several experiments in each animal to explore differing effects in the face-patch network, in which it appeared we were recording.

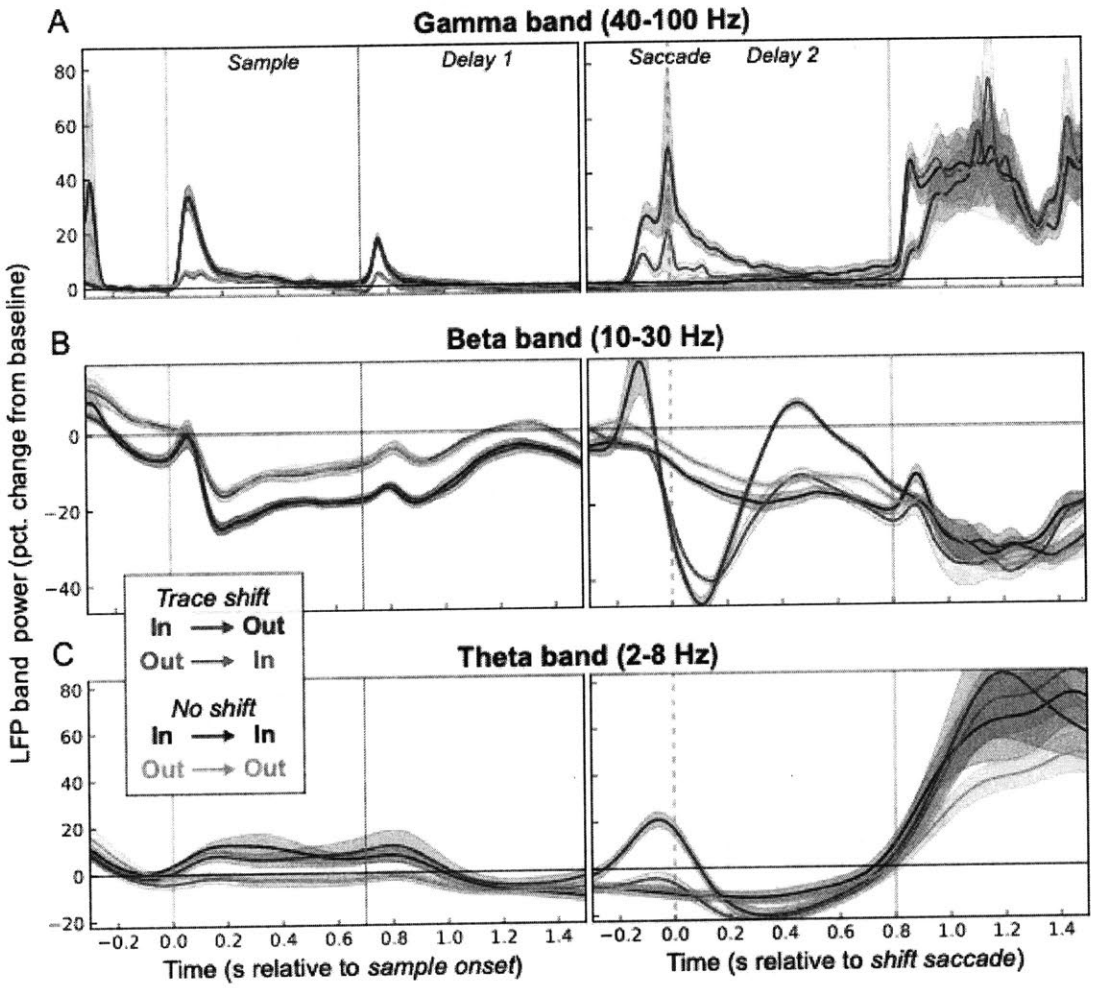

Figure B–2: Memory trace shifts are marked by transient bursts of PFC gamma and theta oscillations, and induce a sign flip of beta oscillations. LFP power in the gamma (A; 40-100 Hz), beta (B; 10-30 Hz), and theta (C; 3-8 Hz) bands, expressed as percent change from the pre-sample baseline. Gamma (A) and theta (C) oscillations are overall stronger for memory traces in the contralateral hemifield (left: red/dark grey vs. green/light gray), and exhibit a transient peak around the time of the saccade, which is stronger for saccades bringing a memory trace into the non-contralateral hemifield (red) than those shifting it into the ipsilateral hemifield (green). **B**, Beta oscillations are instead stronger for memory traces in the ipsilateral hemifield (left: green/light gray vs. red/dark gray), consistent with their putative suppressive role. Following the saccade, the preference flips—the red curve becomes greater than the green—in reflecting the shifted location of the shifted memory trace.

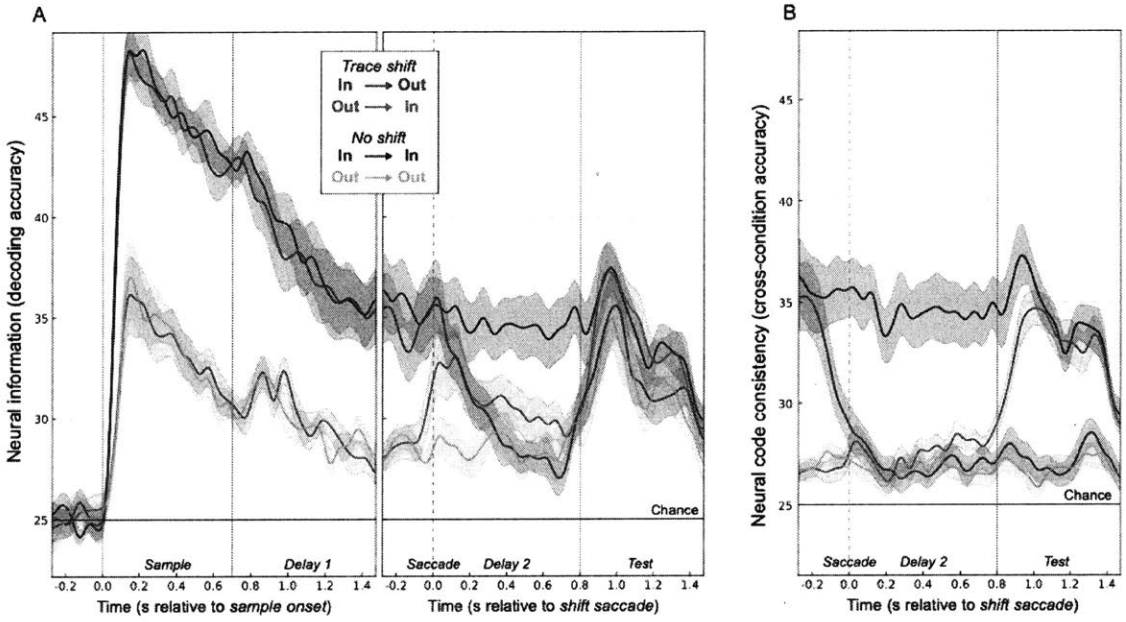

Figure B–3: A memory trace shift activates neurons in the contralateral PFC but with a distinct neural code, as measured by spiking rate. **A**, Accuracy (across-session mean ± SEM percent correct) of decoding a working memory trace from PFC multiunit spiking populations. Accuracy is computed separately for trials where the memory trace in the preferred (contralateral) hemifield (dark gray), the non-preferred (ipsilateral) hemifield (light gray), when the trace is shifted from the non-preferred into the preferred (green), and when it is shifted into the non-preferred hemifield (red). The neural code is stronger overall for the preferred hemifield, but when the trace is shifted into the preferred hemifield (green curve around "saccade"), the contralateral PFC reactivates, as if a new visual stimulus was shown. **B**, Decoding accuracy for training a classifier on the no-shift preferred location condition (dark gray), and testing its generalization to the other conditions. If the shift-reactivated neural code was the same as in the no-shift condition, the green curve should be similar to the one in (A). Instead, it remains at baseline levels, indicating that a distinct code is used when a saccade brings a memory trace into a location vs. an existing memory trace at the same location.

Appendix C

Methods for Evaluating Treatments and Physiology in Human Patients Using Intravenous Alpha-2 Adrenergic Antagonist Agents

Inventors: Jacob A. Donoghue, Noah D. Donoghue, Earl K. Miller, Emery N. Brown

This section contains the patent application referenced in Chapter 5.4, arising from the studies of the arousal system's relation to the emergence from general anesthesia. The following patent application, entitled *"Methods for Evaluating Treatments and Physiology in Human Patients Using Intravenous Alpha-2 Adrenergic Antagonist Agents,"* was filed to the United States Patent and Trademark under the provisional application number 62/806,630.

METHODS FOR EVALUATING TREATMENTS AND PHYSIOLOGY IN HUMAN PATIENTS USING INTRAVENOUS ALPHA-2 ADRENERGIC ANTAGONIST AGENTS

FEDERALLY SPONSORED RESEARCH

This invention was made with Government support under Grant No. R01 MH115592 and R01 GM118269 awarded by the National Institutes of Health. The Government has certain rights in the invention.

FIELD OF THE INVENTION

The invention relates in some aspects to an anesthesia- or sedation-reversing agent and methods for using these agents, for instance, to assess a surgical procedure or a patient's physiologic state during and/or after a surgical procedure.

BACKGROUND

General anesthesia is widely used in clinical and research contexts. It is used to place patients in an insensate state during major surgery, so that surgeons may perform highly invasive, lengthy, and/or complex procedures. Some of general anesthesia's intended immediate effects are to induce analgesia, immobility, unconsciousness, and amnesia while keeping the patient's physiology stable during a surgical procedure. Recovery of consciousness from the drug-induced anesthesia can be achieved by reducing or cessating the administration of the anesthetic drugs.

Lighter forms of general anesthesia are used for attenuating, specifically, the level of consciousness, without necessarily affecting a patient's mobility or analgesia. This state, referred to as sedation, is commonly utilized outside of operating rooms, such as in the intensive care units of hospitals.

SUMMARY

The present disclosure is based, *inter alia*, on the discovery that an α2 adrenergic receptor antagonist, particularly atipamezole, can be used to rapidly reverse the effect of α2 adrenergic receptor agonists used in cases ranging from surgery to ICU and inpatient/ongoing hospital care, and the consequent ability to perform new medical treatments and procedures.

The present disclosure is based, *inter alia,* on methods for administering an α2 adrenergic receptor antagonist, particularly atipamezole, to a human under general anesthesia during a surgical procedure in order to induce a temporary and rapid reversal of unconsciousness (also referred to herein as a planned wakeup) and conduct an intraoperative assessment. Thereafter, the state of unconsciousness is restored for the completion of the surgical procedure.

Accordingly, one aspect of the present disclosure provides a method comprising administering to a subject an effective amount of an α2 adrenergic receptor agonist to perform a surgical procedure, inducing a planned wake-up by administering to the subject an effective amount of α2 adrenergic receptor antagonist (wherein the adrenergic receptor agonist is maintained or reduced), conducting an intraoperative assessment of the subject during the planned wakeup, and ceasing the α2 adrenergic receptor antagonist in order to proceed with the surgical procedure, and optionally administering to the subject an effective amount of a general anesthetic. In some embodiments, the intraoperative assessment is performed in an operating room. In some embodiments, after ceasing the α2 adrenergic receptor antagonist, the amount of the adrenergic receptor agonist is increased to its amount at the initiation of the surgical procedure. In some embodiments, the surgical procedure is a neurosurgery or an orthopedic surgery. In some embodiments, the neurosurgery is a craniotomy. In some embodiments, the orthopedic surgery is a spine surgery. In some embodiments, the intraoperative assessment is a physiologic or functional assessment of an organ, organ system, or anatomical region. In some embodiments, the

intraoperative assessment is an evaluation of the surgical procedure. In some embodiments, the intraoperative assessment is to assess the subject's breathing. In some embodiments, the intraoperative assessment is a standard motor and language mapping of the subject's brain. In some embodiments, the intraoperative assessment is a standard motor mapping technique of the subject's spinal cord or musculature.

A further aspect of the present disclosure provides a method of administering to a subject undergoing a surgical procedure an effective amount of an α2 adrenergic receptor agonist to perform a surgical procedure, ceasing the administration of the α2 adrenergic agonist and administering to the subject an effective amount of α2 adrenergic receptor antagonist at or near the end of the surgery, and conducting a post-operative assessment. In some embodiments, the post-operative assessment is conducted in the operating room after the end of the surgery. In some embodiments, the post-operative assessment is conducted in the intensive care unit (ICU) after the end of the surgery. In some embodiments, the post-operative assessment is conducted in the post-anesthesia care unit (PACU) after the end of the surgery. In some embodiments, the post-operative assessment is conducted in the surgical intensive care unit (SICU) after the end of the surgery. In some embodiments, the post-operative assessment is conducted within 30 minutes of the end of the surgery or within 1 hour of the end of the surgery or within 90 minutes of the end of the surgery. In some embodiments, the post-operative assessment is conducted within 10 minutes of the end of the surgery.

A further aspect of the present disclosure provides a method of administering to a subject undergoing a surgical procedure an effective amount of an α2 adrenergic agonist to perform a surgical procedure, ceasing the administration of the α2 adrenergic agonist and administering to the subject an effective amount of α2 adrenergic receptor antagonist at or near the end of the surgery, wherein the subject's mobility in an intensive or critical care unit is increased. In some embodiments, the subject's mobility is increased within 90 minutes of the end of the surgery or within 10-30 minutes of the end of the surgery.

A further aspect of the present disclosure provides a method of modifying circadian rhythms by administering to a subject in need thereof, treated with an α2 adrenergic agonist, an effective amount of an α2 adrenergic receptor antagonist in order to facilitate normal adaptation to regular day-light cycles or adjust the subject's circadian rhythms. In some embodiments, the subject is a patient at risk of, known to have, or diagnosed with delirium. In some embodiments, the α2 adrenergic agonist is administered for sleep at night time or as desired. In some embodiments, the α2 adrenergic receptor antagonist is administered to restart a circadian rhythms cycle.

A further aspect of the present disclosure provides a method of treating cardiac arrest, the method comprising administering to a subject under general anesthesia and experiencing cardiac arrest, an effective amount of an α2 adrenergic receptor antagonist to treat the cardiac arrest, wherein the subject under general anesthesia had received an α2 adrenergic receptor agonist.

A further aspect of the present disclosure provides a method of treating bradycardia, the method comprising administering to a subject under general anesthesia and experiencing bradycardia, an effective amount of an α2 adrenergic receptor antagonist to treat the bradycardia, wherein the subject under general anesthesia had received an α2 adrenergic receptor agonist.

A further aspect of the present disclosure provides a method of treating hypotension, the method comprising administering to a subject under general anesthesia and experiencing hypotension, an effective amount of an α2 adrenergic receptor antagonist to treat the hypotension, wherein the subject under general anesthesia had received an α2 adrenergic receptor agonist.

A further aspect of the present disclosure provides a method of treating hypotension, the method comprising administering to a subject under sedation and experiencing hypotension, an effective amount of an α2 adrenergic receptor antagonist to

treat the hypotension, wherein the subject under sedation had received an α2 adrenergic receptor agonist.

A further aspect of the present disclosure provides a method comprising administering to a subject an effective amount of an α2 adrenergic receptor agonist to perform a surgical procedure (wherein the subject is given an endotracheal breathing tube), ceasing the administration of the α2 adrenergic agonist, administering to the subject an effective amount of α2 adrenergic receptor antagonist prior to the end of the surgical procedure, and conducting an extubation when the subject displays a brainstem reflex. In some embodiments, prior to the end of the surgical procedure is between 0 and 15 minutes before the end of the surgical procedure. In some embodiments, the brainstem reflex is a pharyngeal reflex or a tracheal reflex.

A further aspect of the present disclosure provides a method comprising administering to a subject an effective amount of an α2 adrenergic receptor agonist to perform a surgical procedure, ceasing the administration of the α2 adrenergic agonist, administering to the subject an effective amount of α2 adrenergic receptor antagonist prior to the end (or at the end) of the surgical procedure, and assessing the subject for a brainstem reflex. In some embodiments, prior to the end of the end of the surgical procedure is between 0 and 15 minutes before the end of the surgical procedure. In some embodiments, the effective amount of α2 adrenergic receptor antagonist is administered after or at the end of the surgical procedure. In some embodiments, the effective amount of α2 adrenergic receptor antagonist is administered within 30 minutes after the end of the surgical procedure.

A further aspect of the present disclosure provides a method for reversing a neural blockade during a surgical procedure by administering to a subject undergoing a surgical procedure who has received a muscle blockade agent and a neural blockade agent, an effective amount of an α2 adrenergic receptor antagonist to reverse the neural blockade. In some embodiments, the method includes conducting an intraoperative assessment of

the subject following the administration of the α2 adrenergic receptor antagonist. In some embodiments, the α2 adrenergic receptor antagonist is given in a dose range of 30:1-400:1 μg/kg α2 adrenergic receptor antagonist to neural blockade agent.

A further aspect of the present disclosure provides a method for reducing or preventing emergence delirium by administering to a subject under general anesthesia, an effective amount of an α2 adrenergic receptor antagonist for the subject to regain consciousness or to minimize symptoms of emergence delirium, wherein the subject under general anesthesia had received an α2 adrenergic receptor agonist. In some embodiments, the α2 adrenergic receptor antagonist is administered before emergence from general anesthesia. In some embodiments, the α2 adrenergic receptor antagonist is administered as the subject begins to regain consciousness. In some embodiments, the α2 adrenergic receptor antagonist is administered in an effective amount to stop at least one symptom of emergence delirium.

In further embodiments of the present disclosure, the α2 adrenergic receptor antagonist is administered in a dose range of 30:1-400:1 μg/kg α2 adrenergic receptor antagonist to agonist (e.g., α2 adrenergic agonist). In further embodiments of the present disclosure, the α2 adrenergic receptor antagonist provides rapid reversal of unconsciousness or sedation. In further embodiments, the α2 adrenergic receptor antagonist is atipamezole. In further embodiments, the α2 adrenergic receptor antagonist is administered intravenously. In further embodiments, the α2 adrenergic receptor antagonist is a composition comprising the α2 adrenergic receptor antagonist and a pharmaceutically acceptable excipient. In further embodiments, the pharmaceutically acceptable excipient is a saline or water-based solution. In further embodiments, the α2 adrenergic receptor antagonist is administered intravenously as a bolus or an infusion. In further embodiments, the α2 adrenergic agonist is dexmedetomidine or clonidine. In further embodiments, the α2 adrenergic agonist is administered in solo or in combination with other general anesthetics or sedative drugs. In further embodiments, the general

anesthetic is propofol, sevoflurane, ketamine, or benzodiazepines. In further embodiments, the subject is a mammal. In further embodiments, the subject is a human.

The methods disclosed herein that apply to a subject under general anesthesia, wherein the subject under general anesthesia had received an α2 adrenergic receptor agonist, may also apply to methods for treating a subject under sedation, wherein the subject under sedation had received an α2 adrenergic receptor agonist.

These and other aspects of the invention, as well as various embodiments thereof, will become more apparent in reference to the detailed description of the invention. This invention is not limited in its application to the details of construction and the arrangement of components set forth in the following description or illustrated in the drawings.

DETAILED DESCRIPTION

The disclosure provides, in certain aspects, methods of rapidly reversing the effects of general anesthesia or sedation by administering an α2 adrenergic receptor antagonist. In a preferred embodiment the α2 adrenergic receptor antagonist is atipamezole. Current drugs used in anesthesia and sedation typically require the subject be intubated and rely on reducing or stopping administration of the drug in order for the patient to regain consciousness, which can be a lengthy process.

Herein, the present disclosure teaches an application for atipamezole in human surgical procedures that has not been used previously and has the potential to shift the paradigm of surgical medicine. Currently, there is no clinical use of atipamezole in humans. The present disclosure teaches methods for administering atipamezole to a subject (e.g., patient, human, etc.) during a surgical procedure in order to conduct a planned wakeup (described further below) and evaluate the subject in the middle (or prior to the end) of the surgical procedure. Atipamezole induces a rapid reversal of unconsciousness (or sedation), thus resulting in the planned wakeup.

Currently, in surgical cases in the operating room, there are no effective methods for the temporary reversal of unconsciousness in human patients, which would allow a clinician to make early (intraoperative) assessments/diagnoses. Clinicians have to wait until after the surgical procedure—after the effects of the general anesthesia have subsided—to assess the patient. Examples of the assessments include checking the patient's motor function and neurological function, cognitive exams, etc. The methods described in the present application would allow an intraoperative assessment of the patient, a determination of how the surgical technique is impacting the patient during surgery, the identification of surgical errors that would impact, for example, motor function and neurological function, and the correction of surgical errors in real-time thus minimizing the requirement for a second (separate) corrective surgical procedure. These would substantially improve surgical outcomes and open up possibilities for new, currently unknown and/or unpracticed surgical procedures. In a preferred embodiment, the α2 adrenergic receptor antagonist, atipamezole, is administered intravenously.

Often in neurosurgical and orthopedic surgery cases, for example, the subject will have received general anesthesia in standard current practices, and surgery will be performed to expose a region of the central nervous system such as the brain or spinal cord. In some embodiments, before surgery can proceed on the sensitive region of interest, the subject can be re-awakened by administering an α2 adrenergic receptor antagonist (*e.g.*, atipamezole) for an intraoperative assessment of nervous system function. This is done in order to determine the functions of the regions of potential surgical intervention in order to avoid damaging regions of critical importance (*e.g.*, avoiding critical language regions in the brain during tumor removal via patient's speaking, ensuring spinal cord integrity by voluntary movements). In contrast, current practice involves turning down the levels of anesthetic drugs and waiting for them to wear off once the surgical site has been exposed and before the surgery can proceed.

It has been discovered herein that the effects of general anesthesia and sedation agents used alone or in combination can be predictably and efficiently reduced through use of an α2 adrenergic receptor antagonist, as described herein. The α2 adrenergic receptor antagonist is sufficient to reverse neurological sedation in an anesthetized/sedated patient in a manner that enables a physician to conduct intra-operative assessments on the patient that was under general anesthesia. The α2 adrenergic receptor antagonists are particularly useful in surgical procedures where a patient has received a full anesthetic treatment including a muscle blockade agent and a neural blockade agent. The α2 adrenergic receptor antagonist is sufficient to reverse the neural blockade and enable the patient to communicate with the surgical team and or regain sufficient cognitive function in order to function at a normal level. In alternative embodiments, rather than waiting for the anesthetic to wear off, the α2 adrenergic receptor antagonist can be administered immediately following an intensive procedure where the patient was under general anesthesia. The rapid reversal of the unconsciousness would allow assessment (e.g., of patient mobility, language skills, cognitive ability) much sooner than previously possible. This can be conducted prior to the transfer of the patient from the operating room to the post-surgical inpatient hospital unit.

Previous studies have shown that about 15% of patients have failed extubations. The high rates of failed extubations lead to unnecessary (and costly) prolongation of intubation in hospitals. The present disclosure teaches a method of using the α2 adrenergic receptor antagonist (*e.g.*, atipamezole) to promote spontaneous breathing or promote brainstem reflexes in a subject that was under general anesthesia. In some embodiments a subject is administered α2 adrenergic receptor agonist and is intubated. Prior to the end of the surgical procedure (*e.g.* 10 minutes prior), the subject is administered an effective amount of the α2 adrenergic receptor antagonist, which promotes (*i.e.*, results in rapid onset of) breathing or promotes a pharyngeal reflex (*i.e.* gag-reflex). Upon observation of the breathing or the pharyngeal reflex, the subject is extubated. Typically, when a patient

is intubated and under general anesthesia, the clinician waits for the subject to start having a gag-reflex, as an indication that the subject has recovered spontaneous breathing, before pulling out the endotracheal breathing tube. Administering atipamezole could accelerate this process. In instances when the subject does not have a gag-reflex towards the end or after the surgery, the clinicians conduct a trial extubation. Here, the use of atipamezole would reduce or obviate the need for trial extubation and lead to new surgical protocols that better facilitate the recovery of breathing.

It has also been discovered herein that α2 adrenergic receptor antagonists may be used to regulate circadian rhythms. In patients that need assistance in regulating circadian rhythms α2 adrenergic receptor antagonists may be delivered alone or in a cyclic combination with an α2 adrenergic agonist in order to facilitate normal adaptation to regular day-light cycles or adjust the subject's circadian rhythms.

The α2 adrenergic receptor antagonists may also be used to treat cardiac arrest occurring while a patient is under general anesthesia. The patient who has gone into cardiac arrest can be administered an α2 adrenergic receptor antagonist to reverse the sedative effects or effects of general anesthesia and enable or support the restoration of cardiac activity in the patient.

GENERAL ANESTHESIA AND SEDATION

General anesthesia is a drug-induced comatose state resulting from the administration of one or more general anesthetic agents and is characterized by a loss of consciousness. Typically, the induction of general anesthesia includes a balance of potent sedatives, muscle relaxants, opioids, neuromuscular blocking agents, and local anesthetics. General anesthesia is widely used in the medical field for highly invasive, lengthy, and/or complex procedures. In addition to unconsciousness, other effects of general anesthesia include amnesia, analgesia, antinociception, akinesia, paralysis, and physiological stability. Analgesia or nociceptive blockage (or antinociception) prevents central nervous system

arousal and cardiovascular and neurohumoral responses to surgery (Sanders, Tononi, Laureys, & Sleigh, 2012). Nociceptive blockage refers to the blockage of pain caused by tissue damage. In standard practice, following a major surgery with general anesthesia, the administration of a general anesthetic is typically reduced or terminated to allow the subject (*e.g.*, patient) to regain consciousness. This is a slow, suboptimal process. In current practice, most of the agents used for the post-operative reversal of the general anesthetics are centered on the use of muscle relaxants. Disclosed herein are methods for accelerating this process and, most importantly, allowing a subject to regain cognitive faculties rapidly through the use of a reversal agent.

The term "general anesthetic" refers to a drug that induces general anesthesia, as defined herein. Non-limiting examples of general anesthetics include nitrous oxide, sevoflurane, halothane, xenon, enflurane, chloroform, isoflurane, methoxyflurane, desflurane, ethyl chloride, cyclopropane, chloral hydrate, ketamine, esketamine, etomidate, propofol, chlorobutanol, guanabenz, guanfacine, clonidine, tizanidine, medetomidine, and dexmedetomidine.

The term "sedation," as used herein, refers to a rousable state or depression in consciousness caused by sedative drugs. In standard practice, sedation is typically used for minor surgical interventions. During sedation, a subject shows decreased arousal or consciousness, wherein consciousness can be described as an awareness of self and environment or the awareness of external stimuli. The effects of sedation include anxiolysis, and/or amnesia, and/or analgesia. The term "sedative drugs" or "sedatives" encompasses a broad spectrum of drugs that slow normal brain function. They have different mechanisms of action, but mainly function by increasing the neurotransmitter gamma-aminobutyric acid (GABA), which in turn depresses the central nervous system (CNS). Types of sedatives include barbiturates, benzodiazepines, nonbenzodiazepine hypnotics, first generation antihistamines, herbal sedatives, methaqualone (and analogues), muscle relaxants, opioids, antidepressants, and antipsychotics.

Examples of barbiturates include Amobarbital, Aprobarbital, Butabarbital, Mephobarbital, Methohexital, Pentobarbital, Phenobarbital, Primidone, Secobarbital, and Thiopental. Examples of benzodiazepines include Alcohol (ethyl alcohol or ethanol), Alprazolam, Chloral hydrate, Chlordiazepoxide, Clorazepate, Clonazepam, Diazepam, Estazolam, Flunitrazepam, Flurazepam, Lorazepam, Midazolam, Nitrazepam, Oxazepam, Temazepam, and Triazolam. Examples of nonbenzodiazepine hypnotics include Eszopiclone, Zaleplon, Zolpidem, and Zopiclone. Examples of first generation antihistamines include Diphenhydramine, Dimenhydrinate, Doxylamine, Promethazine, Hydroxyzine, Brompheniramine, and Chlorpheniramine. Examples of herbal sedatives include *Duboisia hopwoodii*, chamomile, *Prostanthera striatiflora*, catnip, *Piper methysticum*, valerian, cannabis, *Passiflora incarnata*, *Physochlaina*, and menthyl isovalerate. Examples of methaqualone (and analogues) include Afloqualone, Cloroqualone, Diproqualone, Etaqualone, Methaqualone, Methylmethaqualone, Mebroqualone, Mecloqualone, and Nitromethaqualone. Examples of muscle relaxants include Baclofen, Meprobamate, Carisoprodol, Cyclobenzaprine, Metaxalone, Methocarbamol, Tizanidine, Chlorzoxazone, Orphenadrine, Gabapentin, and Pregabalin. Examples of opioids include Tramadol, Tapentadol, Morphine, Hydromorphone, Oxymorphone, Oxycodone, Hydrocodone, Methadone, Propoxyphene, Meperidine, Fentanyl, Codeine, Carfentanil, Remifentanil, Alfentanil, Sufentanil, and Opium. Examples of antidepressants include Amitriptyline, Trazodone, Mirtazapine, Doxepin, Desipramine, Imipramine, Clomipramine, Amoxapine, Trimipramine, Nortriptyline, and Nefazodone. Examples of antipsychotics include Olanzapine, Clozapine, Thiothixene, Haloperidol, Fluphenazine, Prochlorperazine, Trifluoperazine, Loxapine, Quetiapine, and Asenapine.

Medication to induce general anesthesia or sedation can be administered, for example, through a breathing mask or tube, or given as an injection. The injection can be intravenously, intradermally, intraarterially, intralesionally, intratumorally,

intracranially, intraarticularly, intraprostaticaly, intrapleurally, intratracheally, intravitreally, intravaginally, intrarectally, topically, intratumorally, intramuscularly, intraperitoneally, subcutaneously, subconjunctival, intravesicularlly, mucosally, intrapericardially, intraumbilically, and/or intraocularally. In some embodiments, the medication used to induce general anesthesia or sedation can also be administered by infusion, such as intravenous infusion.

General anesthesia and sedation are dose-dependent and there exists a lot of person-to-person variation in response to doses.

In some embodiments, a subject is placed under general anesthesia with a general anesthetic such as propofol, a rapid-activating GABAergic drug that can cause cessation of breathing and require intubation. For medical evaluations, the general anesthetic is turned off until the subject reaches the desired state of consciousness and then turned back on after the evaluation. In some embodiments of this disclosure, with the use of alternative sedatives, such as α2 adrenergic receptor agonists, either alone or in combination with general anesthetics, it is possible to administer an anesthesia-reversing agent to rapidly reverse the effects of the sedative so that the subject's medical evaluation can be carried intraoperatively and more efficiently.

ANESTHESIA-REVERSING AGENTS

Described herein, in some aspects, are methods for administering an anesthesia-reversing agent to a subject who is under general anesthesia or sedation. Anesthesia-reversing agents (*e.g.*, reversal agents), as used herein, reverse the effects of anesthetic drugs or sedative drugs. There are two main types of anesthesia-reversing drugs: receptor-specific antagonists and non-specific analeptic agents. Receptor-specific antagonists, used in the present disclosure, have no intrinsic capacity for anesthesia reversal but have a high affinity for a receptor involved in the anesthetic effect pathway. Non-limiting examples of

such receptor-specific antagonist include atipamezole, anticholinesterases, naloxone, flumazenil, nalmefene, and naltrexone (Pani, Dongare, & Mishra, 2015).

In several major surgical procedures, it would be useful to wake a subject during the surgery. This practice is referred to as a "planned wake-up". In some embodiments of the disclosure, the subject may be returned to a certain level of consciousness during the procedure to evaluate the subject's physiology (*e.g.*, the effectiveness of the treatment or intervention). In yet another embodiment of the disclosure, the subject may be returned to a certain level of consciousness during the procedure in response to an emergency situation. Currently, the standard practice is to reduce or terminate the administration of the anesthetic drug or sedative, and wait for its effects to wear off, which is an impractical solution due to loss of time and space in the operating room. In emergency situations, this practice also increases the risk of secondary complications and/or death to the subject. This practice can have additional adverse effects on the subject: for example, a slow and gradual emergence from unconsciousness or sedation can be disorienting and has been attributed to cases of delirium, post-surgery. Thus, there is a dire need for improved methods to induce rapid reversal of (general anesthesia-related) unconsciousness or sedation, in order to conduct intra-operative or post-operative assessments of a patient's physiology, evaluate treatments or surgical procedures, and improve patient outcomes.

As used herein, the term "emergence" refers to the process of regaining consciousness. This is a process during which a subject regains cognitive and, optionally motor faculties. As used herein, the term "planned wake-up" refers to the process of intentionally inducing consciousness and the return of cognitive faculties in a subject during a surgical procedure. In some embodiments, this planned wake-up is for purposes of an assessment. In alternative embodiments, this planned wake-up is performed in response to an emergency during the surgery.

Typically, the administration of anesthetics and sedatives is terminated to facilitate arousal or emergence from unconsciousness or sedation, which can take a prolonged period

of time and render planning the end or subsequent step of a procedure difficult. Subjects typically do not regain cognitive and/or motor faculties quickly when anesthetic administration is decreased or stopped, which may delay extubation of a patient and thus require intensive care unit (ICU) admission. In order to reduce the time to emergence, additional drugs (*i.e.*, anesthesia-reversing agents) can be administered during or at the end of a procedure.

As used herein, the terms "intensive care unit" and "critical care unit" are used interchangeably. ICU, as used herein, refers to a ward in which subjects (*e.g.*, hospital patients) are cared for. These subjects are in critical condition, have undergone major surgery, and are under constant observation. Subjects are never discharged from the ICU, and instead are moved to standard medical hospital floors once stable.

α2 ADRENERGIC RECEPTOR AGONISTS

As described above, there are a number of general anesthetics and sedatives. Of particular interest to the present disclosure are α2 adrenergic receptor agonists (also known as α2 adrenoceptor agonists). These agonists are widely used as anesthesia adjuncts and, less commonly, used alone (*i.e.* in solo). As used herein, the term "adjunct" refers to an agent that is used in combination (*i.e.* as a supplement) and, in the context of this disclosure, enhances or augments anesthetic effects.

One of the reasons for the broad use of α2 adrenergic receptor agonists as anesthesia adjuncts in the medical field is minimalization of a subject's requirement for additional sedative or anesthetics. Many of the additional surgical anesthetics are not tolerated well, especially in children and the elderly, which makes surgery and sedation less safe. Some of the associated risks with these drugs include, but are not limited to, acute hypertension, rebound hypertension after cessation of the anesthetic or sedative, nausea, delirium after cessation of the anesthetic or sedative, hepatoxicity, elevated serum concentrations, bradycardia, tachyphylaxis, hypoxia, and atrial fibrillation.

An α2 adrenergic receptor inhibits norepinephrine release from the presynaptic neuron. This is accomplished through the inhibition of adenylate cyclase, which decreases the formation of 3,5-cyclic adenosine monophosphate (cAMP). Through modulation of calcium-activated activity, specifically potassium efflux, calcium entry into the nerve channel is blocked and the membrane hyperpolarizes. Norepinephrine secretion and neuronal firing are, in turn, suppressed (Gertler, Brown, Mitchell, & Silvius, 2017; Giovannitti, Thoms, & Crawford, 2015). Non-limiting examples of α2 adrenergic receptor agonists include guanabenz, guanfacine, clonidine, tizanidine, medetomidine, and dexmedetomidine.

Dexmedetomidine (*e.g.*, PRECEDEX™ and DEXDOMITOR®) is a prototypical central α2 adrenergic receptor agonist, a sedative, and has been utilized most broadly in veterinary contexts. It is prescribed for intravenous use. DEXDOMITOR® (dexmedetomidine hydrochloride) is indicated for use in dogs and cats, while PRECEDEX™ (dexmedetomidine hydrochloride) is indicated for use in humans. Dexmedetomidine is an imidazole compound and an active dextroisomer of medetomidine. It has a highly selective affinity for the α2 adrenoceptor and selectively binds to presynaptic α2 adrenoceptor, which inhibits the post-synaptic activation of adrenoceptors, suppresses sympathetic activity, and induces sedation and anxiolysis.

Compared to other more commonly-used anesthetics and sedatives, dexmedetomidine is a safer option that, when supplemented to current anesthesia cocktails, has been shown to dramatically reduce the quantity of other surgical anesthetics required for general anesthesia and sedation. It can be administered orally, transmucosally, transdermally, intravenously, or intramuscularly. When delivered by intravenous (IV) infusion at low doses, it decreases cardiac output and systolic blood pressure. Unlike other anesthetics and sedatives, dexmedetomidine has a minimal effect on the respiratory system and can provide adequate rousable sedation without intubation (Giovannitti et al., 2015).

In previous years, dexmedetomidine was not preferred for human clinical use, primarily due to its terminal elimination half-life of about 2 hours—its prolonged efficacy. It was primarily used for non-human subjects, including, but not limited to monkeys, dogs, and pigs. However, despite its prolonged duration of efficacy, dexmedetomidine is increasingly being used in more human surgeries due to the aforementioned advantages it has over other anesthetic and sedative drugs. Dexmedetomidine is currently approved by the United Stated Food and Drug Administration (FDA) for sedation of initially intubated and mechanically ventilated patients in an intensive care setting and sedation of non-intubated patients prior to and/or during surgical procedures. Methods for administering dexmedetomidine to patients in an intensive care unit are provided in US Patent No. 6,716,867.

Clonidine (*e.g.*, CATAPRES® and KAPVAY™) is an imidazoline derivative and a centrally-acting α2 adrenergic receptor agonist. Clonidine binds to a central α2 adrenergic receptor, thus suppressing norepinephrine release and decreasing the sympathetic outflow to the heart, kidneys, and peripheral vasculature. In doing so, clonidine reduces the blood pressure and heart rate of a subject. Clonidine is used as a sedative and analgesic. It reduces post-operative shivering. Its additional uses are for the treatment of hypertension, ADHD, and cancer pain in human subjects. It has also been used for prophylaxis of vascular migraine headaches, treatment of severe dysmenorrhea, management of vasomotor symptoms associated with menopause, and treatment of opiate, benzodiazepine, alcohol, cocaine, food, and tobacco withdrawal. It is prescribed for oral use and has an elimination half-life ranging from 12 hours to 16 hours. Clonidine has resulted in unpredictable hemodynamic effects (*e.g.*, hypotension and tachycardia), which has limited its use on critically ill subjects (Tryba & Kulka, 1993).

In some aspects, the disclosure provides a means to counter the prolonged efficacy of these α2 adrenergic receptor agonists/sedatives through the use of an anesthesia-reversing agent, for example, an α2 adrenergic receptor antagonist.

α2 ADRENERGIC RECEPTOR ANTAGONISTS

An α2 adrenergic receptor antagonist, as used herein, is a neural blockade reversing agent that specifically antagonizes α2 adrenergic receptors. α2 adrenergic receptor antagonists are known in the art and include but are not limited to Atipamezole, Aripiprazole, Asenapine, Cirazoline, Clozapine, Efaroxan, Idazoxan, Lurasidone, Melperone, Mianserin, Mirtazapine, Napitane, Olanzapine, Paliperidone, Phenoxybenzamine, Phentolamine, Piribedil, Rauwolscine, Risperidone, Rotigotine, Quetiapine, Norquetiapine , Tetiptiline, Tolazoline, Yohimbine, and Ziprasidone.

Atipamezole (MPV-1248) or 4-(2-ethyl-2,3-dihydro-1H-inden-2-yl)-1H-imidazole] (ANTISEDAN®) is a synthetic agent with an imidazole structure. It has the following chemical structure:

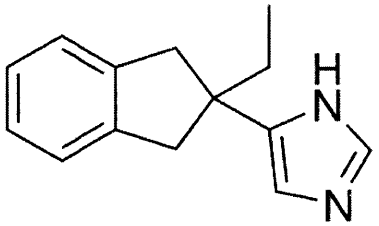

In some embodiments, the methods of the invention use atipamezole, a synthetic α2 adrenergic receptor antagonist, to rapidly reverse the sedative and analgesic effects of α2 adrenergic receptor agonists, such as dexmedetomidine, medetomidine, romifidine, and xylazine. Atipamezole has been used in veterinary medicine. It is currently administered to dogs as an intramuscular injection. Clinically, it has not been used for human surgeries.

After administration, atipamezole rapidly crosses the blood brain barrier. It is highly selective for α2-adrenergic receptors, which are in the central synapses and are located presynaptically and/or postsynaptically. There are three types of α2-adrenergic receptors, α2A, α2B, and α2C. α2A are located on the locus coeruleus, brainstem, cerebral cortex, septum, hypothalamus, hippocampus and amygdala. α2B is located in the

thalamus, and α2C is located in the basal ganglia, olfactory tubercle, hippocampus, and cerebral cortex (Scheinin et al., 1994). Atipamezole competitively displaces α2-adrenergic receptor agonists. In addition, it has no affinity for other receptors, which increases its effectiveness and minimizes adverse effects from the drug. Upon administration, atipamezole has been shown to reverse sedation, increase subject mobility after a non-invasive or minor surgery, and reverse the cardiovascular effects (*e.g.*, bradycardia) of α2-adrenergic receptor agonists (*e.g.*, dexmedetomidine and clonidine). In certain cases, administration of atipamezole results in motor restlessness, hypotension, and/or tachycardia, and thus it has not been recommended for intravenous administration (Bahri, 2008).

Atipamezole has a rapid onset, at which point a subject under sedation regains consciousness and motor and/or cognitive faculties. Intramuscular injection of atipamezole has been shown to reverse the effects of dexmedetomidine (*e.g.*, DEXDOMITOR and DEXDOMITOR 0.1) in 5-10 minutes. As used herein, the term "rapid" or "rapidly" refers to an onset ranging from 1 minute to 20 minutes following the administration of the α2 adrenergic receptor antagonist. According to some aspects of the present disclosure, rapid onset of α2 adrenergic receptor antagonist is 1, 2, 3, 4, 5, 6, 7, 8, 9, 10, 11, 12, 13, 14, 15, 16, 17, 18, 19, or 20 minutes.

The use of atipamezole or other α2 adrenergic receptor antagonists as reversal agents would expand the use of α2 adrenergic receptor agonists such as dexmedetomidine in operating rooms and ICUs and allow subjects to emerge from unconsciousness more rapidly, enabling intraoperative evaluations, post-operative evaluations, and quick discharge. This new application for atipamezole could radically transform current practice and open up possibilities for unknown procedures and treatments in future.

INTRAOPERATIVE AND POST-OPERATIVE SURGERY-RELATED USE OF α2 ADRENERGIC RECEPTOR ANTAGONIST

In surgical cases in the operating room, a temporary reversal of unconsciousness may be desired. Often in neurosurgical and orthopedic surgery cases, for example, the subject will have received general anesthesia in standard current practices and surgery will be performed to expose a region of the central nervous system such as the brain or spinal cord. In some embodiments, before surgery can proceed on the sensitive region of interest, the subject will be re-awakened by administering an α2 adrenergic receptor (*e.g.*, atipamezole) for an intraoperative assessment of nervous system function. This is done in order to determine the functions of the regions of potential surgical intervention in order to avoid damaging regions of critical importance (*e.g.*, avoiding critical language regions in the brain during tumor removal via patient's speaking, ensuring spinal cord integrity by voluntary movements). In contrast, current practice involves turning down the levels of anesthetic drugs and waiting for them to wear off once the surgical site has been exposed and before the surgery can proceed.

In some aspects of the present disclosure, a subject treated with general anesthetic agents, including an α2 adrenergic receptor agonist, will undergo the initial stages of relevant surgical procedures. Upon the clinician's decision to evaluate the functions and/or physiologic status of an organ, organ system, or anatomical region of importance to the clinicians, administration of an α2 adrenergic receptor antagonist will be carried out as either a single bolus, multiple boluses, or as a continuous infusion. At this time (or prior to or following this administration), the standard anesthetic protocol for facilitating reversal of intraoperative sedation may be begun or the pre-reversal protocol may be maintained. Part way through or following the conclusion of the physiologic or functional assessment, intravenous α2 adrenergic receptor antagonist will cease infusion, and the surgical procedure will proceed following current practices with re-initiation of general anesthesia, after a planned wake-up.

In some embodiments of the present disclosure, an α2 adrenergic receptor antagonist is used for rapid reversal of unconsciousness in an awake craniotomy, whereby

a subject is administered an α2 adrenergic receptor agonist (*e.g.*, dexmedetomidine) and is fully unconscious under general anesthesia. The subject is administered an α2 adrenergic receptor antagonist to regain cognitive faculties (while standard anesthetics remain on or are reduced prior to infusion), and standard motor and language mapping of the brain are carried out. The surgery proceeds as normal because the subject is fully anesthetized following intraoperative cognitive or physiological testing.

In some embodiments of the present disclosure, an α2 adrenergic receptor antagonist is used for rapid reversal of unconsciousness in a neurosurgery or orthopedic spine surgery, whereby a subject is administered an α2 adrenergic receptor agonist (*e.g.*, dexmedetomidine) and is fully unconscious under general anesthesia. The subject is administered an α2 adrenergic receptor antagonist to regain active (awake) or improve passive/conductive motor faculties (while standard anesthetics remain on or are reduced prior to infusion), and standard motor mapping techniques of the spinal cord and musculature carried out. The surgery proceeds as normal because the subject is fully anesthetized following intraoperative testing.

Often in neurosurgical and orthopedic surgery cases, for example, the subject will have received general anesthesia in standard current practices and surgery will be performed on sensitive regions of interest within or approximating structures of the central or peripheral nervous system. It is of critical importance to know if the intervention succeeded or caused unacceptable side effects (*e.g.*, in surgery on the spine that approximates the spinal cord, it is essential to know if the surgery placed pressure on the nerves and was blocking motor and sensory functions). Current practice involves turning down the levels of anesthetic drugs and waiting for them to wear off and allowing the patient to begin the wake-up process and be transferred to the post-operative care unit or a critical care unit. Often here, in these sites outside of the operating room, the first exams are done on the patients to evaluate the presence or absence of side-effects and overall effectiveness resulting from the surgery.

In some embodiments, a subject is treated with general anesthetic agents, including the addition of an α2 adrenergic receptor agonist, and will undergo the initial stages of relevant surgical procedures. Prior to or upon conclusion of the surgical procedure, general anesthetic doses are reduced to help facilitate awakening of the subject. At these times, an α2 adrenergic receptor antagonist will be administered as either a single bolus, multiple boluses, or as a continuous infusion. The intended effect of the drug is to wake up the subject rapidly from a state of unconsciousness such that a clinical exam can be carried out in the operating room. Before the subject is relocated to the main hospital floor, the rapid arousal will allow the surgeons or additional medical clinical team members to evaluate the functions and/or physiologic status of an organ, organ system, or anatomical region of relevance to the surgical procedure previously completed. This is a critical diagnostic maneuver. This will allow for immediate evaluation of the subject's physiological state post-surgery. This rapid induction of wake-up may allow immediate diagnosis of potentially untoward events that can require further diagnostic evaluation and/or treatment. An anesthesia-reversal agent such as an α2 adrenergic receptor antagonist could open the possibility of evaluating the surgeries effectiveness still in the operating room because the subject will be sufficiently awake for clinical exams. This could radically change the practice of care, for example, as surgeries could be re-initiated in the operating room immediately to rectify otherwise devastating side effects, without reinitiating a whole new surgery at a different time.

The intensive care unit (ICU) receives patients following major trauma health events and following majorly invasive or complicated surgeries. In the ICU, human patients are often sedated with propofol, a rapid-acting GABAergic drug that can stop breathing and thus requires patients to be intubated. Patients in the ICU are continuously observed and receive regular health exams from the healthcare team to evaluate progress of symptoms and recovery of physiological functions. Currently, propofol infusions are scheduled to be turned off prior to these clinical exams. Dexmedetomidine, however, has

shown promise in trials that α2-adrenergic drugs can be used in the critical care setting for sedation without the need for intubation. The prolonged duration of action of this dexmedetomidine make it extremely difficult, if not impossible, to efficiently schedule and perform clinical exams on patients requiring them. Administration of an α2 adrenergic receptor antagonist such as atipamezole would allow for rapid reversal of α2 adrenergic receptor agonist (*e.g.*, dexmedetomidine) in the ICU, and allow clinical teams to evaluate a subject's physiologic functions efficiently and more safely.

In some aspects of the present disclosure, subjects in an intensive or critical care unit (e.g. medical ICU, post-surgical ICU, cardiac ICU, neurological ICU) receive α2 adrenergic receptor agonists such as dexmedetomidine or clonidine with or without supplementation of other general anesthetics, such as propofol, sevoflurane, ketamine, or benzodiazepines. During their inpatient stay under continuous monitoring, the addition of an α2 adrenergic receptor antagonist, such as atipamezole, is used to reverse the sedative effects of the anesthetic drugs, specifically such that physical and physiological assessments can take place unencumbered. Once the assessment has taken place, next steps in treatment can be more accurately planned and a decision to restore or remove sedation from the patient can be made.

In some embodiments, the α2 adrenergic receptor antagonist (e.g., atipamezol) is administered with a second anesthesia-reversing agent. Non-limiting examples of anesthesia-reversing agents include neuromuscular blockade reversal agents (anticholinesterases, cyclodextrins, cysteine, 4-aminopyridine, galanthamine, suramin, etc.), opioid antagonists (naloxone, nalmefene, naltrexone etc.), sedative reversal agents (flumazenil, atipamezole, etc.), analeptic agents (doxapram, nikethamide, pentylenetetrazol, bemegride, amphetamine, methylphenidate, etc.), and anticoagulant reversal agents (e.g., platelet factor 4).

As used herein, the term "inpatient" refers to a setting wherein the patient is admitted and currently staying in the hospital. An inpatient facility is for patients that have not been discharged.

In some embodiments, a subject suffering from a traumatic injury and requiring a clinical exam in the ICU receives α2 adrenergic receptor agonist (*e.g.*, dexmedetomidine) sedation with or without other anesthetic drugs. Sedative and anesthetic agents administered to subjects are either maintained or changed at the time of the clinical exam. An α2 adrenergic receptor antagonists, for example, are administered intravenously either as a bolus, multiple boluses, or an infusion in order to reverse sedation sufficiently such that a clinical exam can be initiated. Following the exam or at the cessation of its attempt, standard ICU sedation protocols restart at the discretion of the physician based on the new clinical findings.

An alternative embodiment is an intubated subject that has suppressed breathing and is in the ICU receiving adrenergic receptor agonist (*e.g.*, dexmedetomidine) sedation with or without other anesthetic drugs. In order to assess the viability of that subject's breathing abilities, intravenous α2 adrenergic receptor antagonist is administered via bolus, multiple boluses, or steady infusion. Spontaneous breathing is assessed following the administration of the α2 adrenergic receptor antagonist, and a new clinical decision is able to be made at this time to discern if extubation if indicated or sedation should be reinstated.

An alternative embodiment is the use of an α2 adrenergic receptor antagonist on subjects in the ICU following major surgery to improve long-term patient outcomes. An α2 adrenergic receptor antagonist is administered via bolus, multiple boluses, or steady infusion in order to get these subjects ambulatory. Reduction in sedation increases the time the subjects will spend walking and moving around during their stay, and will improve the chances for a better health outcome.

The term surgery (*e.g.*, surgical procedure) refers to the use of a manual or instrumental technique on a subject to diagnose or treat a pathological condition, to improve a physiologic condition, or to enhance the appearance of an organ, organ system, or anatomical region. It includes any procedure (e.g., laparoscopic or otherwise requiring suturing or wound closure). Surgery can be performed by a doctor, surgeon, veterinarian, or dentist and can be performed in a hospital, veterinary clinic, dentist's office, or an equivalent health care facility. Surgery can also be performed bedside in an ICU/PACU /Surgical ICU, as emergencies arise, and make-shift operating areas are established at the bedside to deal with the urgent nature of the matter. The term "major surgery", as used herein, refers to an invasive surgery for which the use of sedation or general anesthesia is recommended.

In some embodiments, the surgery is performed in an operating room (OR). The term "operating room" as used herein refers to a room within a hospital, veterinary clinic, or health care facility in which surgical procedures are performed under sterile conditions. To maintain the sterility of the operating room all the individuals wear personal protective equipment and have their nose and mouth covered, with the exception, in some instances, of the patient.

As used herein, the "end of the surgery" (or end of the surgical procedure) refers to the time of the assumed final role of the individual conducting the surgery (e.g., the surgeon, dentist, etc.) The end of the surgical procedure can refer to the point when the anesthesiologist takes over the surgery for extubation, the point when extubation has been completed (or successfully completed), the transfer of patient out of the operating room, the point of final wound closure (sutures set), the final surgical evaluation in the operating room, etc. In some embodiments, the end of the surgery can be defined as the completion time of the last medical procedure (e.g., billable medical procedure) carried out by a member of the surgical team before the transfer of acute management to a member of

another staff (anesthesiologists, medical ICU docs, etc.). A person of ordinary skill in the art would recognize the end of the surgery (surgical procedure).

As used herein, the terms "subject" and "patient" are used interchangeably. In some embodiments, subject refers to a human, in other embodiments subject refers to a mammal, wherein the mammal is selected from a group including but not limited to non-human primate, cow, horse, pig, sheep, goat, dog, cat, rabbit, ferret, hippopotamus, giraffe, okapi, or rodent. In further embodiments, subject refers to a reptile, wherein the reptile is selected from a group including tortoises, turtles, alligators, and armadillos.
In some embodiments, an α2 adrenergic receptor antagonist is administered to a subject undergoing day-stay surgery, wherein "day-stay surgery" refers to surgery for more minor procedure, wherein the subject is discharged the same day of the surgery, generally without ICU admission. In some embodiments, an α2 adrenergic receptor antagonist is administered to a subject undergoing major surgery. In further embodiments, an α2 adrenergic receptor antagonist is administered to a subject that is undergoing a surgical procedure and will not be discharged on the same-day.

A surgical procedure, as used herein, includes but is not limited to a neurosurgery, orthopedic surgery, thoracic or cardiovascular surgery, gynecologic surgery, ophthalmologic surgery, oral or maxillofacial surgery, otolaryngological surgery, urological surgery, and cosmetic surgery. Non-limiting examples of neurosurgeries include spinal fusion, ventriculostomy, craniotomy, cranioplasty, decompressive craniectomy, trepanning, pallidotomy, anterior temporal lobectomy, thalamotomy, hemispherectomy, endoscopic thoracic sympathectomy, sympathectomy, bilateral cingulotomy, and lobotomy. Non-limiting examples of orthopedic surgery include spine surgery, scoliosis surgery, hand surgery, shoulder surgery, elbow surgery, total joint reconstruction (arthroplasty), skull reconstruction, foot surgery, and ankle surgery. Non-limiting examples of thoracic or cardiovascular surgery include Angioplasty, coronary artery bypass surgery, Valvuloplasty, Pericardiectomy, Endarterectomy, Cardiotomy,

Thoracotomy, Pericardiotomy, Pneumonectomy, Pleurodesis, heart transplantation, and lung transplantation. Non-limiting examples of gynecologic surgery include Vaginoplasty, Clitoroplasty, Labiaplasty, Tuboplasty, Fimbrioplasty, Cervicectomy, Clitoridectomy, Oophorectomy, Salpingoophorectomy, Salpingectomy, Hysterectomy, Vaginectomy, Vulvectomy, Salpingostomy, Amniotomy, Clitoridotomy, Hysterotomy, Hymenotomy, Episiotomy, Symphysiotomy , Tubal ligation, Tubal reversal, Colporrhaphy, Cesarean section, Hymenorrhaphy, and Endometrial biopsy. Non-limiting examples of ophthalmologic surgery include Punctoplasty, Trabeculoplasty, Photorefractive keratectomy, Trabeculectomy, Iridectomy, Vitrectomy, Dacryocystorhinostomy, Radial keratotomy, Mini Asymmetric Radial Keratotomy, and Corneal transplantation. Non-limiting examples of oral or maxillofacial surgery include Tracheal intubation, Distraction osteogenesis, Cranioplasty, Sling, Labial frenectomy, Jaw reduction, Microsurgery, Genioglossus advancement, Osteotomy, Bone grafting, Flap, Cheiloplasty, Maxillomandibular advancement, Facial feminization surgery, Face transplant, and Forehead lift. Non-limiting examples of otolaryngological surgery include insertion of grommets for glue ear, tonsillectomy, septoplasty, microlaryngoscopy, oesophagoscopy, endoscopic sinus surgery, tympanomastoid surgery, and tracheostomy. Non-limiting examples of urological surgery include Urethroplasty, Pyeloplasty, Nephrectomy, Cystectomy, Nephrostomy, Ureterostomy, Cystostomy (Suprapubic cystostomy), Urostomy, Nephrotomy, Nephropexy, Urethropexy, Lithotripsy, Kidney transplantation, and Renal biopsy. Non-limiting examples of plastic surgery include Abdominoplasty, Blepharoplasty, Phalloplasty, Mammoplasty, Buttock augmentation, Cryolipolysis, Cryoneuromodulation, Labiaplasty, Lip enhancement, Rhinoplasty, Otoplasty, Rhytidectomy, Genioplasty, Cheek augmentation, Orthognathic Surgery, Fillers injections, Brachioplasty, Liposuction, Zygoma reduction plasty, and Jaw reduction.

The methods and compositions of the present disclosure can also be used in a medical procedure in which an α2 adrenergic receptor agonist is used (e.g., colonoscopy, sigmoidoscopy, esophagogastroduodenoscopy, etc.)

The term "intraoperative", as used herein, refers to any time period during the surgical procedure and prior to the end of the surgical procedure. In some embodiments, the end of the surgical procedure is when all manual and instrumental techniques being conducted on the subject for the surgical procedure have been completed. In other embodiments, the end of the surgical procedure is when the subject is removed from the operating room. The term "post-operative", as used herein, refers to any time period after the end of the surgical procedure. In some embodiments, the term "post-operative" refers to any time following the surgical procedure when the subject is in the ICU.

The present disclosure provides methods to administer to a subject under general anesthesia or sedation an effective amount of an α2 adrenergic receptor antagonist in order to conduct an intraoperative assessment or post-operative assessment (*e.g.*, clinical or physical examination). In one embodiment, the surgery is a neurosurgery, more specifically a craniotomy and the assessment performed is a standard motor and language mapping of the brain. Standard motor and language mapping of the brain are examples of cortical stimulation mapping, which is a highly invasive surgical procedure that involves the placement of electrodes on exposed brain tissue and delivery of an electric stimulus to identify the role of that part of the brain or to test the function of the part of the brain. In the context of a craniotomy, an assessment can be a standard motor mapping of the brain, wherein the standard motor mapping of the brain is the use of cortical stimulation mapping to stimulate a motor or sensory response within the body. In the context of a craniotomy, an assessment can be a standard language mapping, wherein the standard language mapping is the use of cortical stimulation mapping while a language-related assessment is performed on the subject. Non-limiting examples of language-related assessments are known to one of ordinary skill in the art and include reading sentences,

completing sentences, auditory comprehension, answering basic questions, spontaneous speech, verb generation, fluency tasks (*e.g.*, listing words that start with a specific letter), naming objects, listing letters, and counting. In some embodiment the standard language mapping is performed with functional magnetic resonance imaging (fMRI). In some aspects, the intraoperative assessment is an evaluation of the surgical procedure. For example the motor and language mapping of the brain when performed intraoperatively can reveal whether the preceding portions of the surgical procedure have resulted in any functional damage to the nervous system.

In the context of an orthopedic surgery, non-limiting examples of assessments are asking the subject to move a body part, asking a subject whether a body part can be felt, and asking a subject whether a physical stimulus can be felt. In the example of a spine surgery, the intraoperative assessment is an evaluation of the surgical procedure, because it reveals and functional damage sustained by the spine and any unintended pressure on the subject's spinal cord or nerves.

In some embodiments, an assessment is a measurement of the following parameters in a subject: heart rate, respiratory rate, blood pressure, urine output, knee reflex test, post-operative pain, and responsiveness to verbal communication.

In some embodiments a subject is administered α2 adrenergic receptor agonist and is intubated. As used herein, the term "intubated" or "intubation" refers to the insertion of a tube (*e.g.*, endotracheal tube) into the trachea in order to connect a subject to a ventilator, which assists with breathing. Intubation is often used to assist with breathing when a subject is under general anesthesia or receiving certain types of sedation in critical care settings (e.g. ICU). As used herein, the term "extubate" or "extubation" refers to the removal of the endotracheal tube, often at the end of the surgery to allow the subject to breath unassisted. In some embodiments, the subject is administered α2 adrenergic receptor antagonist prior to the end of surgery. "Prior to the end of the surgical procedure", as used herein, can be 0, 1, 2, 3, 4, 5, 6, 7, 8, 9, 10, 11, 12, 13, 14, 15, 16, 17, 18, 19, or 20

minutes prior to the end of surgery or in any range of time between 0 to 20 minutes prior to the end of surgery (e.g. 0-10 minutes, 0-15 minutes, etc.). The subject is then observed for a pharyngeal reflex (*i.e.* gag-reflex) before extubation.

Typically, when a subject does not have a gag-reflex towards the end or after the surgery, the clinicians conduct a trial extubation or a spontaneous breathing trial. In a trial extubation, the tube is removed before the subject displays a gag-reflex and is spontaneously breathing. It is done in the hope that the subject will begin breathing spontaneously. A failed trial extubation, may require reintubation. In a spontaneous breathing trial, the subject is still intubated and connected to the mechanical ventilator. The mechanical ventilator is set to minimal ventilator settings and the ability of the subject to begin their own breathing at these settings is observed. For such protocols, the patient is extubated if they pass the spontaneous breathing trial (i.e. demonstrate sufficient physiological evidence that they will be able to breath on their own without mechanical support). If not, the spontaneous breathing trial is repeated and/or lengthened. As explained above, the use of atipamezole would reduce or obviate the need for trial extubation and minimize time required for spontaneous breathing trials. It has the potential to reduce the number of failed extubations, and the potentially dangerous and expensive complications arising therefrom.

In some embodiments, a subject is administered an effective amount of an α2 adrenergic receptor agonist to perform a surgical procedure, then the subject is administered an effective amount of α2 adrenergic receptor antagonist prior to the end of the surgical procedure (or at the end of the surgical procedure), and the clinician observes the subject (performs an intraoperative assessment or post-operative assessment) for a brainstem reflex. Examples of brainstem reflexes include, but are not limited to, pharyngeal reflex, tracheal reflex, pupillary reflex, corneal reflex, spontaneous eye position and movements, occulocephalic (Doll's eye) reflex, occulovestibular (caloric) reflex, and jaw reflex.

In some embodiments, the post-operative assessment is conducted in the operating room. Alternatively, it is conducted after the patient has been transferred to the ICU. The post-operative assessments occurring after the end of the surgical procedure can occur within 1, 2, 3, 4, 5, 6, 7, 8, 9, 10, 11, 12, 13, 14, 15, 16, 17, 18, 19, 20, 21, 22, 23, 24, 25, 26, 27, 28, 29, 30, 35, 40, 45, 50, or 60 minutes of the end of surgery. In some embodiments, the postoperative assessment is conducted 1.5, 2, 2.5, or 3 hours after the end of the surgery.

CARDIAC ARREST

Patients receiving α2 adrenergic agonists can suffer from cardiovascular side-effects including reduced heart rate. It has been previously reported that patients can suffer from cardiac arrest when receiving dexmedetomidine. Currently, patients receive a standard regime of pharmacological agents to restart the heart including atropine and epinephrine. Contemplated in this disclosure is a α2-agonists adrenergic antagonist and methods for using the α2-agonists adrenergic antagonist to reduce the agent causing the cardiac arrest, which would identify the cause of the stopped heart as arising from the α2 adrenergic agonist and restart the heart beating in these cases. As disclosed herein, the α2-agonists adrenergic antagonist can be used to determine if the cause of the cardiac arrest is due to the α2-receptor agonist drugs, which would be confirmed if the heart resumes beating. Thus, the methods used according to this disclosure allow the use of an α2 adrenergic receptor antagonist to diagnose/identify cardiac arrest intraoperatively. Additionally, the methods according to this disclosure allow the use of an α2 adrenergic receptor antagonist to treat cardiac arrest.

As used herein, the term "cardiac arrest" refers to the abrupt loss of heart function—whereby the heart ceases beating. In some cases it is preceded by abnormal heart rhythms, for example, an irregular heart rhythm, bradycardia (*i.e.*, a depressed heart rate), tachycardia (*i.e.*, an accelerated heart rhythm), and the like.

The term "treat," as used herein refers to the process of administering an agent (*e.g.*, therapeutic agent), wherein the object is to lessen or reverse an undesired physiological condition, disorder or disease, or to obtain beneficial or desired clinical results. The term "treat" implies that the agent elicits a clinically significant response, as determined by one of ordinary skill in the art.

In some aspects of the disclosure, a subject is in an inpatient setting or in an operating room receives α2 adrenergic agonist, alone or in combination with other sedative drugs. Upon the code alerting the clinical care team that the subject's heart has ceased beating, an α2-receptor antagonist is administered. In some embodiment, the α2 adrenergic agonist is injected, infused, or oral. In some embodiments, the α2 adrenergic antagonist is administered as an injection. In some embodiments, the α2 adrenergic antagonist is administered as an infusion. In some embodiments, the α2 adrenergic antagonist is administered as either a single bolus, multiple boluses, or as a continuous infusion. In some embodiments, when the patient is under cardiac arrest, boluses of α2-adrenergic receptor antagonist are progressively administered until the patient's heart resumes beating.

In alternative embodiments, the methods of the present disclosure are used for treating bradycardia. As used herein, the term "bradycardia" refers to low heart rate or abnormally slow heart rate. The α2 adrenergic antagonist is administered to a subject under general anesthesia and experiencing bradycardia. Without being bound by theory, the administration of the α2 adrenergic antagonist reverses the effects of the agent causing the bradycardia.

In alternative embodiments, the methods of the present disclosure are used for treating hypotension. As used herein, the term "hypotension" refers to low blood pressure. The α2 adrenergic antagonist is administered to a subject under general anesthesia and experiencing hypotension. Without being bound by theory, the administration of the α2 adrenergic antagonist reverses the effects of the agent causing the hypotension.

CIRCADIAN RHYTHMS

Circadian rhythms are the mental, physical, and behavioral changes that follow a 24-hour cycle and are driven by a master clock in the hypothalamus and environmental cues, such as daylight. Circadian rhythms are guided by day-light cycles. Chronic disruptions to a subject's circadian rhythms are correlated with secondary health problems, such as sleep disorders, obesity, diabetes, depression, and bipolar disorder.

In the ICU and other inpatient facilities, patients often suffer disruptions to their circadian rhythms, lose track of time and place, and as a result, can suffer from devastating delirium. It has been shown that delirium is linked to poor sleep and disruption of circadian rhythms. Sedation in the ICU for delirium typically relies on antipsychotic drugs such as haldol and quetiapine. More recently, α2 agonists such as dexmedetomidine (IV) or clonidine (oral) have shown promise as improved sedative agents for patients at risk for or suffering from delirium.

In one aspect of the present disclosure, a specific reversal agent for dexmedetomidine is administered to a subject, which enables proper initiating of circadian rhythms with a day-light cycle and reduces the risks of delirium onset and its persistence.

In some embodiments, a subject with delirium in the ICU would receive an α2 adrenergic agonist for sleep at night time or as desired. Subsequently, to restart the circadian rhythms cycle and decrease the chance for delirium recurrence, the subject receives an α2 adrenergic antagonist agent to cause waking-up from their pharmacologically-aided sleep and properly begin their day-light schedule for initializing their circadian rhythms. In some embodiments, the α2 adrenergic agonist is dexmedetomidine or clonidine. In some embodiments, the dexmedetomidine is administered as an injection. In some embodiments, the dexmedetomidine is administered intravenously. In some embodiments the clonidine is administered orally or by nasogastric tube. In some embodiments, the α2 adrenergic antagonist is atipamezole. In some

embodiments, the α2-agonists adrenergic antagonist is administered as an injection. In some embodiment, the α2-agonists adrenergic antagonist is administered intravenously.

EMERGENCE DELIRIUM

Upon emergence from general anesthesia, patients often become disoriented, combative, and disruptive, endangering themselves and, in extreme cases, the surrounding medical staff. This state is referred to as emergence delirium and can persist well after the patient leaves the operating room to another unit (e.g., ICU). The estimated incidence of emergence delirium, when a patient is waking up from general anesthesia, is 4-31% overall. In children, the incidence of emergence delirium has been estimated to be as high as 50-80%. As a result, many patients have to be restrained upon emergence from general anesthesia in the operating room and post-op unit (ICU, PACU, etc.).

In some embodiments, an α2 adrenergic antagonist is administered to prevent or reduce emergence delirium (i.e., the irritable, combative, inconsolable, or uncompromising, disorientation, emotional distress, and the physical manifestations thereof). In some embodiments, the α2 adrenergic receptor antagonist is administered before emergence (e.g., prophylactically). In some embodiments, the α2 adrenergic receptor antagonist is administered as the subject is regaining consciousness. In some embodiments, the α2 adrenergic receptor antagonist is administered as soon as the subject starts showing any symptoms of emergence delirium (e.g., distress, combativeness, etc.). In some embodiments, the α2 adrenergic receptor antagonist is administered by infusion. In alternative embodiments, the α2 adrenergic receptor antagonist is administered as a single bolus or multiple boluses (optionally rapidly administered boluses). These methods help reorient the patient, possibly through an increased state of arousal, to become less combative and minimize trauma during emergence from general anesthesia.

Compositions and Administration

In some embodiments, α2 adrenergic receptor antagonist can be formulated in compositions for administration. In some embodiments, the α2 adrenergic receptor antagonist is a solution, for example, a saline/water-based solution.

The compounds described herein can be administered in combination with other therapeutic agents and such administration may be simultaneous or sequential. When the other therapeutic agents are administered simultaneously they can be administered in the same or separate formulations, but are administered at the same time. The administration of the other therapeutic agent can also be temporally separated, meaning that the therapeutic agents are administered at a different time, either before or after, the administration of the therapeutics described herein. The separation in time between the administration of these compounds may be a matter of minutes or it may be longer.

The invention described herein, in some aspects, includes methods for administering an α2 adrenergic receptor antagonist as a composition in the doses described herein, wherein the composition is a pharmaceutically acceptable composition. In embodiments where the composition is in a liquid form, a carrier can be a solvent or dispersion medium comprising but not limited to, water, and saline.

A "pharmaceutical composition" or "pharmaceutically acceptable composition" comprises the compound of the invention dissolved or dispersed in a pharmaceutically acceptable carrier. The term "pharmaceutical" or "pharmacologically acceptable" refers to molecular entities and compositions that do not produce an adverse, allergic or other untoward reaction when administered to an animal, such as, for example, a human, as appropriate. Moreover, for animal (*e.g.*, human) administration, it will be understood that preparations should meet sterility, pyrogenicity, general safety and purity standards as required by FDA Office of Biological Standards. The compounds are generally suitable for administration to humans or mammals. This term requires that a compound or composition be nontoxic and sufficiently pure so that no further manipulation of the compound or composition is needed prior to administration to the subject.

As used herein, "pharmaceutically acceptable carrier" includes any and all solvents, dispersion media, coatings, surfactants, antioxidants, preservatives (*e.g.*, antibacterial agents, antifungal agents), isotonic agents, absorption delaying agents, salts, preservatives, drugs, drug stabilizers (*e.g.*, antioxidants), gels, binders, excipients, disintegration agents, lubricants, sweetening agents, flavoring agents, dyes, such like materials and combinations thereof, as would be known to one of ordinary skill in the art (see, for example, Remington's Pharmaceutical Sciences (1990), incorporated herein by reference). Except insofar as any conventional carrier is incompatible with the active ingredient, its use in the therapeutic or pharmaceutical compositions is contemplated. The agent may comprise different types of carriers depending on whether it is to be administered in solid, liquid or aerosol form, and whether it need to be sterile for such routes of administration as injection. In any case, the composition may comprise various antioxidants to retard oxidation of one or more components. Exemplary pharmaceutically acceptable carriers for α-adrenergic receptor antagonists in particular are described in US Patent No. 6,294,517.

In embodiments where the composition is in a liquid form, a carrier can be a solvent or dispersion medium comprising but not limited to, water, ethanol, polyol (*e.g.*, glycerol, propylene glycol, liquid polyethylene glycol, etc.), lipids (*e.g.*, triglycerides, vegetable oils, liposomes) and combinations thereof. The proper fluidity can be maintained, for example, by the use of a coating, such as lecithin; by the maintenance of the required particle size by dispersion in carriers such as, for example liquid polyol or lipids; by the use of surfactants such as, for example hydroxypropylcellulose; or combinations thereof such methods. In many cases, it will be preferable to include isotonic agents, such as, for example, sugars, sodium chloride or combinations thereof.

The term "excipient", as used herein, includes preservatives, suspending agents, stabilizers, dyes, buffers, antibacterial agents, antifungal agents, and isotonic agents, for example, sugars or sodium chloride. As used herein, the term "stabilizer" refers to a

compound optionally used in the pharmaceutical compositions of the present invention in order to avoid the need for sulphite salts and increase storage life. Non-limiting examples of buffers include acetic acid, citric acid, boric acid, and phosphoric acid.

Preservatives can include anti-microbials, antioxidants, and agents that enhance sterility. Exemplary preservatives include ascorbic acid, ascorbyl palmitate, benzyl alcohol, BHA, BHT, citric acid, erythorbic acid, fumaric acid, malic 5 acid, propyl gallate, sodium ascorbate, sodium benzoate, sodium bisulfate, sodium metabisulfite, sodium sulfite, parabens (methyl-, ethyl-, butyl-), benzoic acid, potassium sorbate, and vanillin. The prevention of the action of microorganisms can be brought about by preservatives such as various antibacterial and antifungal agents, including but not limited to parabens (*e.g.*, methylparabens, propylparabens), chlorobutanol, phenol, sorbic acid, thimerosal or combinations thereof.

In embodiments where the composition is in a liquid form, a carrier can be a solvent or dispersion medium comprising but not limited to, water, ethanol, polyol (*e.g.*, glycerol, propylene glycol, liquid polyethylene glycol, etc.), lipids (*e.g.*, triglycerides, vegetable oils, liposomes) and combinations thereof. The proper fluidity can be maintained, for example, by the use of a coating, such as lecithin; by the maintenance of the required particle size by dispersion in carriers such as, for example liquid polyol or lipids; by the use of surfactants such as, for example hydroxypropylcellulose; or combinations thereof such methods. In many cases, it will be preferable to include isotonic agents, such as, for example, sugars, sodium chloride or combinations thereof.

The composition of the present invention can comprise pharmaceutically acceptable salts. Such salts include, but are not limited to, those prepared from the following acids: hydrochloric, hydrobromic, sulphuric, nitric, phosphoric, maleic, acetic, salicylic, p-toluene sulphonic, tartaric, citric, methane sulphonic, formic, malonic, succinic, naphthalene-2-sulphonic, gluconic, and benzene sulphonic.

The compositions may take such forms as suspensions, solutions or emulsions in oily or aqueous vehicles, and may contain formulatory agents such as suspending, stabilizing and/or dispersing agents.

In some embodiments, the α2-adrenergic receptor antagonist is administered as a bolus or as an infusion. Bolus, as used herein, is a defined, discrete amount of a substance (*e.g.*, a dose) delivered intravenously, intramuscularly, intrathecally, or subcutaneously. A bolus can also be a dose delivered by inhalation. In some embodiments, a subject is given one bolus of the α2-adrenergic receptor antagonist. In further embodiments, the subject is given more than one bolus of the α2-adrenergic receptor antagonist, wherein the more than one bolus of the α2-adrenergic receptor antagonist is 2, 3, 4, or 5 boluses of an α2 adrenergic receptor antagonist, in order to facilitate emergence from sedation or unconsciousness. The boluses can be administered during a surgical procedure, immediately after a surgical procedure, over the course of a day, or over the course of multiple days. In some embodiments, the subject is given more than 5 boluses of the α2-adrenergic receptor antagonist over the course of multiple days. In the case of cardiac arrest, where urgency is needed, the α2-adrenergic receptor antagonist needs to be administered rapidly and/or in the form of multiple boluses. Alternatively or in addition, the medication to reverse unconsciousness or sedation is administered by infusion, such as intravenous infusion. Preferably the material is infused into the body (*e.g.*, via intravenous means), but could also be administered by other delivery methods. For instance, the compounds of the present invention can be administered by any available or effective delivery method including, but not limited to, intravenously, intradermally, intraarterially, intralesionally, intratumorally, intracranially, intraarticularly, intraprostaticaly, intrapleurally, intratracheally, intravitreally, intravaginally, intrarectally, topically, intratumorally, intramuscularly, intraperitoneally, subcutaneously, subconjunctival, intravesicularlly, mucosally, intrapericardially, intraumbilically, intraocularally, orally, topically, locally, transdermal drug delivery,

injection, infusion, continuous infusion, localized perfusion bathing target cells directly, via a catheter, via a lavage, in creams, in lipid compositions (*e.g.*, liposomes), or by other method or any combination of the forgoing as would be known to one of ordinary skill in the art (see, for example, Remington's Pharmaceutical Sciences (1990), incorporated herein by reference). In some embodiments, the α2-adrenergic receptor antagonist is administered as a buccal spray. In preferred embodiments, the methods and compositions of the present disclosure involve intravenous administration of the α2-adrenergic receptor antagonist.

The compounds of the invention may be administered directly to a tissue. Direct tissue administration may be achieved by direct injection. In some embodiment, the compounds of the invention are administered intravenously. The compounds may be administered once, or alternatively they may be administered in a plurality of administrations. If administered multiple times, the compounds may be administered via different routes. For example, the first (or the first few) administrations may be made directly into the affected tissue while later administrations may be systemic.

Dosing

The invention described herein, in some aspects, includes methods for administering to a subject that is under general anesthesia or sedation, an effective amount of an α2 adrenergic receptor antagonist. The term "therapeutically effective amount" or "effective amount" as used herein, refers to the amount of active compound or pharmaceutical agent that elicits a biological or medicinal response in a tissue, system, animal, individual or human that is being sought by a researcher, veterinarian, medical doctor or other clinician, which includes one or more of the following: (1) the amount sufficient for the subject to regain full consciousness, (2) the amount sufficient to regain any motor and/or cognitive faculties required to perform the intraoperative or post-operative assessment on the subject, (3) the amount sufficient to make a subject ambulatory while staying in an ICU,

(4) the amount sufficient to reverse cardiac arrest occurring during a surgical procedure. The effective amount of a compound of the invention described herein (*e.g.*, an α2 adrenergic receptor antagonist) may vary depending upon the specific compound used, the mode of delivery of the compound, and whether it is used alone or in combination. The effective amount for any particular application can also vary depending on such factors as the disease being assessed or treated, the particular compound being administered, the size of the subject, the severity of the disease or condition, the detection method, as well as the amount of anesthetic/sedation agent used. One of ordinary skill in the art can empirically determine the effective amount of a particular molecule of the invention without necessitating undue experimentation. Combined with the teachings provided herein, by choosing among the various active compounds and weighing factors such as potency, relative bioavailability, patient body weight, severity of adverse side-effects and preferred mode of administration, an effective regimen can be planned.

Multiple doses of α2 adrenergic receptor antagonist are contemplated herein. In some embodiments, the dose range of α2 adrenergic receptor antagonist given subsequent to the administration of the anesthetic or sedative is 30:1-400:1: μg/kg (antagonist:agonist). In some embodiments, the dose range is 5:1, 10:1, 15:1, 20:1, 25:1, 30:1, 35:1, 37:1, 38:1, or 39:1 μg/kg. In some embodiments, the dose of α2 adrenergic receptor antagonist given subsequent to the administration of the anesthetic or sedative is 40:1, 41:1, 42:1, 43:1, 44:1, 45:1, 46:1, 47:1, 48:1, 49:1, 50:1, 51:1, 52:1, 53:1, 54:1, 55:1: 56:1, 57:1, 58:1, 59:1, 60:1, 62:1, 64:1, 66:1, 68:1, 70:1, 72:1, 74:1, 76:1, 78:1, 80:1, 85:1, 90:1, 95:1, 100:1, 110:1, 120:1, 130:1, 140 150:1, 160:1, 170:1, 180:1, 190:1, 200:1, 220:1, 240:1, 260:1, 280:1, 300:1, 320:1, 340:1, 360:1, 380:1, 400:1, 420:1, 440:1, 460:1, 480:1, or 500:1 μg/kg. In some embodiments, the dose range is 5:1-20:1, 5:1-30:1, 5:1-50:1, 5:1-70:1, 5:1-100:1, 5:1-100:1, 20:1-40:1, 20:1-60:1, 20:1-80:1, 20:1-100:1, 20:1-150:1, 20:1-200:1, 20:1-400:1, 30:1-60:1, 30:1-80:1, 30:1-100-1, 30:1-125:1, 30:1-150:1, 30:1-175:1, 30:1-200:1, 30:1-250:1, 30:1-300:1, 30:1-350:1, 30:1-400:1, 30:1-450:1, 30:1-500:1, 40:1-60:1, 40:1-80:1, 40:1-100-1, 40:1-125:1,

40:1-150:1, 40:1-175:1, 40:1-200:1, 40:1-250:1, 40:1-300:1, 40:1-350:1, 40:1-400:1, 40:1-500:1, 80:1-100:1, 80:1-120:1, 80:1-140:1, 80:1-160:1, 80:1-180:1, 80:1-200:1, 80:1-225:1, 80:1-250:1, 80:1-275:1, 80:1-300:1, 80:1-350:1, 80:1-400:1, 80:1-500:1, 100:1-120:1, 100:1-140:1, 100:1-160:1, 100:1-180:1, 100:1-200:1, 100:1-240:1, 100:1-280:1, 100:1-300:1, 100:1-325:1, 100:1-350:1, 100:1-375:1, 100:1-400:1, 100:1-500:1, 150:1-175:1, 150:1-200:1, 150:1-225:1, 150:1-250:1, 150:1-275:1, 150:1-300:1, 150:1-325:1, 150:1-350:1, 150:1-375:1, 150:1-400:1, 150:1-425:1, 150:1-450:1, 150:1-500:1, 200:1-250:1, 200:1-300:1, 200:1-350:1, 200:1-400:1, 200:1-450:1 or 200:1-500:1 μg/kg (antagonist:agonist). In some embodiments, the α2 adrenergic receptor antagonist is atipamezole.

In some embodiments, the pre-anesthetic dose is an α2 adrenergic receptor agonist (e.g. dexmedetomidine) and can range from 0.15 μg/kg to 2 μg/kg. In some embodiments 0.05, 0.10, 0.15, 0.20, 0.25, 0.30, 0.30, 0.35, 0.40, 0.45, 0.50, 0.55, 0.60, 0.65, 0.70, 0.75, 0.80, 0.85, 0.90, 0.95, 1.00, 1.25, 1.50, 1.75, 2.00, 2.25, 2.50, 2.75, 3.00, 3.5, 4.00, 4.50, or 5.00 μg/kg.

In some embodiments, the α2 adrenergic receptor antagonist is administered by infusion at rates ranging from 0.2-2 μg/kg/hr. In some embodiments, the α2 adrenergic receptor antagonist is administered by infusion at rates up to 20 μg/kg/min. In some embodiments, the α2 adrenergic receptor antagonist is administered by infusion at 0.2, 0.4, 0.6, 0.8, 1.0, 1.2, 1.4, 1.6, 1.8, 2.0, 2.2, 2.4, 2.6, 2.8, 3.0, 3.2, 3.4, 3.6, 3.8, 4.0, 4.2, 4.4, 4.6, 4.8, 5.0, 6, 7, 8, 9, 10, 11, 12, 13, 14, 15, 16, 17, 18, 19, or 20 μg/kg/min. In some embodiments, the α2 adrenergic receptor antagonist is administered by infusion at a rate greater than 20 μg/kg/min. In alternative embodiments, the α2 adrenergic receptor antagonist is administered by bolus.

Generally, the dosage required to constitute an effective amount can be adjusted by one of ordinary skill in the art. The dosage can also vary from one subject to another, based on age, health, physical condition, sex, weight, and contraindications.

Having thus described several aspects of at least one embodiment of this invention, it is to be appreciated various alterations, modifications, and improvements will readily occur to those skilled in the art. Such alterations, modifications, and improvements are intended to be part of this disclosure, and are intended to be within the spirit and scope of the invention. Accordingly, the foregoing description and drawings are by way of example only.

OTHER EMBODIMENTS

All of the features disclosed in this specification may be combined in any combination. Each feature disclosed in this specification may be replaced by an alternative feature serving the same, equivalent, or similar purpose. Thus, unless expressly stated otherwise, each feature disclosed is only an example of a generic series of equivalent or similar features.

From the above description, one skilled in the art can easily ascertain the essential characteristics of the present invention, and without departing from the spirit and scope thereof, can make various changes and modifications of the invention to adapt it to various usages and conditions. Thus, other embodiments are also within the claims.

EQUIVALENTS

While several inventive embodiments have been described and illustrated herein, those of ordinary skill in the art will readily envision a variety of other means and/or structures for performing the function and/or obtaining the results and/or one or more of the advantages described herein, and each of such variations and/or modifications is deemed to be within the scope of the inventive embodiments described herein. More generally, those skilled in the art will readily appreciate that all parameters, dimensions, materials, and configurations described herein are meant to be exemplary and that the actual parameters, dimensions, materials, and/or configurations will depend upon the specific application or applications for which the inventive teachings is/are used. Those

skilled in the art will recognize, or be able to ascertain using no more than routine experimentation, many equivalents to the specific inventive embodiments described herein. It is, therefore, to be understood that the foregoing embodiments are presented by way of example only and that, within the scope of the appended claims and equivalents thereto, inventive embodiments may be practiced otherwise than as specifically described and claimed. Inventive embodiments of the present disclosure are directed to each individual feature, system, article, material, kit, and/or method described herein. In addition, any combination of two or more such features, systems, articles, materials, kits, and/or methods, if such features, systems, articles, materials, kits, and/or methods are not mutually inconsistent, is included within the inventive scope of the present disclosure.

All definitions, as defined and used herein, should be understood to control over dictionary definitions, definitions in documents incorporated by reference, and/or ordinary meanings of the defined terms.

All references, patents and patent applications disclosed herein are incorporated by reference with respect to the subject matter for which each is cited, which in some cases may encompass the entirety of the document.

The indefinite articles "a" and "an," as used herein in the specification and in the claims, unless clearly indicated to the contrary, should be understood to mean "at least one."

The phrase "and/or," as used herein in the specification and in the claims, should be understood to mean "either or both" of the elements so conjoined, i.e., elements that are conjunctively present in some cases and disjunctively present in other cases. Multiple elements listed with "and/or" should be construed in the same fashion, i.e., "one or more" of the elements so conjoined. Other elements may optionally be present other than the elements specifically identified by the "and/or" clause, whether related or unrelated to those elements specifically identified. Thus, as a non-limiting example, a reference to "A and/or B", when used in conjunction with open-ended language such as "comprising" can

refer, in one embodiment, to A only (optionally including elements other than B); in another embodiment, to B only (optionally including elements other than A); in yet another embodiment, to both A and B (optionally including other elements); etc.

As used herein in the specification and in the claims, "or" should be understood to have the same meaning as "and/or" as defined above. For example, when separating items in a list, "or" or "and/or" shall be interpreted as being inclusive, i.e., the inclusion of at least one, but also including more than one, of a number or list of elements, and, optionally, additional unlisted items. Only terms clearly indicated to the contrary, such as "only one of" or "exactly one of," or, when used in the claims, "consisting of," will refer to the inclusion of exactly one element of a number or list of elements. In general, the term "or" as used herein shall only be interpreted as indicating exclusive alternatives (i.e. "one or the other but not both") when preceded by terms of exclusivity, such as "either," "one of," "only one of," or "exactly one of." "Consisting essentially of," when used in the claims, shall have its ordinary meaning as used in the field of patent law.

As used herein in the specification and in the claims, the phrase "at least one," in reference to a list of one or more elements, should be understood to mean at least one element selected from any one or more of the elements in the list of elements, but not necessarily including at least one of each and every element specifically listed within the list of elements and not excluding any combinations of elements in the list of elements. This definition also allows that elements may optionally be present other than the elements specifically identified within the list of elements to which the phrase "at least one" refers, whether related or unrelated to those elements specifically identified. Thus, as a non-limiting example, "at least one of A and B" (or, equivalently, "at least one of A or B," or, equivalently "at least one of A and/or B") can refer, in one embodiment, to at least one, optionally including more than one, A, with no B present (and optionally including elements other than B); in another embodiment, to at least one, optionally including more than one, B, with no A present (and optionally including elements other

than A); in yet another embodiment, to at least one, optionally including more than one, A, and at least one, optionally including more than one, B (and optionally including other elements); etc.

Also, the phraseology and terminology used herein is for the purpose of description and should not be regarded as limiting. The use of "including," "comprising," or "having," "containing," "involving," and variations thereof herein, is meant to encompass the items listed thereafter and equivalents thereof as well as additional items.

It should also be understood that, unless clearly indicated to the contrary, in any methods claimed herein that include more than one step or act, the order of the steps or acts of the method is not necessarily limited to the order in which the steps or acts of the method are recited.

What is claimed is:

CLAIMS

1. A method comprising:
    a) administering to a subject an effective amount of an α2 adrenergic receptor agonist to perform a surgical procedure;
    b) inducing a planned wake-up by administering to the subject an effective amount of α2 adrenergic receptor antagonist, wherein the adrenergic receptor agonist is maintained or reduced;
    c) conducting an intraoperative assessment of the subject during the planned wakeup; and
    d) ceasing the administration of the α2 adrenergic receptor antagonist in order to proceed with the surgical procedure.
2. The method of claim 1, wherein the intraoperative assessment is performed in an operating room.
3. The method of claim 1, wherein after ceasing the α2 adrenergic receptor antagonist, the amount of the adrenergic receptor agonist is increased to its amount at the initiation of the surgical procedure.
4. The method of claim 1 or claim 3, wherein the surgical procedure is a neurosurgery or an orthopedic surgery.
5. The method of claim 4, wherein the neurosurgery is a craniotomy.
6. The method of claim 4, wherein the orthopedic surgery is a spine surgery.
7. The method of any one of claims 1-3, wherein the intraoperative assessment is a physiologic or functional assessment of an organ, organ system, or anatomical region.
8. The method of any one of claims 1-3, wherein the intraoperative assessment is an evaluation of the surgical procedure.

9. The method of any one of claims 1-3, wherein the intraoperative assessment is to assess the subject's breathing.

10. The method of claim 4 or claim 5, wherein the intraoperative assessment is a standard motor and language mapping of the subject's brain.

11. The method of claim 4 or claim 6, wherein the intraoperative assessment is a standard motor mapping technique of the subject's spinal cord or musculature.

12. The method of claim 1, further comprising administering to the subject an effective amount of a general anesthetic.

13. A method comprising:

    a) administering to a subject undergoing a surgical procedure an effective amount of an α2 adrenergic receptor agonist to perform a surgical procedure,

    b) ceasing the administration of the α2 adrenergic agonist and administering to the subject an effective amount of α2 adrenergic receptor antagonist at or near the end of the surgery, and

    c) conducting a post-operative assessment.

14. The method of claim 13, wherein the post-operative assessment is conducted within 30 minutes of the end of the surgery.

15. The method of claim 13, wherein the post-operative assessment is conducted in the operating room after the end of surgery.

16. The method of claim 13 or claim 14B, wherein the post-operative assessment is conducted within 10 minutes of the end of surgery.

17. The method of 13, wherein the post-operative assessment is conducted within 1 hour of the end of surgery.

18. A method comprising administering to a subject undergoing a surgical procedure an effective amount of an α2 adrenergic agonist to perform a

surgical procedure, ceasing the administration of the α2 adrenergic agonist and administering to the subject an effective amount of α2 adrenergic receptor antagonist at or near the end of the surgery, wherein the subject's mobility in an intensive or critical care unit is increased.

19. The method of claim 18, wherein the subject's mobility is increased within 90 minutes of the end of the surgery.

20. A method of modifying circadian rhythms, the method comprising administering to a subject in need thereof, treated with an α2 adrenergic agonist, an effective amount of an α2 adrenergic receptor antagonist in order to facilitate normal adaptation to regular day-light cycles or adjust the subject's circadian rhythms.

21. The method of claim 20, wherein the subject is a patient at risk of delirium.

22. The method of claim 20 or claim 21, wherein the α2 adrenergic agonist is administered for sleep at night time or as desired.

23. The method of any one of claims 20-22, wherein the α2 adrenergic receptor antagonist is administered to restart a circadian rhythms cycle.

24. A method of treating cardiac arrest, the method comprising administering to a subject under general anesthesia and experiencing cardiac arrest, an effective amount of an α2 adrenergic receptor antagonist to treat the cardiac arrest, wherein the subject under general anesthesia had received an α2 adrenergic receptor agonist.

25. A method of treating bradycardia, the method comprising administering to a subject under general anesthesia and experiencing bradycardia, an effective amount of an α2 adrenergic receptor antagonist to treat the bradycardia, wherein the subject under general anesthesia had received an α2 adrenergic receptor agonist.

26. A method of treating hypotension, the method comprising administering to a subject under general anesthesia and experiencing hypotension, an effective amount of an α2 adrenergic receptor antagonist to treat the hypotension, wherein the subject under general anesthesia had received an α2 adrenergic receptor agonist.

27. A method comprising:

a) administering to a subject an effective amount of an α2 adrenergic receptor agonist to perform a surgical procedure, wherein the subject is given an endotracheal breathing tube;

b) ceasing the administration of the α2 adrenergic agonist;

c) administering to the subject an effective amount of α2 adrenergic receptor antagonist prior to the end of the surgical procedure; and

d) conducting an extubation when the subject displays a brainstem reflex.

28. The method of claim 27, wherein (c) is conducted between 0 and 15 minutes before the end of the surgical procedure.

29. The method of claim 27, wherein the brainstem reflex is a pharyngeal reflex.

30. The method of claim 27, wherein the brainstem reflex is a tracheal reflex.

31. A method comprising:

a) administering to a subject an effective amount of an α2 adrenergic receptor agonist to perform a surgical procedure;

b) ceasing the administration of the α2 adrenergic agonist;

(c) administering to the subject an effective amount of α2 adrenergic receptor antagonist prior to the end of the surgical procedure; and

(d) conducting an intraoperative or post-operative assessment to determine if the subject displays a brainstem reflex.

32. The method of claim 31, wherein (c) is conducted between 0 and 15 minutes before the end of the surgical procedure.

33. The method of claim 31, wherein (c) is conducted after the end of the surgical procedure.

34. The method of claim 33, wherein (c) is conducted within 30 minutes after the end of the surgical procedure.

35. A method for reversing a neural blockade during a surgical procedure, comprising:

administering to a subject undergoing a surgical procedure who has received a muscle blockade agent and a neural blockade agent, an effective amount of an α2 adrenergic receptor antagonist to reverse the neural blockade.

36. The method of claim 35, further comprising conducting an intraoperative assessment of the subject following the administration of the α2 adrenergic receptor antagonist.

37. The method of claim 35 or 36, wherein the α2 adrenergic receptor antagonist is given in a dose range of 30:1-400:1 μg/kg α2 adrenergic receptor antagonist to neural blockade agent.

38. A method for reducing or preventing emergence delirium, the method comprising:

administering to a subject under general anesthesia, an effective amount of an α2 adrenergic receptor antagonist, wherein the subject under general anesthesia had received an α2 adrenergic receptor agonist.

39. The method of claim 38, wherein the α2 adrenergic receptor antagonist is administered before emergence from general anesthesia.

40. The method of claim 39, wherein the α2 adrenergic receptor antagonist is administered as the subject begins to regain consciousness.

41. The method of claim 39, wherein the α2 adrenergic receptor antagonist is administered in an effective amount to stop at least one symptom of emergence delirium.

42. The method of any one of claim 1-40, wherein the α2 adrenergic receptor antagonist is given in a dose range of 30:1-400:1 μg/kg α2 adrenergic receptor antagonist to α2 adrenergic agonist.

43. The method of any one of claims 1-42, wherein α2 adrenergic receptor antagonist provides rapid reversal of unconsciousness or sedation.

44. The method of any one of claims 1-43, wherein the α2 adrenergic receptor antagonist is atipamezole.

45. The method of any one of claims 1-44, wherein the α2 adrenergic receptor antagonist is administered intravenously.

46. The method of any one of claims 1-45, wherein the α2 adrenergic receptor antagonist is a composition comprising the α2 adrenergic receptor antagonist and a pharmaceutically acceptable excipient.

47. The method of claim 46, wherein the pharmaceutically acceptable excipient is a saline or water-based solution.

48. The method of any one of claims 1-47, wherein the α2 adrenergic receptor antagonist is administered intravenously as a bolus or an infusion.

49. The method of any one of claims 1-38, wherein the α2 adrenergic agonist is dexmedetomidine or clonidine.

50. The method of claim 49, wherein the α2 adrenergic agonist is administered in solo or in combination with other general anesthetics or sedative drugs.

51. The method of 38, wherein the general anesthetic is propofol, sevoflurane, ketamine, or benzodiazepines.

53. The method of any one of claims 1-51, wherein the subject is a mammal.

54. The method of any one of claims 1-52, wherein the subject is a human.

ABSTRACT

Disclosed herein are methods and compositions for reversing the effects of a sedation agent or general anesthetic agents. The methods are useful for example for assessing a patient during a surgical procedure or a patient's physiologic state during and/or after a surgical procedure. Other uses for the methods and compositions include modulating a circadian rhythm, treating cardiac arrest, hypotension and bradycardia, and preventing emergence delirium.

Bibliography

Absalom, A., & Kenny, G. (2003). Closed-loop control of propofol anaesthesia using bispectral index^{TM}: performance assessment in patients receiving computer-controlled propofol and manually controlled remifentanil infusions for minor surgery†. *BJA: British Journal of Anaesthesia*, *90*(6), 737–741. doi: 10.1093/bja/aeg137

Absalom, A., Mani, V., Smet, D. T., & Struys, M. (2009). Pharmacokinetic models for propofol—defining and illuminating the devil in the detail. *BJA: British Journal of Anaesthesia*, *103*(1), 26–37. doi: 10.1093/bja/aep143

Absalom, A. R., Keyser, R., & Struys, M. M. (2011). Closed Loop Anesthesia. *Anesthesia & Analgesia*, *112*(3), 516–518. doi: 10.1213/ane.0b013e318203f5ad

Achermann, P., & Borbély, A. A. (1998). Coherence analysis of the human sleep electroencephalogram. *Neuroscience*, *85*(4), 1195–1208. doi: 10.1016/s0306-4522(97)00692-1

Adhikari, A., Sigurdsson, T., Topiwala, M. A., & Gordon, J. A. (2010). Cross-correlation of instantaneous amplitudes of field potential oscillations: A straightforward method to estimate the directionality and lag between brain areas. *Journal of Neuroscience Methods*, *191*(2), 191–200. doi: 10.1016/j.jneumeth.2010.06.019

Akeju, O., Song, A. H., Hamilos, A. E., Pavone, K. J., Flores, F. J., Brown, E. N., & Purdon, P. L. (2016). Electroencephalogram signatures of ketamine anesthesia-induced unconsciousness. *Clinical Neurophysiology*, *127*(6), 2414–2422. doi:

10.1016/j.clinph.2016.03.005

Alkire, M. T. (1998). Quantitative EEG Correlations with Brain Glucose Metabolic Rate during Anesthesia in Volunteers. *Anesthesiology*, *89*(2), 323–333. doi: 10.1097/00000542-199808000-00007

Alkire, M. T. (2008). Loss of Effective Connectivity During General Anesthesia. *International Anesthesiology Clinics*, *46*(3), 55–73. doi: 10.1097/aia.0b013e3181755dc6

Alkire, M. T., Hudetz, A. G., & Tononi, G. (2008). Consciousness and Anesthesia. *Science*, *322*(5903), 876–880. doi: 10.1126/science.1149213

Alkire, M. T., & Nathan, S. V. (2005). Does the Amygdala Mediate Anesthetic-induced Amnesia? *Anesthesiology*, *102*(4), 754–760. doi: 10.1097/00000542-200504000-00010

Alpert, M., & Angrist, B. (2003). The ketamine model for schizophrenia. *Behavioral and Brain Sciences*, *26*(1), 82–83. doi: 10.1017/s0140525x03220021

Baker, J. L., Ryou, J.-W., Wei, X. F., Butson, C. R., Schiff, N. D., & Purpura, K. P. (2016). Robust modulation of arousal regulation, performance and frontostriatal activity through central thalamic deep brain stimulation in healthy non-human primates. *Journal of Neurophysiology*, *116*(5), jn.01129.2015. doi: 10.1152/jn.01129.2015

Barr, J., Egan, T. D., Sandoval, N. F., Zomorodi, K., Cohane, C., Gambus, P. L., & Shafer, S. L. (2001). Propofol Dosing Regimens for ICU Sedation Based upon an Integrated Pharmacokinetic– Pharmacodynamic Model. *Anesthesiology*, *95*(2), 324–333. doi: 10.1097/00000542-200108000-00011

Bar-Shalom, Y., Li, X. -Ron., & Kirubarajan, T. (2002). *Estimation with Applications to Tracking and Navigation: Theory, Algorithms and Software.* 89–119. doi: 10.1002/0471221279.ch2

Bastos, A. M., Loonis, R., Kornblith, S., Lundqvist, M., & Miller, E. K. (2018). Laminar recordings in frontal cortex suggest distinct layers for maintenance and control of working memory. *Proceedings of the National Academy of Sciences*, *115*(5), 1117–1122. doi: 10.1073/pnas.1710323115

Bernardi, G., Betta, M., Ricciardi, E., Pietrini, P., Tononi, G., & Siclari, F. (2019). Regional Delta Waves In Human Rapid Eye Movement Sleep. *Journal of Neuroscience*, *39*(14), 2686–2697. doi: 10.1523/jneurosci.2298-18.2019

Betjemann, J. P., & Lowenstein, D. H. (2015). Status epilepticus in adults. *The Lancet Neurology*, *14*(6), 615–624. doi: 10.1016/s1474-4422(15)00042-3

Billard, V., Gambus, P. L., Chamoun, N., Stanski, D. R., & Shafer, S. L. (1997). A comparison of spectral edge, delta power, and bispectral index as EEG measures of alfentanil, propofol, and midazolam drug effect. *Clinical Pharmacology & Therapeutics*, *61*(1), 45–58. doi: 10.1016/s0009-9236(97)90181-8

Blumenfeld, H. (2014). A master switch for consciousness? *Epilepsy & Behavior*, *37*, 234–235. doi: 10.1016/j.yebeh.2014.07.008

Boly, M., Moran, R., Murphy, M., Boveroux, P., Bruno, M.-A., Noirhomme, Q., ... Friston, K. (2012). Connectivity Changes Underlying Spectral EEG Changes during Propofol-Induced Loss of Consciousness. *The Journal of Neuroscience*, *32*(20), 7082–7090. doi: 10.1523/jneurosci.3769-11.2012

Brown, E. N., Lydic, R., & Schiff, N. D. (2010). General Anesthesia, Sleep, and Coma. *The New England Journal of Medicine*, *363*(27), 2638–2650. doi: 10.1056/nejmra0808281

Brown, E. N., Purdon, P. L., & Dort, C. J. (2011). General Anesthesia and Altered States of Arousal: A Systems Neuroscience Analysis. *Neuroscience*, *34*(1), 601–628. doi: 10.1146/annurev-neuro-060909-153200

Buzsáki, G., & Moser, E. I. (2013). Memory, navigation and theta rhythm in the hippocampal-entorhinal system. *Nature Neuroscience*, *16*(2), 130. doi: 10.1038/nn.3304

Caixeta, F. V., Cornélio, A. M., Scheffer-Teixeira, R., Ribeiro, S., & Tort, A. B. (2013). Ketamine alters oscillatory coupling in the hippocampus. *Scientific Reports*, *3*(1), 2348. doi: 10.1038/srep02348

Castro-Zaballa, S., Cavelli, M., Gonzalez, J., Nardi, A., Machado, S., Scorza, C., & Torterolo, P. (2019). EEG 40 Hz Coherence Decreases in REM Sleep and Ketamine Model of Psychosis. *Frontiers in Psychiatry*, *9*, 766. doi: 10.3389/fpsyt.2018.00766

Chakravarty, S., Nikolaeva, K., Kishnan, D., Flores, F. J., Purdon, P. L., & Brown, E. N. (2017). Pharmacodynamic Modeling of Propofol-Induced General Anesthesia in Young Adults. *2017 IEEE Healthcare Innovations and Point of Care Technologies (HI-POCT)*, 44–47. doi: 10.1109/hic.2017.8227580

Chau, A., Salazar, A. M., Krueger, F., Cristofori, I., & Grafman, J. (2015). The effect of claustrum lesions on human consciousness and recovery of function. *Consciousness and Cognition*, *36*, 256–264. doi: 10.1016/j.concog.2015.06.017

Chemali, J., Ching, S., Purdon, P. L., Solt, K., & Brown, E. N. (2013). Burst suppression probability algorithms: state-space methods for tracking EEG burst suppression. *Journal of Neural Engineering*, *10*(5), 056017. doi: 10.1088/1741-2560/10/5/056017

Ching, S., Liberman, M. Y., Chemali, J. J., Westover, B. M., Kenny, J. D., Solt, K., ... Brown, E. N. (2013). Real-time Closed-loop Control in a Rodent Model of Medically Induced Coma Using Burst Suppression. *Anesthesiology*, *119*(4), 848–860. doi: 10.1097/aln.0b013e31829d4ab4

Ching, S., Purdon, P. L., Vijayan, S., Kopell, N. J., & Brown, E. N. (2012). A neurophysiological–metabolic model for burst suppression. *Proceedings of the National Academy of Sciences*, *109*(8), 3095–3100. doi: 10.1073/pnas.1121461109

Cole, S. R., van der Meij, R., Peterson, E. J., de Hemptinne, C., Starr, P. A., & Voytek, B. (2017). Nonsinusoidal Beta Oscillations Reflect Cortical Pathophysiology in Parkinson's Disease. *Journal of Neuroscience*, *37*(18), 4830–4840. doi: 10.1523/jneurosci.2208-16.2017

Covvey, J. R., Crawford, A., & Lowe, D. K. (2012). Intravenous Ketamine for Treatment-Resistant Major Depressive Disorder. *Annals of Pharmacotherapy*, *46*(1), 117–123. doi: 10.1345/aph.1q371

Crick, F. C., & Koch, C. (2005). What is the function of the claustrum? *Philosophical Transactions of the Royal Society B: Biological Sciences*, *360*(1458), 1271–1279. doi: 10.1098/rstb.2005.1661

Dahaba, A. A. (2005). Different Conditions That Could Result in the Bispectral Index Indicating an Incorrect Hypnotic State. *Anesthesia & Analgesia*, *101*(3), 765–773. doi: 10.1213/01.ane.0000167269.62966.af

Darracq, M., Funk, C. M., Polyakov, D., Riedner, B., Gosseries, O., Nieminen, J. O., ... Sanders, R. D. (2018). Evoked Alpha Power is Reduced in Disconnected Consciousness During Sleep and Anesthesia. *Scientific Reports*, *8*(1), 16664. doi: 10.1038/s41598-018-34957-9

de Hemptinne, C., Swann, N. C., Ostrem, J. L., Ryapolova-Webb, E. S., Luciano, M., Galifianakis, N. B., & Starr, P. A. (2015). Therapeutic deep brain stimulation reduces cortical phase-amplitude coupling in Parkinson's disease. *Nature Neuroscience*, *18*(5), nn.3997. doi: 10.1038/nn.3997

Destexhe, A., Hughes, S. W., Rudolph, M., & Crunelli, V. (2007). Are corticothalamic 'up' states fragments of wakefulness? *Trends in Neurosciences*, *30*(7), 334–342. doi: 10.1016/j.tins.2007.04.006

Different Conditions that Could Result in the Bispectral Index Indicating an Incorrect Hypnotic State. (2006). *Survey of Anesthesiology*, *50*(1), 49–50. doi: 10.1097/01.sa.0000193592.67363.fc

Domino, E. F., Chodoff, P., & Corssen, G. (1965). Pharmacologic effects of CI-581, a new dissociative anesthetic, in man. *Clinical Pharmacology & Therapeutics*, *6*(3), 279–291. doi: 10.1002/cpt196563279

Donoghue, J. P., Kerman, K. L., & Ebner, F. F. (1979). Evidence for two organizational plans within the somatic sensory-motor cortex of the rat. *Journal of Comparative Neurology*, *183*(3), 647–663. doi: 10.1002/cne.901830312

Dumont, G. A. (2012). IFAC Proceedings Volumes. *IFAC Proceedings Volumes*, *45*(18), 373–378. doi: 10.3182/20120829-3-hu-2029.00102

Dumont, G. A., Martinez, A., & Ansermino, M. J. (2009). Robust control of depth of anesthesia. *International Journal of Adaptive Control and Signal Processing*, *23*(5), 435–454. doi: 10.1002/acs.1087

Dussaussoy, C., Peres, M., Jaoul, V., Liu, N., Chazot, T., Picquet, J., ... Beydon, L. (2014). Automated titration of propofol and remifentanil decreases the anesthesiologist's workload during vascular or thoracic surgery: a randomized prospective study. *Journal of Clinical Monitoring and Computing*, *28*(1), 35–40. doi: 10.1007/s10877-013-9453-6

Eldar, Y. C., & Oppenheim, A. V. (2003). MMSE Whitening and Subspace Whitening. *IEEE Transactions on Information Theory*, *49*(7), 1846. doi: 10.1109/tit.2003.813507

Frohlich, J., & Horn, J. D. (2014). Reviewing the ketamine model for schizophrenia. *Journal of Psychopharmacology*, *28*(4), 287–302. doi: 10.1177/0269881113512909

Gent, T. C., Bandarabadi, M., Herrera, C., & Adamantidis, A. R. (2018). Thalamic dual

control of sleep and wakefulness. *Nature Neuroscience*, *21*(7), 974–984. doi: 10.1038/s41593-018-0164-7

Gentilini, A., Rossoni-Gerosa, M., Frei, C. W., Wymann, R., Morari, M., Zbinden, A. M., & Schnider, T. W. (2001). Modeling and closed-loop control of hypnosis by means of bispectral index (BIS) with isoflurane. *IEEE Transactions on Biomedical Engineering*, *48*(8), 874–889. doi: 10.1109/10.936364

Gertler, R., Brown, C. H., Mitchell, D. H., & Silvius, E. N. (2017). Dexmedetomidine: A Novel Sedative-Analgesic Agent. *Baylor University Medical Center Proceedings*, *14*(1), 13–21. doi: 10.1080/08998280.2001.11927725

Gil-da-Costa, R., Stoner, G. R., Fung, R., & Albright, T. D. (2013). Nonhuman primate model of schizophrenia using a noninvasive EEG method. *Proceedings of the National Academy of Sciences*, *110*(38), 15425–15430. doi: 10.1073/pnas.1312264110

Gill, P., Shah, J., & Ogilvy, A. (2001). Midazolam reduces the dose of propofol required for induction of anaesthesia and laryngeal mask airway insertion. *European Journal of Anaesthesiology*, *18*(3), 166–170. doi: 10.1097/00003643-200103000-00005

Giovannitti, J. A., Thoms, S. M., & Crawford, J. J. (2015). Alpha-2 Adrenergic Receptor Agonists: A Review of Current Clinical Applications. *Anesthesia Progress*, *62*(1), 31–39. doi: 10.2344/0003-3006-62.1.31

Grady, S. E., Marsh, T. A., Tenhouse, A., & Klein, K. (2017). Ketamine for the treatment of major depressive disorder and bipolar depression: A review of the literature. *Mental Health Clinician*, *7*(1), 16–23. doi: 10.9740/mhc.2017.01.016

Graziano, M. S. (2018). The temporoparietal junction and awareness. *Neuroscience of Consciousness*, *2018*(1), niy005-. doi: 10.1093/nc/niy005

Gregoriou, G. G., Gotts, S. J., Zhou, H., & Desimone, R. (2009). High-Frequency, Long-Range Coupling Between Prefrontal and Visual Cortex During Attention. *Science*, *324*(5931), 1207–1210. doi: 10.1126/science.1171402

Guillery, R. W., & Sherman, S. M. (2002). Thalamic Relay Functions and Their Role in Corticocortical Communication Generalizations from the Visual System. *Neuron*, *33*(2), 163–175. doi: 10.1016/s0896-6273(01)00582-7

Haefely, W. E. (1989). Pharmacology of the benzodiazepine receptor. *European Archives*

of Psychiatry and Neurological Sciences, *238*(5–6), 294–301. doi: 10.1007/bf00449811

Hafting, T., Fyhn, M., Bonnevie, T., Moser, M.-B., & Moser, E. I. (2008). Hippocampus-independent phase precession in entorhinal grid cells. *Nature*, *453*(7199), 1248. doi: 10.1038/nature06957

Homayoun, H., & Moghaddam, B. (2007). NMDA Receptor Hypofunction Produces Opposite Effects on Prefrontal Cortex Interneurons and Pyramidal Neurons. *The Journal of Neuroscience*, *27*(43), 11496–11500. doi: 10.1523/jneurosci.2213-07.2007

Hubel, D. H. (1963). Integrative Processes in Central Visual Pathways of the Cat*. *Journal of the Optical Society of America*, *53*(1), 58. doi: 10.1364/josa.53.000058

Hubel, D. H. (1982). Exploration of the primary visual cortex, 1955–78. *Nature*, *299*(5883), 515–524. doi: 10.1038/299515a0

Hutchison, M. R., & Everling, S. (2012). Monkey in the middle: why non-human primates are needed to bridge the gap in resting-state investigations. *Frontiers in Neuroanatomy*, *6*, 29. doi: 10.3389/fnana.2012.00029

Insanally, M. N., Carcea, I., Field, R. E., Rodgers, C. C., DePasquale, B., Rajan, K., ... Froemke, R. C. (2019). Spike-timing-dependent ensemble encoding by non-classically responsive cortical neurons. *ELife*, *8*, e42409. doi: 10.7554/elife.42409

Jacobs, J. (2013). Hippocampal theta oscillations are slower in humans than in rodents: implications for models of spatial navigation and memory. *Philosophical Transactions of the Royal Society of London. Series B, Biological Sciences*, *369*(1635), 20130304. doi: 10.1098/rstb.2013.0304

Jobert, M., Wilson, F. J., Ruigt, G. S., Brunovsky, M., Prichep, L. S., inkenburg, W. H., & Committee, I. (2012). Guidelines for the Recording and Evaluation of Pharmaco-EEG Data in Man: The International Pharmaco-EEG Society (IPEG). *Neuropsychobiology*, *66*(4), 201–220. doi: 10.1159/000343478

Kaneko, K., Koyanagi, Y., Oi, Y., & Kobayashi, M. (2016). Propofol-induced spike firing suppression is more pronounced in pyramidal neurons than in fast-spiking neurons in the rat insular cortex. *Neuroscience*, *339*, 548–560. doi: 10.1016/j.neuroscience.2016.10.016

Koubeissi, M. Z., Bartolomei, F., Beltagy, A., & Picard, F. (2014). Electrical stimulation

of a small brain area reversibly disrupts consciousness. *Epilepsy & Behavior*, *37*, 32–35. doi: 10.1016/j.yebeh.2014.05.027

Kreuzer, M., Zanner, R., Pilge, S., Paprotny, S., Kochs, E. F., & Schneider, G. (2012). Time Delay of Monitors of the Hypnotic Component of Anesthesia. *Anesthesia & Analgesia*, *115*(2), 315–319. doi: 10.1213/ane.0b013e31825801ea

Kurada, L., Bayat, A., Joshi, S., & Koubeissi, M. Z. (2019). The Claustrum in Relation to Seizures and Electrical Stimulation. *Frontiers in Neuroanatomy*, *13*, 8. doi: 10.3389/fnana.2019.00008

Lapidus, K., Levitch, C. F., Perez, A. M., Brallier, J. W., Parides, M. K., Soleimani, L., ... Murrough, J. W. (2014). A Randomized Controlled Trial of Intranasal Ketamine in Major Depressive Disorder. *Biological Psychiatry*, *76*(12), 970–976. doi: 10.1016/j.biopsych.2014.03.026

Latchoumane, C.-F. V., Ngo, H.-V. V., Born, J., & Shin, H.-S. (2017). Thalamic Spindles Promote Memory Formation during Sleep through Triple Phase-Locking of Cortical, Thalamic, and Hippocampal Rhythms. *Neuron*, *95*(2), 424-435.e6. doi: 10.1016/j.neuron.2017.06.025

Lazarewicz, M. T., Ehrlichman, R. S., Maxwell, C. R., Gandal, M. J., Finkel, L. H., & Siegel, S. J. (2010). Ketamine Modulates Theta and Gamma Oscillations. *Journal of Cognitive Neuroscience*, *22*(7), 1452–1464. doi: 10.1162/jocn.2009.21305

Lee, S.-H., & Cox, C. L. (2003). Vasoactive Intestinal Peptide Selectively Depolarizes Thalamic Relay Neurons and Attenuates Intrathalamic Rhythmic Activity. *Journal of Neurophysiology*, *90*(2), 1224–1234. doi: 10.1152/jn.00280.2003

Lewis, L. D., Ching, S., Weiner, V. S., Peterfreund, R. A., Eskandar, E. N., Cash, S. S., ... Purdon, P. L. (2013). Local cortical dynamics of burst suppression in the anaesthetized brain. *Brain*, *136*(9), 2727–2737. doi: 10.1093/brain/awt174

Lewis, L. D., Weiner, V. S., Mukamel, E. A., Donoghue, J. A., Eskandar, E. N., Madsen, J. R., ... Purdon, P. L. (2012). Rapid fragmentation of neuronal networks at the onset of propofol-induced unconsciousness. *Proceedings of the National Academy of Sciences*, *109*(49), E3377–E3386. doi: 10.1073/pnas.1210907109

Liberman, M. Y., Ching, S., Chemali, J., & Brown, E. N. (2013). A closed-loop anesthetic delivery system for real-time control of burst suppression. *Journal of Neural*

Engineering, *10*(4), 046004. doi: 10.1088/1741-2560/10/4/046004

Liebe, S., Hoerzer, G. M., Logothetis, N. K., & Rainer, G. (2012). Theta coupling between V4 and prefrontal cortex predicts visual short-term memory performance. *Nature Neuroscience*, *15*(3), 456. doi: 10.1038/nn.3038

Liu, N. (2017). *Total Intravenous Anesthesia and Target Controlled Infusions, A Comprehensive Global Anthology*. 649–666. doi: 10.1007/978-3-319-47609-4_35

Liu, N., Chazot, T., Hamada, S., Landais, A., Boichut, N., Dussaussoy, C., ... Fischler, M. (2011). Closed-Loop Coadministration of Propofol and Remifentanil Guided by Bispectral Index. *Anesthesia & Analgesia*, *112*(3), 546–557. doi: 10.1213/ane.0b013e318205680b

Liu, N., & Rinehart, J. (2016). Closed-Loop Propofol Administration. *Anesthesia & Analgesia*, *122*(1), 4–6. doi: 10.1213/ane.0000000000000665

Loonis, R. F., Brincat, S. L., Antzoulatos, E. G., & Miller, E. K. (2017). A Meta-Analysis Suggests Different Neural Correlates for Implicit and Explicit Learning. *Neuron*, *96*(2), 521-534.e7. doi: 10.1016/j.neuron.2017.09.032

Mahon, P., Greene, B., Greene, C., Boylan, G., & Shorten, G. (2008). Behaviour of spectral entropy, spectral edge frequency 90%, and alpha and beta power parameters during low-dose propofol infusion. *BJA: British Journal of Anaesthesia*, *101*(2), 213–221. doi: 10.1093/bja/aen161

Malekmohammadi, M., AuYong, N., Ricks-Oddie, J., Bordelon, Y., & Pouratian, N. (2018). Pallidal deep brain stimulation modulates excessive cortical high β phase amplitude coupling in Parkinson disease. *Brain Stimulation*, (Brain 125 2002). doi: 10.1016/j.brs.2018.01.028

Marsh, B., White, M., Morton, N., & Kenny, G. N. C. (1991). PHARMACOKINETIC MODEL DRIVEN INFUSION OF PROPOFOL IN CHILDREN. *BJA: British Journal of Anaesthesia*, *67*(1), 41–48. doi: 10.1093/bja/67.1.41

Mashour, G. A., & Alkire, M. T. (2013). Consciousness, Anesthesia, and the Thalamocortical System. *Anesthesiology*, *118*(1), 13–15. doi: 10.1097/aln.0b013e318277a9c6

Masson, G., Masson, S., Debay, D., & Bal, T. (2002). Feedback inhibition controls spike

transfer in hybrid thalamic circuits. *Nature*, *417*(6891), 854. doi: 10.1038/nature00825

McLaren, D. G., Kosmatka, K. J., Oakes, T. R., Kroenke, C. D., Kohama, S. G., Matochik, J. A., ... Johnson, S. C. (2009). A population-average MRI-based atlas collection of the rhesus macaque. *NeuroImage*, *45*(1), 52–59. doi: 10.1016/j.neuroimage.2008.10.058

Miyasaka, M., & Domino, E. F. (1968). Neuronal mechanisms of ketamine-induced anesthesia. *International Journal of Neuropharmacology*, *7*(6), 557–573. doi: 10.1016/0028-3908(68)90067-1

Münch, M., Knoblauch, V., Blatter, K., Schröder, C., Schnitzler, C., Kräuchi, K., ... Cajochen, C. (2004). The frontal predominance in human EEG delta activity after sleep loss decreases with age. *European Journal of Neuroscience*, *20*(5), 1402–1410. doi: 10.1111/j.1460-9568.2004.03580.x

Nir, Y., Staba, R. J., Andrillon, T., Vyazovskiy, V. V., Cirelli, C., Fried, I., & Tononi, G. (2011). Regional Slow Waves and Spindles in Human Sleep. *Neuron*, *70*(1), 153–169. doi: 10.1016/j.neuron.2011.02.043

Oostenveld, R., Fries, P., Maris, E., & Schoffelen, J.-M. (2011). FieldTrip: Open Source Software for Advanced Analysis of MEG, EEG, and Invasive Electrophysiological Data. *Computational Intelligence and Neuroscience*, *2011*, 156869. doi: 10.1155/2011/156869

Pani, N., Dongare, P. A., & Mishra, R. (2015). Reversal agents in anaesthesia and critical care. *Indian Journal of Anaesthesia*, *59*(10), 664–669. doi: 10.4103/0019-5049.167484

Pedrazzini, E., & Ptak, R. (2019). Damage to the right temporoparietal junction, but not lateral prefrontal or insular cortex, amplifies the role of goal-directed attention. *Scientific Reports*, *9*(1), 306. doi: 10.1038/s41598-018-36537-3

Pilge, S., Zanner, R., Schneider, G., Blum, J., Kreuzer, M., & Kochs, E. F. (2006). Time Delay of Index Calculation. *Anesthesiology*, *104*(3), 488–494. doi: 10.1097/00000542-200603000-00016

Purdon, P. L., Pierce, E. T., Mukamel, E. A., Prerau, M. J., Walsh, J. L., Wong, K. K., ... Brown, E. N. (2013). Electroencephalogram signatures of loss and recovery of consciousness from propofol. *Proceedings of the National Academy of Sciences*, *110*(12), E1142–E1151. doi: 10.1073/pnas.1221180110

Puri, G. D., Mathew, P. J., Biswas, I., Dutta, A., Sood, J., Gombar, S., ... Singh, G. (2016). A Multicenter Evaluation of a Closed-Loop Anesthesia Delivery System. *Anesthesia & Analgesia*, *122*(1), 106–114. doi: 10.1213/ane.0000000000000769

Radek, L., Kallionpää, R. E., Karvonen, M., Scheinin, A., Maksimow, A., Långsjö, J., ... Valli, K. (2018). Dreaming and awareness during dexmedetomidine- and propofol-induced unresponsiveness. *British Journal of Anaesthesia*, *121*(1), 260–269. doi: 10.1016/j.bja.2018.03.014

Rainer, G., Asaad, W. F., & Miller, E. K. (1998). Memory fields of neurons in the primate prefrontal cortex. *Proceedings of the National Academy of Sciences*, *95*(25), 15008–15013. doi: 10.1073/pnas.95.25.15008

Robinson, D. H., & Toledo, A. H. (2012). Historical Development of Modern Anesthesia. *Journal of Investigative Surgery*, *25*(3), 141–149. doi: 10.3109/08941939.2012.690328

Rohan, D., Buggy, D. J., Crowley, S., Ling, F. K., Gallagher, H., Regan, C., & Moriarty, D. C. (2005). Increased incidence of postoperative cognitive dysfunction 24 hr after minor surgery in the elderly. *Canadian Journal of Anesthesia*, *52*(2), 137–142. doi: 10.1007/bf03027718

Saalmann, Y. B. (2014). Intralaminar and medial thalamic influence on cortical synchrony, information transmission and cognition. *Frontiers in Systems Neuroscience*, *8*, 83. doi: 10.3389/fnsys.2014.00083

Sanders, R. D., Tononi, G., Laureys, S., & Sleigh, J. W. (2012). Unresponsiveness ≠ Unconsciousness. *Anesthesiology*, *116*(4), 946–959. doi: 10.1097/aln.0b013e318249d0a7

Saxe, R., & Kanwisher, N. (2003). People thinking about thinking people The role of the temporo-parietal junction in "theory of mind." *NeuroImage*, *19*(4), 1835–1842. doi: 10.1016/s1053-8119(03)00230-1

Scheinin, M., Lomasney, J. W., Hayden-Hixson, D. M., Schambra, U. B., Caron, M. G., Lefkowitz, R. J., & Fremeau, R. T. (1994). Distribution of α2-adrenergic receptor subtype gene expression in rat brain. *Molecular Brain Research*, *21*(1–2), 133–149. doi: 10.1016/0169-328x(94)90386-7

Schiff, N., Giacino, J., Kalmar, K., Victor, J., Baker, K., Gerber, M., ... Rezai, A. (2007). Behavioural improvements with thalamic stimulation after severe traumatic

brain injury. *Nature*, *448*(7153), 600. doi: 10.1038/nature06041

Schnider, T. W., Minto, C. F., Shafer, S. L., Gambus, P. L., Andresen, C., Goodale, D. B., & Youngs, E. J. (1999). The Influence of Age on Propofol Pharmacodynamics. *Anesthesiology*, *90*(6), 1502-1516. doi: 10.1097/00000542-199906000-00003

Schwender, D., underer, Mulzer, S., Klasing, S., Finsterer, U., & Peter, K. (1996). Spectral edge frequency of the electroencephalogram to monitor depth of anaesthesia with isoflurane or propofol. *BJA: British Journal of Anaesthesia*, *77*(2), 179–184. doi: 10.1093/bja/77.2.179

Schwilden, H., Stoeckel, H., & Schüttler, J. (1989). CLOSED-LOOP FEEDBACK CONTROL OF PROPOFOL ANAESTHESIA BY QUANTITATIVE EEG ANALYSIS IN HUMANS. *BJA: British Journal of Anaesthesia*, *62*(3), 290–296. doi: 10.1093/bja/62.3.290

Sederberg, P. B., Kahana, M. J., Howard, M. W., Donner, E. J., & Madsen, J. R. (2003). Theta and Gamma Oscillations during Encoding Predict Subsequent Recall. *Journal of Neuroscience*, *23*(34), 10809–10814. doi: 10.1523/jneurosci.23-34-10809.2003

Shafer, S. L., & Gregg, K. M. (1992). Algorithms to rapidly achieve and maintain stable drug concentrations at the site of drug effect with a computer-controlled infusion pump. *Journal of Pharmacokinetics and Biopharmaceutics*, *20*(2), 147–169. doi: 10.1007/bf01070999

Shanechi, M. M., Chemali, J. J., Liberman, M., Solt, K., & Brown, E. N. (2013). A Brain-Machine Interface for Control of Medically-Induced Coma. *PLoS Computational Biology*, *9*(10), e1003284. doi: 10.1371/journal.pcbi.1003284

Siegel, M., Warden, M. R., & Miller, E. K. (2009). Phase-dependent neuronal coding of objects in short-term memory. *Proceedings of the National Academy of Sciences*, *106*(50), 21341–21346. doi: 10.1073/pnas.0908193106

Singh, V., Gillespie, T. W., & Harvey, R. (2018). Intranasal Ketamine and Its Potential Role in Cancer-Related Pain. *Pharmacotherapy: The Journal of Human Pharmacology and Drug Therapy*, *38*(3), 390–401. doi: 10.1002/phar.2090

Sinyor, M., Williams, M., Belo, S., Orser, B., Vincent, M., Mah, L., ... Schaffer, A. (2018). Ketamine augmentation for major depressive disorder and suicidal ideation: Preliminary experience in an inpatient psychiatry setting. *Journal of Affective*

Disorders, *241*(Biol. Psychiatry 72 2012), 103–109. doi: 10.1016/j.jad.2018.07.073

Sklar, G. S., Zukin, S. R., & Reilly, T. A. (1981). Adverse reactions to ketamine Anaesthesia. *Anaesthesia*, *36*(2), 183–187. doi: 10.1111/j.1365-2044.1981.tb08721.x

Smith, C., McEwan, A. I., Jhaveri, R., Wilkinson, M., Goodman, D., Smith, R. L., ... Glass, P. S. (1994). The Interaction of Fentanyl on the Cp50 of Propofol for Loss of Consciousness and Skin Incision. *Anesthesiology*, *81*(4), 820–828. doi: 10.1097/00000542-199410000-00008

Supp, G. G., Siegel, M., Hipp, J. F., & Engel, A. K. (2011). Cortical Hypersynchrony Predicts Breakdown of Sensory Processing during Loss of Consciousness. *Current Biology*, *21*(23), 1988–1993. doi: 10.1016/j.cub.2011.10.017

Szurhaj, W., Lamblin, Kaminska, A., & Sediri, H. (2015). EEG guidelines in the diagnosis of brain death. *Neurophysiologie Clinique/Clinical Neurophysiology*, *45*(1), 97–104. doi: 10.1016/j.neucli.2014.11.005

Tonner, P. H., & Bein, B. (2006). Classic electroencephalographic parameters: Median frequency, spectral edge frequency etc. *Best Practice & Research Clinical Anaesthesiology*, *20*(1), 147–159. doi: 10.1016/j.bpa.2005.08.008

Tóth, K., Hofer, K. T., Kandrács, Á., Entz, L., Bagó, A., Erőss, L., ... Wittner, L. (2018). Hyperexcitability of the network contributes to synchronization processes in the human epileptic neocortex. *The Journal of Physiology*, *596*(2), 317–342. doi: 10.1113/jp275413

Tryba, M., & Kulka, P. (1993). Critical Care Pharmacotherapy. *Drugs*, *45*(3), 338–352. doi: 10.2165/00003495-199345030-00003

van Vugt, B., Dagnino, B., Vartak, D., Safaai, H., Panzeri, S., Dehaene, S., & Roelfsema, P. R. (2018). The threshold for conscious report: Signal loss and response bias in visual and frontal cortex. *Science*, *360*(6388), eaar7186. doi: 10.1126/science.aar7186

Vidyasagar, T. R., & Levichkina, E. (2019). An Integrated Neuronal Model of Claustral Function in Timing the Synchrony Between Cortical Areas. *Frontiers in Neural Circuits*, *13*, 3. doi: 10.3389/fncir.2019.00003

Vijayan, S., Ching, S., Purdon, P. L., Brown, E. N., & Kopell, N. J. (2013).

Thalamocortical Mechanisms for the Anteriorization of Alpha Rhythms during Propofol-Induced Unconsciousness. *The Journal of Neuroscience*, *33*(27), 11070–11075. doi: 10.1523/jneurosci.5670-12.2013

Vyazovsky, V. V., & Tobler, I. (2005). Regional differences in NREM sleep slow-wave activity in mice with congenital callosal dysgenesis. *Journal of Sleep Research*, *14*(3), 299–304. doi: 10.1111/j.1365-2869.2005.00456.x

Watson, B. O., Levenstein, D., Greene, P. J., Gelinas, J. N., & Buzsáki, G. (2016). Network Homeostasis and State Dynamics of Neocortical Sleep. *Neuron*, *90*(4), 839–852. doi: 10.1016/j.neuron.2016.03.036

Westover, B. M., Ching, S., Kumaraswamy, V. M., Akeju, O., Pierce, E., Cash, S. S., ... Purdon, P. L. (2015). The human burst suppression electroencephalogram of deep hypothermia. *Clinical Neurophysiology*, *126*(10), 1901–1914. doi: 10.1016/j.clinph.2014.12.022

Womelsdorf, T., Schoffelen, J.-M., Oostenveld, R., Singer, W., Desimone, R., Engel, A. K., & Fries, P. (2007). Modulation of Neuronal Interactions Through Neuronal Synchronization. *Science*, *316*(5831), 1609–1612. doi: 10.1126/science.1139597

Yang, Y., & Shanechi, M. M. (2016). An adaptive and generalizable closed-loop system for control of medically induced coma and other states of anesthesia. *Journal of Neural Engineering*, *13*(6), 066019. doi: 10.1088/1741-2560/13/6/066019

Yin, B., Terhune, D. B., Smythies, J., & Meck, W. H. (2016). Claustrum, consciousness, and time perception. *Current Opinion in Behavioral Sciences*, *8*, 258–267. doi: 10.1016/j.cobeha.2016.02.032

Young, B. G. (2000). The EEG in Coma. *Journal of Clinical Neurophysiology*, *17*(5), 473–485. doi: 10.1097/00004691-200009000-00006

Zanner, R., Pilge, S., Kochs, E., Kreuzer, M., & Schneider, G. (2009). Time delay of electroencephalogram index calculation: analysis of cerebral state, bispectral, and Narcotrend indices using perioperatively recorded electroencephalographic signals. *BJA: British Journal of Anaesthesia*, *103*(3), 394–399. doi: 10.1093/bja/aep198

We shall not cease from exploration
And the end of all our exploring
Will be to arrive where we started
And know the place for the first time.

-- T.S. Eliot, Little Gidding (1942)